

Nucleobase catalysts for the enzymatic activation of 8-oxoguanine DNA glycosylase 1

Emily C. Hank,^{1, #} Nicholas D. D'Arcy-Evans,¹ Emma Rose Scaletti,² Carlos Benítez-Buelga,^{3, 4} Olov Wallner,¹ Florian Ortis,¹ Kaixin Zhou,¹ Liuzhen Meng,¹ Alicia del Prado,⁵ Patricia Calvo,⁵ Ingrid Almlöf,¹ Elisée Wiita,¹ Karen Nierlin,¹ Sara Košenina,² Andreas Krämer,⁶ Mario Kehler,¹ Maeve Long,¹ Ann-Sofie Jemth,¹ Holly Dawson,¹ Josephine Stewart,¹ Adam Dickey,¹ Mikhael E. Astorga,¹ Marek Varga,¹ Evert J. Homan,¹ Martin Scobie,¹ Stefan Knapp,⁶ Leandro Sastre,^{3, 7} Pål Stenmark,^{2, 8} Miguel de Vega,⁵ Thomas Helleday,^{1, 9} Maurice Michel^{1, 10 *}

AUTHOR ADDRESS

1 Science for Life Laboratory, Department of Oncology-Pathology, Karolinska Institutet, Stockholm, Sweden

2 Department of Biochemistry and Biophysics, Stockholm University, Stockholm, Sweden

3 Instituto de Investigaciones Biomédicas Alberto Sols CSIC/UAM, Madrid, Spain

4 Molecular Genetics Unit, Instituto de Investigación de Enfermedades Raras (IIER), Instituto de Salud Carlos III (ISCIII), Madrid, Spain.

5 Centro de Biología Molecular 'Severo Ochoa' (CSIC-UAM), Madrid, Spain

6 Institute of Pharmaceutical Chemistry & Structural Genomics Consortium (SGC), Goethe University, Frankfurt, Germany

7 Centro de Investigación Biomédica en Red de Enfermedades Raras (CIBERER). Instituto de Salud Carlos III. C., Madrid, Spain

8 Department of Experimental Medical Science, Lund University, Lund, Sweden

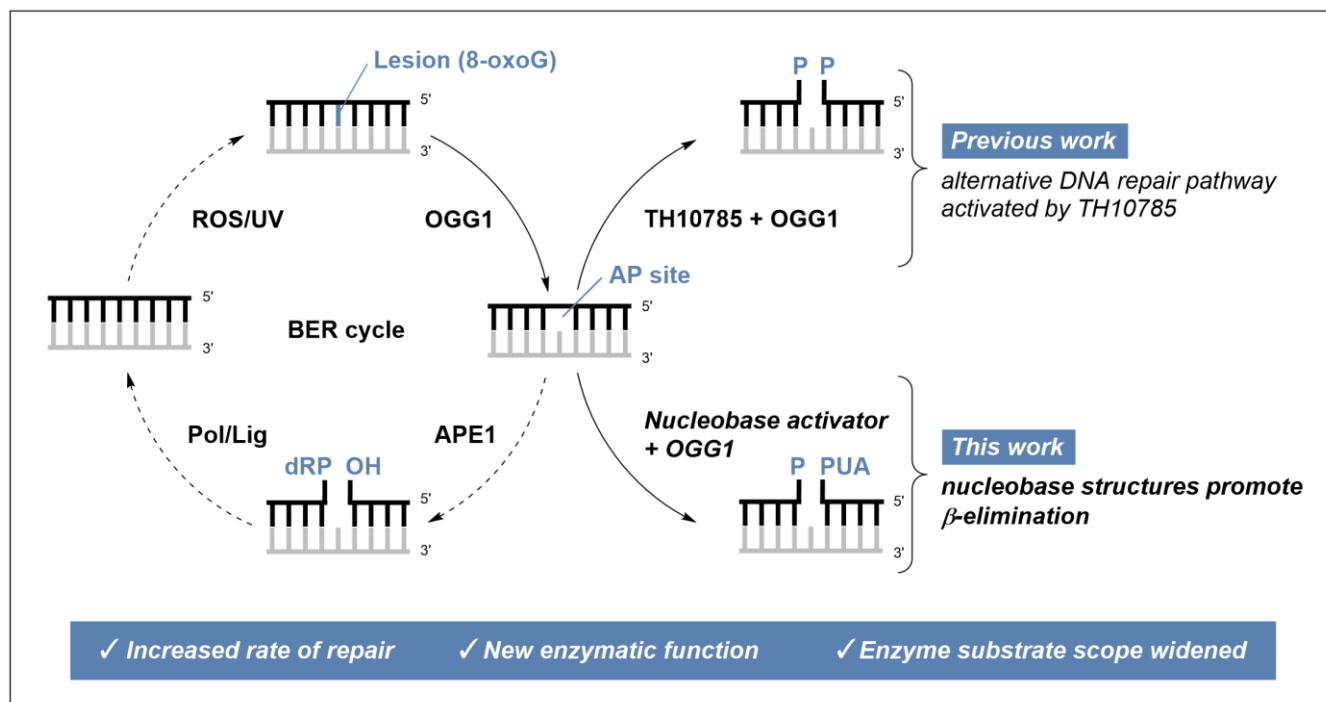
9 Weston Park Cancer Centre and Division of Clinical Medicine, School of Medicine and Population Health, University of Sheffield, Sheffield, United Kingdom

10 Center for Molecular Medicine, Karolinska Institute and Karolinska Hospital, Stockholm, Sweden

Current Address: Department of Pharmacy, Ludwig-Maximilians-Universität Munich, Germany

KEYWORDS: Base excision repair, OGG1, organocatalytic switch, DNA glycosylase, thioguanine

Graphical abstract: OGG1 lyase-activators acting from within the catalytic pocket are organocatalytic switches that enhance OGG1 initiated DNA repair through stimulating rudimentary activities by partaking in the reaction, establishing de novo enzymatic functions on a widened substrate scope.



ABSTRACT: Bifunctional DNA glycosylases employ an active site lysine or the N-terminus to form a Schiff base with the abasic (AP) site base excision repair intermediate. For the 8-oxoguanine DNA glycosylase 1 (OGG1), cleaving this reversible structure is the rate-determining step in the initiation of 8-oxoguanine (8-oxoG) repair in DNA. Evolution has led OGG1 to use a product-assisted catalysis approach, where the excised 8-oxoG acts as a Brønsted base for cleavage of a Schiff base intermediate. However, the physicochemical properties of 8-oxoG significantly limit the inherent enzymatic turnover leading to a weak, cellularly absent, AP lyase activity. We hypothesized that chemical synthesis of purine analogues enables access to complex structures that are suitable as product-like catalysts. Here, the nucleobase landscape is profiled for its potential to increase OGG1 Schiff base cleavage. 8-Substituted 6-thioguanines emerge as potent and selective scaffolds enabling OGG1 to cleave AP sites opposite any canonical nucleobase by β -elimination. This effectively broadens the enzymatic substrate scope of OGG1, shaping a complete, artificial AP-lyase function. In addition, a second class of compounds, 6-substituted pyrazolo-[3,4-*d*]-pyrimidines, stimulate OGG1 function at high pH, while thioguanines govern enzymatic control at acidic pH. This enables up to 20-fold increased enzyme turnover and a *de novo* OGG1 β -elimination in conditions commonly not tolerated. The tool compounds employed here are non-toxic in cells and stimulate the repair of AP sites through a natural, APE1 dependent, pathway, as opposed to previously reported β,δ -lyase stimulator TH10785.

Oxidative damage in the form of 8-oxoG is the most common DNA lesion in our cells. An accumulation of 8-oxoG, its oxidation products or subsequent mutations caused through their presence leads to deterioration of cellular health and ultimately to neurodegenerative^[1,2] and cardiovascular^[3,4] diseases, as well as cancer.^[5,6] OGG1 is the enzyme responsible for the removal of 8-oxoG through its glycosylase function. Thus, literature suggests that targeting of OGG1 function may be a viable strategy to counter-act the above effects.^[7,8]

Interestingly, so far, the necessary OGG1 activation has been achieved by an allosteric mechanism^[9] or by activation of the otherwise rudimentary AP-lyase activity.^[10] This AP-lyase activity is most likely controlled by product-assisted catalysis; a distinct mode of action compared to classic allosteric regulation.^[11] For detailed mechanistic insight, please visit Scheme S1. Briefly, the previously excised 8-oxoG acts as a weak chemical base and abstracts a proton from the Schiff base intermediate formed between the AP site and OGG1 active site Lys249 during the glycosylase step. *In vitro*, this process results in a weak AP-lyase activity through β -elimination, which leads to 3'-DNA strand incision and removal of OGG1 from the product. In cells, this effect is negligible and OGG1 is thus a monofunctional glycosylase.^[12] Here, instead recruited apurinic/aprimidinic endonuclease 1 (APE1) prevents rebinding of AP sites through OGG1 by its nuclease function, effectively preventing duration of Schiff Base complexes.^[10,13,14] Since the recruitment and binding to the AP site by APE1 requires time,^[15] release of OGG1 from the Schiff Base or alternatively its cleavage is the rate-determining step in the initiation of base excision repair (BER).^[16] Activating the AP-lyase activity of OGG1 through small molecules would therefore lead to increased repair of AP sites by avoidance of APE1 recruitment. Accelerated release of OGG1 from the Schiff Base would then a) immediately stimulate AP site repair and b) increase the capacity for 8-oxoG repair as an effect of increased OGG1 release.^[10,17]

In agreement with the product-assisted catalysis mechanism postulated by Fromme *et al.*,^[11] we have recently reported OGG1 lyase-activators that establish proton-abstraction events to foster an artificial β,δ -elimination generating a gap flanked by 5'P and 3'P ends. The kinetics of this novel elimination overwrote the dominant glycosylase function of OGG1 in cells, rendering it a β,δ -AP lyase that creates products whose repair pathways are independent of APE1. We termed the bifunctional compounds organocatalytic switches since they:

- a) contain a heterocyclic nitrogen center with Brønsted base-like character,
- b) bear a structural handle with active site affinity,^[10]
- c) partake in the biochemical reaction,
- d) are not changed in the process, and

e) as a result, alter, *i.e.* switch, the protein function

In the same study, we used 8-bromoguanine as a more soluble analogue of 8-oxoG and confirmed it to be an activator of the residual β -elimination (Figure 1). Controlling OGG1 incision through either β - or β,δ -elimination leads to distinct repair pathways depending on either APE1 or bifunctional polynucleotide phosphatase/kinase (PNKP1) function for end cleansing.^[18] To be able to investigate both mechanisms in more detail and the chemical space surrounding 8-bromoguanine we sought to establish a series of purine-based organocatalytic switches of OGG1.

Here, we screened a library of nucleoside and nucleobase analogues and discovered two chemical series of nucleobase based organocatalytic switches acting within OGG1. Chemical modification revealed the detailed structure-activity-relationship (SAR) and enzymatic assays as well as co-crystal structures confirmed active site binding, and not allosteric regulation as the mode of action. We further observed that very potent organocatalytic switches control OGG1 function opposite any canonical nucleobase and that different scaffolds can be employed to govern enzymatic function in a pH range distinct from naïve OGG1. The compounds developed enable OGG1-mediated repair of AP sites dependent on APE1 and are powerful tools to investigate increased loading of this canonical pathway within base excision repair.

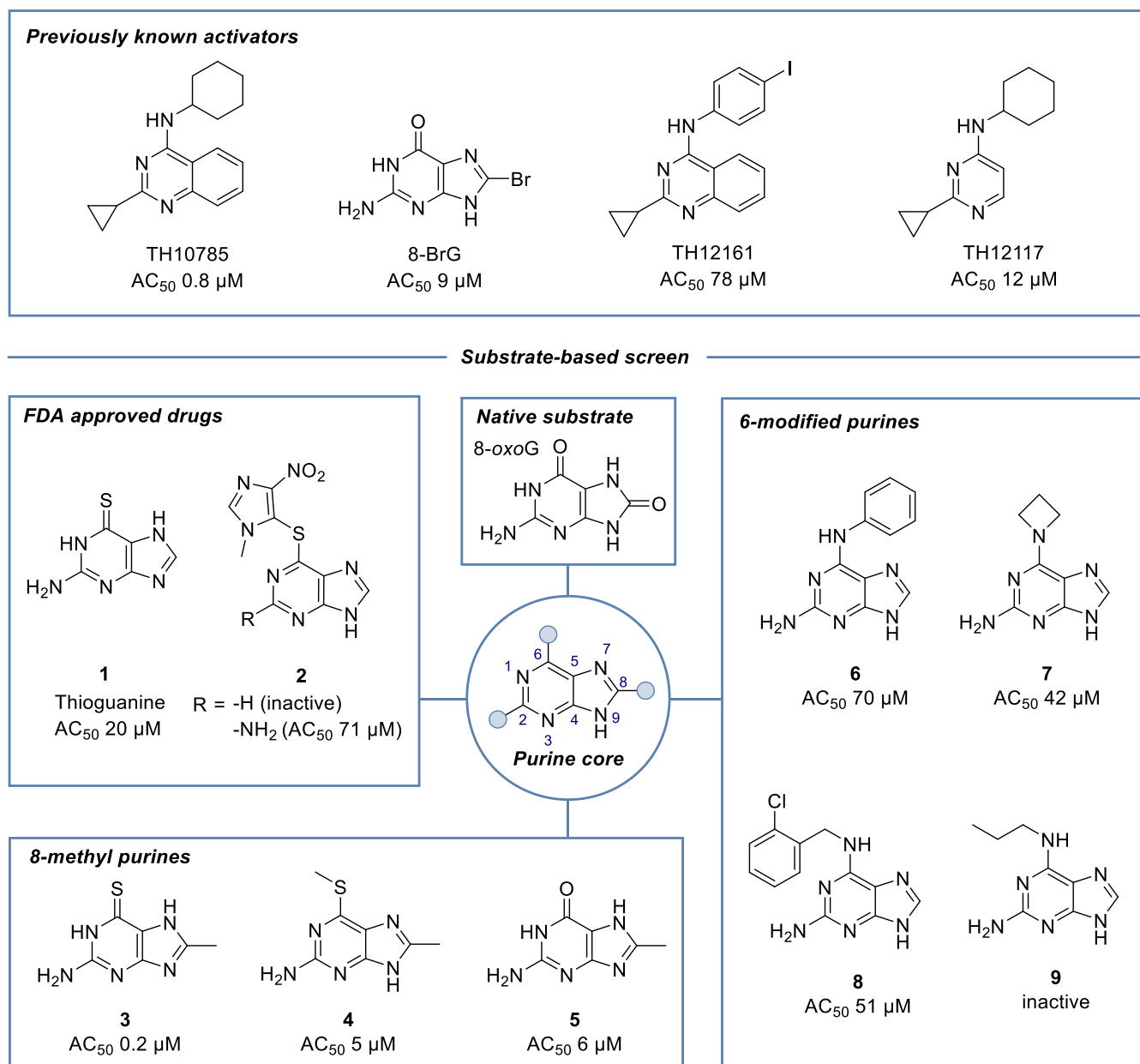


Figure 1: Screening for OGG1 organocatalytic switches based on substrate similarity: A number of OGG1 organocatalytic switches have previously been reported. As an 8-oxoG analogue, 8-bromoguanine is a known OGG1 lyase-activator catalyzing the inherent β -elimination activity of OGG1. Based on substrate similarity, we screened an in-house library of diverse modified nucleobases and discovered 8-methylpurines as potent OGG1 organocatalytic switches (3-5). Additional classes covered thioguanine analogues including FDA-approved drugs (1, 2), as well as 6-amino-substituted guanines (6-9) but not adenines or 9-substituted nucleobases. Assay Details in Materials and Methods.

Results

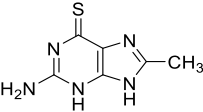
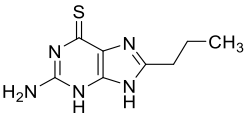
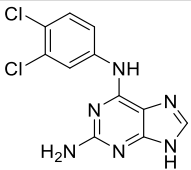
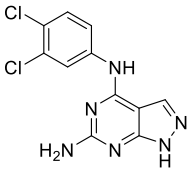
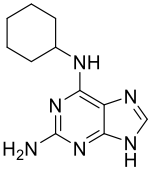
Screening of in-house library

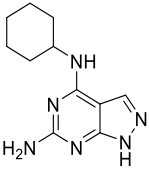
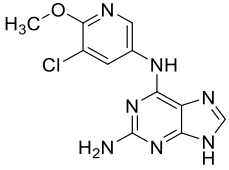
We started by screening a 500-compound in-house library enriched for nucleosides and nucleobases, which was built up from compounds available through the National Cancer Institute's Developmental Therapeutics Platform (NCI DTP). Additionally, we manually added compounds that were synthesized during our campaigns for nucleobase binding proteins, such as the NUDIX proteins and alternative DNA

glycosylases to OGG1.^[19–23] Previously, we have introduced the concentration of half-maximal activation (AC_{50}), which is the activity of 10 nM OGG1 with a given compound concentration that reaches 50% assay turnover compared to 10 nM OGG1 with 2 nM APE1. Consequently, the AC_{50} may be altered depending on assay conditions and the amount of APE1 used. Thus, as a quantitative readout to compare compound activity with APE1 function, we determined AC_{50} for all screened compounds on the substrate 8oxoA:C through kinetic readout instead of a single point read for inhibitors. For details of this screening assay ($Z' = 0.853$), the workflow and data handling, please see Figure S1.^[24]

Among the primary hits were the FDA approved drugs thioguanine **1** and azathioprine **2** (Figure 1, Figure S2), 8-substituted thioguanines **3-5** and compounds combining guanine with amines in the 6-position (**6-9**). Interestingly, a number of 8-monosubstituted guanines, but not adenines, were found to be particularly active. In addition, we found that N9-modified analogues or nucleoside structures, were inactive in the assay, suggesting the necessity of an unsubstituted nitrogen in that position (Figure S2).

Table 1: Optimization towards potent and selective OGG1 organocatalytic switches: Assay Details in Materials and Methods. AC_{50} in μM , CI95 confidence interval 95% in μM ; * compound only reaches AC_{35} due to a bell-shape activity curve.

#	structure	AC_{50} (CI 95) [μM]
3		0.32 (0.27 - 0.39)
10		0.55 (0.26 - 1.20)
11		12.5*
12		13.1 (2.3-75.1)
13		>100

14		11.7 (5.5-24.9)
15		28.2 (10.0-79.8)

Investigation of thioguanine analogues

Based on the promising screening results for the 6-thioguanine chemotype, we initially directed our attention towards hits within this series. First, we confirmed, purity, identity, reordered solid material from NCI DTP and determined AC_{50} . Then we generated a number of analogues of 8-substituted 6-thioguanines with larger substituents (Table 1, Table S1A). Interestingly, only small substituents were tolerated in the 8-position, as observed for compounds **3** and **10**. We observed a decrease in potency upon extension of the synthetic system via propyl (**10**), methylamino (**S25**) and inactivity for a more extended N-Boc substituent (**S26**). Next, we explored the apparent necessity of an unsubstituted 6-thio modification by generating analogues with thioether or sulfone modifications (Table S1B). Again, small substituents such as ethyl (**S28**), iso-propyl (**S29**) and propene (**S31**) gave better results, while extended systems (**S14**, **S15** and **S36-39**) were inactive below 100 μ M. Finally, a combination of small substituents in both the 6-thioether as well as the 8-position failed to further improve the activity of thioguanine based organocatalytic switches of OGG1 (**S33-S35**). These studies suggest a highly specific SAR for thioguanines, allowing only minor modifications to the core system.

Investigation of 6-Amino substituted purines

To follow up on the primary hits with a 6-amino substituted guanine core (Table 1, Table S2), we confirmed identity, reordered solid material from NCI DTP and determined AC_{50} as before. Previously, we had shown that OGG1 inhibitor modifications^[24] combined with the quinazoline core of TH10785 would still yield activating molecules, such as TH12161.^[10] This exercise was performed to show, that the combination of affinity to the target and reactivity on the substrate within one small molecule was both possible and necessary. To build on the screening results for **6-9** and to assess whether these earlier observations could be further corroborated in a scaffold hopping approach, we generated matched pairs of different amines with guanines (Table S2). Using a mix of acidic and alkaline coupling conditions, a number of derivatives were synthesized. As a readout for activity, the biochemical assay was performed which showed that with the exception of **6** and **11**, 6-aniline modified guanine analogues are not significantly activating OGG1 below 100 μ M. Thereby, **11**, bearing a 3,4-dichloro aniline substituent, exhibited a bell-shaped activity curve peaking at a concentration of 12.5 μ M but below an AC_{50} value (AC_{35} , Figure S3). Previously, we observed similar behavior for TH10785 and concluded that this curve reflects a competition with the 8-oxoA substrate in higher concentrations.

Further, we generated matched pair compounds for the some of the thioguanines synthesized previously and observed improved activity of the amine analogues (**S36** vs. **13** and **S38** vs. **6**, Table S2). Given active site binding, this comparison suggested that guanines require a secondary amine, namely an R_1R_2-NH , between the nucleobase core (R_1) and the 6-modification (R_2) to be able to activate OGG1. This apparent requirement for H-donor-bonding in addition to a π -stacking with the bicyclic hetero-aryl system agreed

with the current knowledge or organocatalytic switch binding, requiring both interactions with OGG1 active site amino acids Gly42 and Phe319. In contrast, a panel of additional sp²-richer amines (**S18-20**, **S42** and **S43**) indicated a preference for small substituted tertiary amine rings. Previously, we had observed that the N-methyl versions of TH10785 and TH11735 were still able to induce activation of OGG1, albeit with more modest turnover.^[10] SAR analysis of these compounds highlighted a preference for a secondary amine linker over a tertiary alternative, as observed in TH10785, TH11735, and TH12161.

6-Substituted pyrazolo-[3,4-d]-pyrimidine are organocatalytic switches of OGG1

Having identified the 3,4-dichloroaniline substituent as the most promising modification in **11**, we then investigated the scope of accepted nucleobase analogues and purine scaffolds, replacing guanine with adenine, uracil and other heterocycles (Table S3A). Interestingly, while 9-methylated analogue **S49** and uracil derivative **S48** remained inactive, the 6-amino-pyrazolo-[3,4-d]-pyrimidine derivative **12** surpassed guanine analogue **11** in the biochemical assay, with an AC₅₀ similar to the peak effect of **11**. In addition, 6-unsubstituted pyrazolo-[3,4-d]-pyrimidine **S47** activated OGG1, while adenine analogue **S46** remained inactive. Following this finding, we assembled a number of matched pairs based on previously synthesized 6-aminoaryl-guanines (Table S3B) and observed that all members of the pyrazolo-[3,4-d]-pyrimidine series surpassed the activity of their guanine counterparts (**11** vs. **12**, **13** vs. **14**). These results suggest that previously optimized OGG1 inhibitor chemical space can be utilized to optimize the affinity handle of a series of OGG1 organocatalytic switches.^[24] At the same time, the polar and nitrogen-rich scaffold of nucleobases appears suitable to stimulate proton abstraction during OGG1 catalysis.

Nucleobase based organocatalytic switches increase β -lyase activity of OGG1 depending on pH

To determine whether the synthesized structures were activating a β,δ -elimination in OGG1 similar to previously reported structures TH10785 and analogues,^[10] we first elucidated the exact nature of the observed biochemical activity, *i.e.* β - or β,δ -AP-lyase. Therefore, we orthogonally assessed the reaction of compound and protein on the substrate using a ³²P-radiolabelled substrate (see Materials and Methods) and further resolution of the products by PAGE. Compounds **13** and **3** as members of their respective nucleobase series were evaluated with regard to the products being generated. Depending on their individual potency, both compounds **3** and **13** were confirmed as activators of the inherent β -lyase functionality of OGG1 after 2 and 4 minutes respectively (Figure 2). The corresponding reaction product of β -elimination, 3'-phospho unsaturated aldehyde (3'-PUA), was rapidly formed by OGG1 in the presence of **13** and **3**. This product was also observed with TH10785, although in this case OGG1 rendered an additional band with a higher electrophoretic mobility and corresponding to a β,δ -elimination 3'-P product, as previously reported.^[10] As expected, the phosphatase activity of T4PNK had no effect on the 3'-PUA product common to **3**, **13**, and TH10785 (Figure S4). For TH10785, the enzyme removed the phosphate group from the 3'P product, generating a product with slightly reduced electrophoretic mobility, confirming its identity as the β,δ -elimination product. Extended incubation periods of 30 minutes or longer gave the β,δ -elimination product in the cases of **3** and **13**, possibly through unspecific cleavage since DMSO and the OGG1 inhibitor TH5487 showed a similar response (Figure S4). Although devoid of β,δ -AP-lyase activity, the intensity of the substrate and product bands confirmed **3** was a quantitatively stronger organocatalytic switch than TH10785 and **13**.

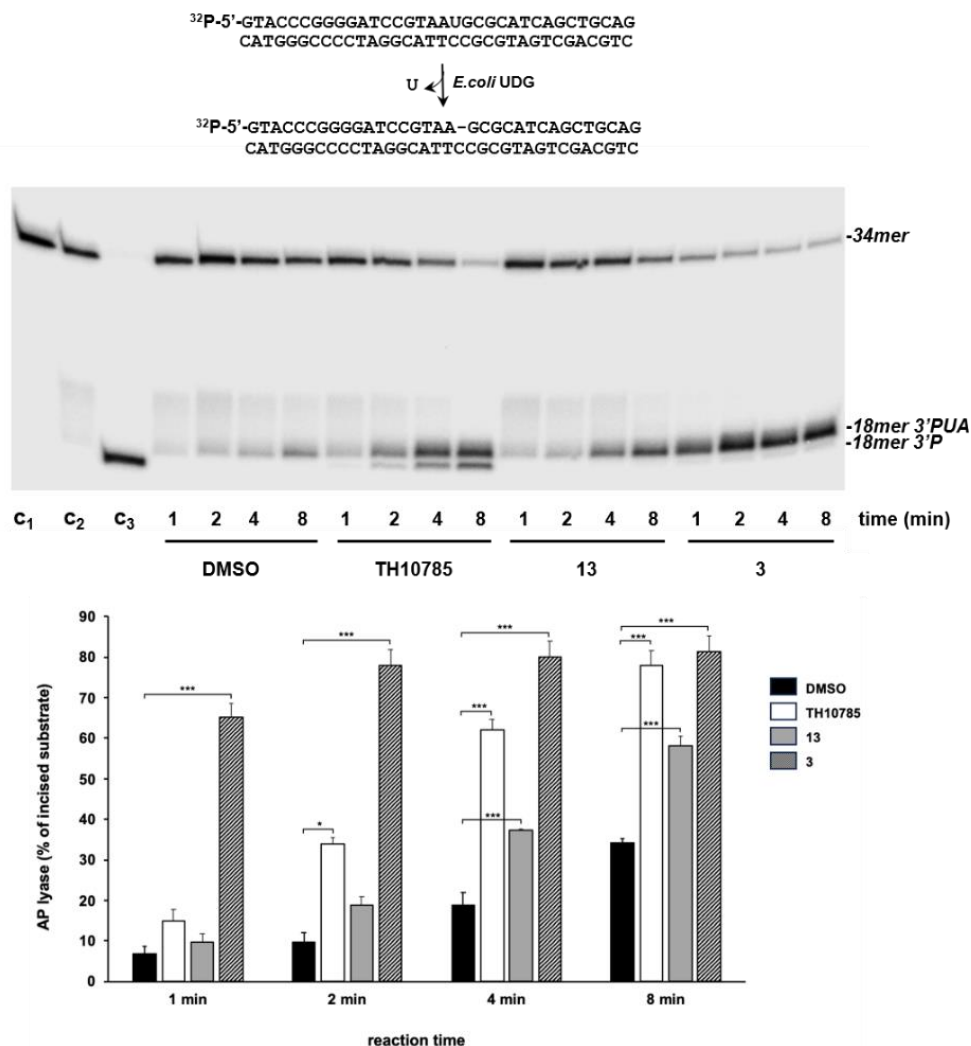


Figure 2: Effect of compounds 3 and 13 on the AP-lyase activity of hOGG1 on 8oxoG:C-containing DNA. Upper panel; the assay was performed using 1 nM of the [³²P]5'-labeled uridin-containing substrate, previously treated with 0.2 U of *E. coli* UDG to obtain a natural AP site, incubated with 10 nM hOGG1, 20 mM EDTA and either 10% DMSO or 6.25 μM TH10785, 20 μM 13 and 20 μM 3. After incubation for the indicated times at 37°C, reactions were stopped and samples further analyzed by 7M urea-20% PAGE and autoradiography. C₁: control of no UDG-treated DNA incubated for 8 min at 37°C; C₂: control of UDG treated DNA incubated for 8 min at 37°C; C₃: alkaline degradation of the UDG treated DNA. Lower panel, bar chart of the AP lyase activity (n=3; means ± SEM). Significance of the results was determined with a two-tailed paired t-test. *P<0.05; P<0.01; ***P<0.001. 3'-PUA – 3' phospho unsaturated aldehyde.

Due to the necessity of employing a nucleophilic lysine residue and cleavage of a Schiff base via proton abstraction, OGG1 functions optimally in a pH close to 8, where both processes are ensured to progress in a reasonable time frame. Since we previously have observed a pH preference for TH10785, all AC₅₀ measurements during screening and optimization were performed at a pH of 7.5. This ensured that compounds were profiled in a way that also included their possible activity in more acidic or more alkaline conditions. Due to this dynamic interplay between OGG1 modulator and enzyme, we next assessed the artificially controlled AP-lyase activity across a pH range of 6.7 to 8.4. For this, we measured the initial rate of the reaction in the fluorescence-based biochemical assay using the 8-oxoA substrate and compounds TH10785, 3 and 14. We chose the most potent concentrations of each compound, according to their activity profile. As indicated in Figure 3, 14 pronounced the already increased OGG1 enzymatic turnover at higher pH close to or over 8. The highest fold increase in function was however observed at

lower pH. Like **3** (5 μ M) and TH10785 (6.25 μ M), **14** (100 μ M) also allowed OGG1 to cleave AP-sites even in a slightly acidic reaction buffer of pH 6.7, installing a de novo function. Interestingly, the effect of **3** was the strongest at low pH. However, **3** exerted less of an effect on OGG1 at higher pH. Finally, TH10785 stimulated OGG1 function the most around a pH of 7.5. A weakened effect was seen for high pH, where OGG1 function was unchanged in the presence of TH10785. These findings pointed towards the presence of a basic nitrogen or a changed protonation state of the enzyme binding site. With respect to the former, the observed activity enhancement was in accordance with the calculated^[25] pKa of the nitrogen bases within the used compounds, TH10785 (1N: 6.55 ± 1.13), **3** (9N: 2.59 ± 2.22) and **59** (9N, 13.53 ± 2.00). Since the AC₅₀ is dependent on pH, compound pKa can have important ramifications on attenuating activity in different biological compartments.

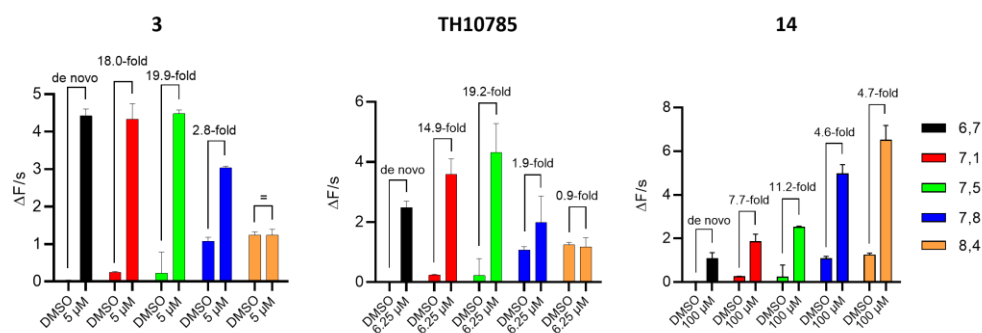


Figure 3: Compound pKa governs pH range of enzymatic activity: left: **3** activates OGG1 at a pH closer to 7 and below; middle: TH10785 follows a bell-shaped curve with a maximum at pH 7.5; right: **14** has a high pKa and thus controls OGG1 function at a pH above 8. 10 nM 8-oxoA was used as substrate and was incubated with 10 nM hOGG1. Compounds were used at most effective concentration as indicated and v_0 was measured within the initial linear slope of the reaction in the fluorescence-quencher assay.

Further investigating the effects of compound binding to OGG1, we assessed protein stability using the melting temperature at different pH and in the presence of the compounds using Nano-DSF (Table S4). The presence of the employed compounds led to a general increase in protein stability, as well as an increase in stability at extreme pH similar to compound pKa, which may partly explain the observed enhancement of enzymatic activity in the biochemical assay through binding of the compounds to OGG1. Lastly, to assess whether proton transfer reactions have an influence on compound activity, we applied D₂O as solvent, investigating a potential solvent isotope effect. Within the fluorescence-based assay we observed challenged incision efficacy evidenced by the slower rate of the reaction compared to conditions using H₂O (Figure S5). The active center nitrogen of the compounds experiences a vivid proton or deuterium exchange in solution. Thus, this result points towards challenged proton abstraction from the α -carbon of the Schiff base intermediate. Altogether, these investigations draw a complex picture of protein stability, compound binding, proton abstraction and transfer, as well as substrate and leaving group solvation during elimination events.

Strongly activated OGG1 cleaves AP-sites opposite all canonical nucleobases

Since OGG1 has a preference for 8-oxoG opposite cytosine,^[26] we hypothesized that a substantially increased AP-lyase function could overwrite this cytosine selectivity. Thus, we performed saturation kinetics with OGG1 against the substrates 8-oxoA:C and AP:A, AP:C, AP:G and AP:T, generated from their respective uracil containing precursors using UNG2. Using **3** and TH10785 to evaluate a potential influence of β - or β,δ -elimination capabilities, we found that both compounds pronounced the inherent preference for cytosine (Figure 4, Figure S6). Further, both compounds exhibited a competition effect for the 8-

oxoA substrate, where higher concentrations lead to reduced rates. This effect was less prominent for AP-site substrates, where the rate is plateauing instead. These observations indicated competition with substrates that require extended active site binding.^[10] In contrast to TH10785, **3** was able to stimulate a significant OGG1 AP-lyase function on all substrates, suggesting that compound potency and not the type of AP-lyase function governs the reaction on AP-sites.

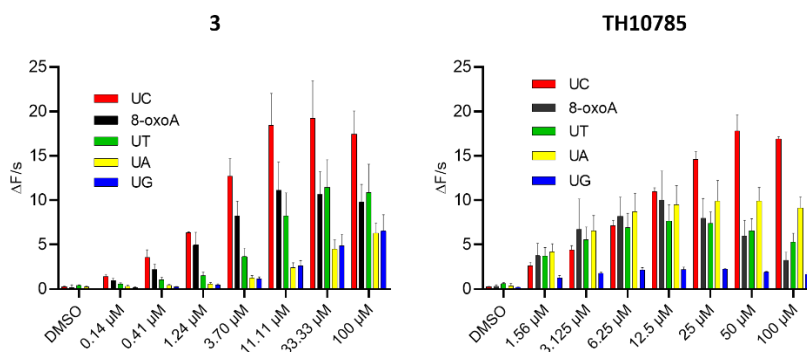


Figure 4: Saturation kinetics for TH10785 and **3 against a number of AP site substrates and 8-oxoA:C:** left: **3** activates OGG1 on AP sites opposite any canonical nucleobase; right: TH10785 activates OGG1 on AP sites in the same manner and no incision dependant efficiency is observed; v_0 of reaction was measured. 10 nM 8-oxo:A was used as substrate and was incubated with 10 nM hOGG1. U:X substrate was used to generate AP sites opposite canonical nucleobases using 1 nM UNG2. v_0 was measured within the initial linear slope of the reaction in the fluorophore-quencher assay. Details in Materials and Methods.

Organocatalytic switches bind the active site of OGG1

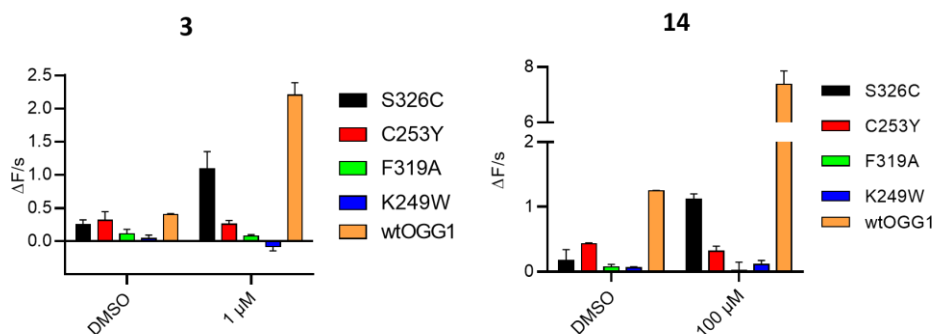


Figure 5: Assessment of OGG1 mutants confirms activation of variants with changes outside but not within the active site: left: **3** and right: **14** are enhancing wtOGG1 and the S326C mutant, but not F319A, C253Y and K249W. 10 nM 8-oxo:A was used as substrate and was incubated with 10 nM hOGG1. Compounds were assayed with the respective mutants and the initial slope was measured in the fluorophore-quencher assay. Assay details in Materials and Methods

To confirm active site binding we evaluated the biochemical activity of **3** and **14** on OGG1 mutant variants in the fluorescence-based assay. While incision through wtOGG1 and Ser326Cys were enhanced, active site mutants Phe319Ala, Cys253Tyr and Lys249Trp were not affected by incubation with the compounds, suggesting that the activity of the compounds is exerted from within the active site (Figure 5). This finding was corroborated by solving the X-ray co-crystal structures of mouse OGG1 in complex with **3**, **10**, **14** and **15** confirming active site binding (Figure 6A-D, Figure S7). The binding poses of compounds **14** and **15**, interacting both with Phe319 and Gly42, confirmed the selectivity observed within the structure activity relationship. An overlay with the 8-oxoG-bound human OGG1 (PDB ID: 1HU0)^[11] indicated no

significant rearrangements in the core protein structure for all structures solved. Identical placement of **3**, **10** and 8-oxoG (Figure 6C and D, Figure S7) suggests a binding mode that allows for enhanced product-assisted like catalysis. The heterocyclic ring systems of **14** and **15** are observed to be shifted outwards due to their more spacious 6-amino substitution and are also flipped compared to one another, which may explain the lower activity observed for this series in all assays (Figure S7).

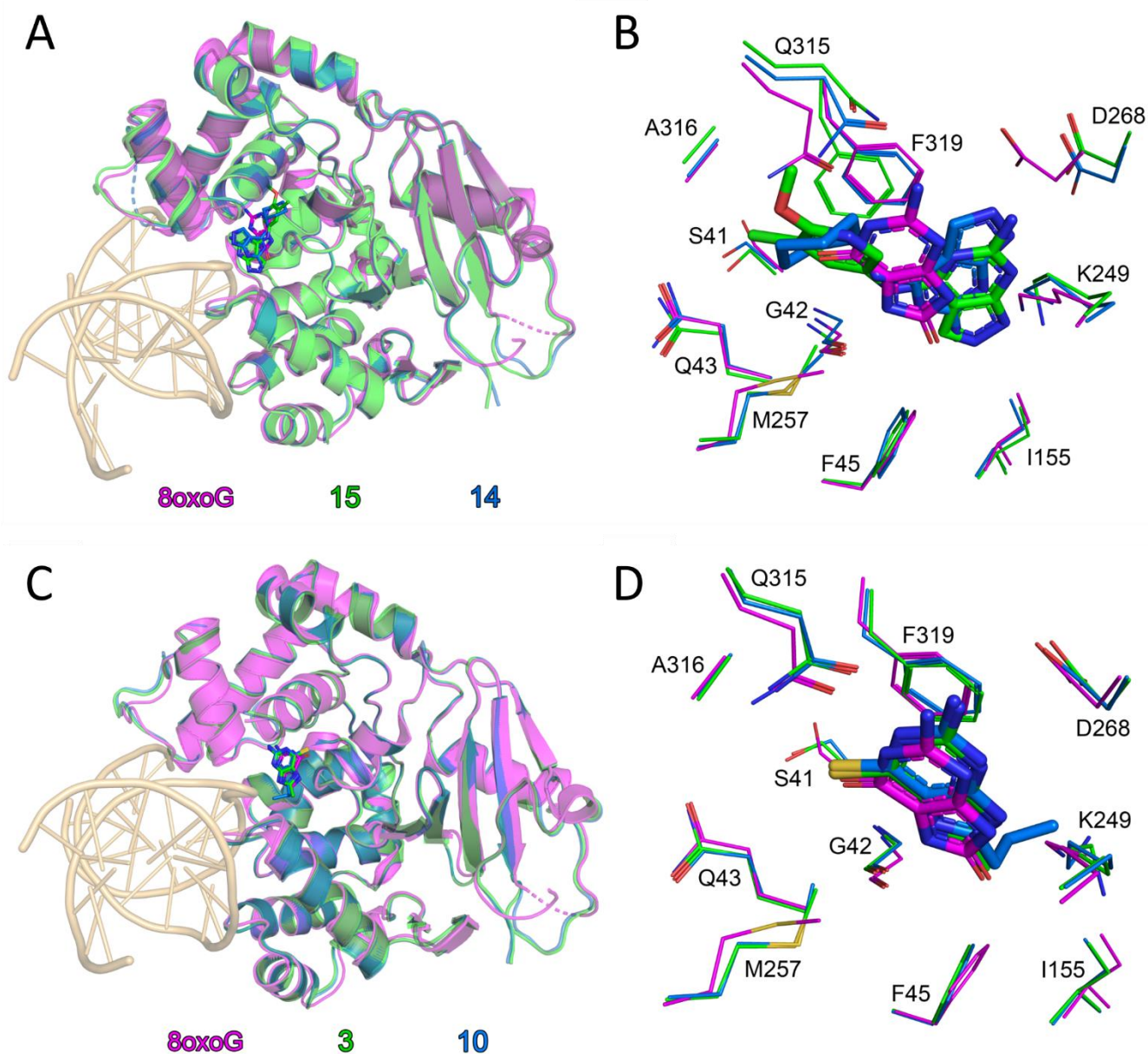


Figure 6: Organocatalytic switches bind the active site of OGG1 and closely overlap with 8-oxoG position: A) Superposition of mouse OGG1 bound **15** (green) and mouse OGG1 bound **14** (blue) and human OGG1 bound DNA-8-oxoG (magenta, PDB ID: 1HU0) monomers. DNA from the 8-oxoG complex is coloured light orange. Ligands are depicted as sticks; C atoms are coloured green (**15**), blue (**14**) or magenta (8-oxoG), O atoms red, and N atoms dark blue; **B)** Close up comparison of ligand binding between the structures in A). Amino acids which contribute to ligand positioning are depicted as thin sticks; **C)** Superposition of mouse OGG1 bound **3** (green) and mouse OGG1 bound **10** (blue) and human OGG1 bound DNA-8-oxoG (magenta, PDB ID: 1HU0) monomers. DNA from the 8-oxoG complex is coloured light orange. Ligands are depicted as sticks; C atoms are coloured green (**3**), blue (**10**) or magenta (8-oxoG), O atoms red, N

atoms dark blue and S atoms gold; **D**) Close up comparison of ligand binding between the structures in C). Amino acids which contribute to ligand positioning are depicted as thin sticks;

Organocatalytic switches are selective, non-toxic and stimulate the repair of AP sites in cells

To rule out any unwanted effects of the molecules regarding potential toxicity or off-target effects, we extensively profiled TH10785, **3** and **14** using an in-house functional panel of enzymes consisting of DNA glycosylases,^[20] NUDIX family members^[19,27] and a set of protein kinases which was probed using thermal stability.^[28] Limited inhibition below 50% was observed within the family of DNA glycosylase at 100 μ M, indicating over 100-fold selectivity for **3** and TH10785. All other tests returned negative for off-targets (Table S6-7, Figure S8-S9).

Further, considering that thioguanines are approved cytotoxic drugs we sought to exclude an effect on cell viability. Cultivation of an immortalized cell line, BJ-TERT, and an oncogene driven cell line, BJ-Ras,^[22,29] over several days in the presence of a dose response of the compounds confirmed the absence of any toxicity between these two cell lines (Table S8).

Using the selective and non-cytotoxic scaffolds, we investigated whether either of the OGG1 functions was indeed improved in a cellular setting. Determining thermal stabilization using DSF revealed that **10** (1.5 K) and **14** (0.5 K) stabilized OGG1 more than **3** (0.5 K) and **13** (0.1 K). Thus, we applied **10** and **14** moving forward and induced DNA damage using KBrO₃ and profiled 8-oxoG, AP sites and γ H2AX. As before, we observed increased levels of nuclear 8-oxoG over 6 hours post exposure (Figure 7A). This effect was rescued by OGG1 organocatalytic switches. The cellular efficacy thereby followed the biochemical activity for organocatalytic switches of the β -elimination, as **10** was superior to **14**, with TH10785 being most efficient as a stimulator of β,δ -elimination. This indeed indicated an increased cellular repair of 8-oxoG lesions in DNA, possibly through more free protein after accelerated repair.^[10] However, considering that the compounds redirect OGG1 function towards resolving AP sites, we expected a more pronounced effect for analogues **10** and **14** when assessing the levels of this particular type of DNA damage. Using the aldehyde reactive probe^[30] and fluorescence-activated cell sorting we indeed observed reduced numbers of AP sites for compound **10**, performing at the level of TH10785 (Figure 7B). **14** was found to be inactive at these concentrations, indicating a suboptimal concentration in relation to its biochemical activity. Lastly, γ H2AX levels were unaltered when using the different compounds (Figure S10), indicating sustainable DNA repair upon faster initiation of base excision repair. Collectively, these studies confirm enhanced, compound-mediated OGG1 activity in canonical repair of oxidative DNA damage *in vitro* and in cells. The effects observed suggest OGG1 being rendered an AP-lyase in presence of potent organocatalytic switches.

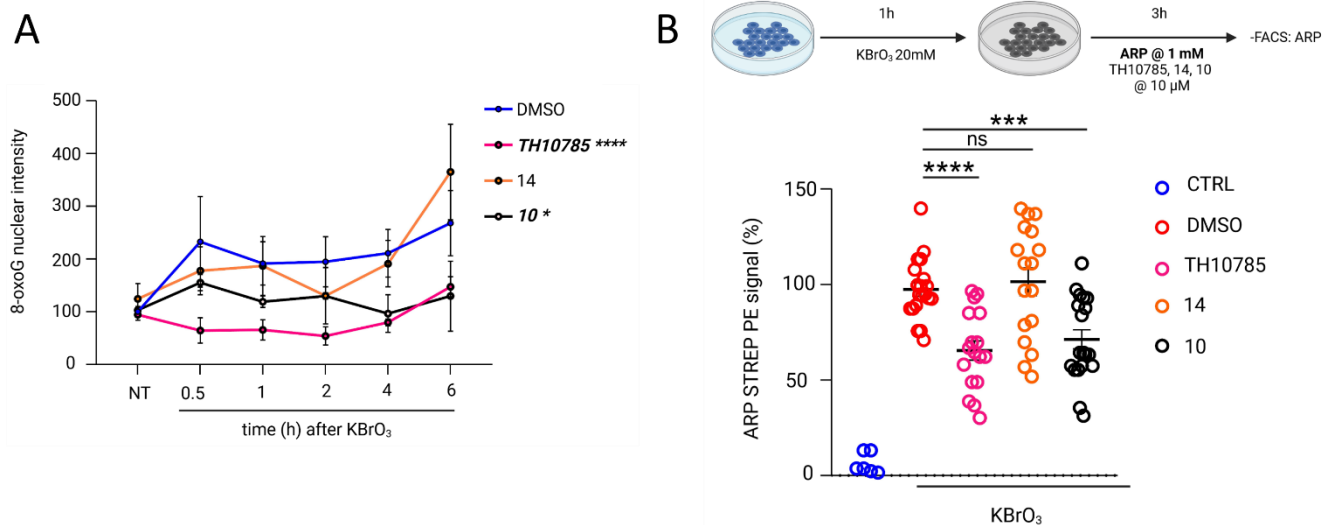


Figure 7: Organocatalytic switches stimulate removal of 8-oxoG and AP sites: A) Effect for compounds TH10785, **14** and **10** at 10 μ M in cells. Quantification of nuclear 8-oxoG levels across different time points in U2OS cells exposed to organocatalytic switches or DMSO, under oxidative stress conditions (20mM of KBrO₃ for 1h). Each bar represents the mean \pm SEM. Data are the average of three independent experiments. For each experiment, 25 fields and around 1000 cells were captured per condition. Statistical significance was calculated using two-way ANOVA for multiple comparisons. ns, non-significant; *P < 0.05; ****P < 0.0001; **B)** A comparative analysis of ARP-STREP_PE signal induction over DMSO, reported in percentage, is shown for compounds TH10785, **14** and **10** at 10 μ M. Each bar represents the mean \pm SD. Data are the average of five independent experiments with at least three biological replicates each. Statistical significance was calculated using an unpaired two-tailed Student's t-test. ns, non-significant; ***P < 0.001; ****P < 0.0001.

Discussion

Removal of 8-oxoG from DNA is necessary to maintain cellular health and genomic integrity. At the same time, the presence of 8-oxoG is crucial to recruit repair enzymes and transcription factors to remodel cellular responses in inflammation,^[31,32] after physical activity and in human disease.^[33,34] Both scenarios benefit from a tight control of human base excision repair, in which OGG1 recognizes and removes 8-oxoG as the initiating enzyme. While bifunctional enzymes with similar substrate scope exist in lower organisms,^[35] OGG1 appears to have lost a robust AP lyase function which cleaves the reaction product, an AP site. Whether this occurred as a result of an evolutionary advantage has not been thoroughly investigated. However, literature indicates that an AP lyase function is at the center of transcriptional processes, since both OGG1 and the succeeding enzyme APE1 are implicated in the recruitment of transcription factors to regions of the genome rich in potential substrates.^[16,36]

Still, APE1 is recruited to relieve OGG1 from the AP site. Due to the required unbinding of the AP site from OGG1, rebinding of APE1 and incision through APE1, significant rearrangements are accomplished within the repair complex. Furthermore, when bound to an AP site via a reversible Schiff Base, OGG1 remains unavailable for additional excision events. In scenarios, such as neurodegenerative and cardiometabolic diseases as well as rapid aging, this delay of repair may cause an accumulation of 8-oxoG as well as AP sites. Mutations and excessive DNA damage may be the result, threatening genomic integrity. Thus, improving OGG1 function by enhancing a weak AP lyase activity has recently gained traction with first applications in patient-derived models of liver fibrosis.^[37]

The discovery of TH10785, an organocatalytic switch, has been reported that improves AP site cleavage of OGG1 in the presence of APE1.^[10] The small molecule binds the active site and removes an activated proton from the Schiff Base intermediate. This effectively shapes an β,δ -elimination reaction that resembles the AP lyase function of DNA glycosylases from lower organisms, such as Fpg from bacteria.^[35]

At the same time, human base excision repair has evolved to accomplish DNA end cleansing depending on the elimination reaction that was performed. β -eliminations generate a 3'-PUA which is still a substrate of APE1. β,δ -eliminations, however, require PNKP1 before the reaction product converges again with the stream resulting from β -elimination. Thus, TH10785 rewires the initiation of base excision repair to become independent of APE1 and to rely on PNKP1 instead.

OGG1 can employ the excised 8-oxoG for a weak β -elimination and we have shown that 8-bromo guanine indeed activates this reaction further. Thus, we hypothesized that complex nucleobase space may present more potent analogues to significantly enhance APE1 dependent repair of 8-oxoG and AP site. We then profiled the nucleobase chemical space for organocatalytic switches of OGG1 using a fluorophore-quencher assay and discovered two distinct selective chemical series, including 6-thioguanines and 6-aminoguanines. An early indication of active site binding was observed in the inactivity of 9-substituted analogues during the screen. Assuming an orientation similar to 8-oxoG during catalysis, these analogues would not be able to abstract protons from the intermediate Schiff Base.

Investigation of the structure activity relationship revealed that 6-thioguanine tolerated only minor groups in the 8-position, with an AC₅₀ of up to 0.32 μ M. 6-aminoguanine derivatives on the other hand were optimized to bear 3,4-dichloroaniline substituents, reaching moderate μ M activity. Finally, investigating the space of alternative scaffolds we observed that members of a pyrazolo-[3,4-*d*]-pyrimidine series surpassed the activity of the corresponding guanine series.

Assessment in the fluorophore-quencher assay allowed to compare compounds to a pathway stimulated by APE1, but does not provide the identity of the reaction product. We then used a ³²P-labelled DNA substrate and resolved the reaction of OGG1 with **3**, **13** and TH10785 by PAGE. As before TH10785 induced β,δ -elimination while **3** and **13** catalyzed an β -elimination according to their previously established AC₅₀. This confirmed the earlier observation of Fromme *et al.* that guanine analogues are assisting in catalysis driven by product-alike properties.

However, since proton abstraction and the lysine attack are both processes that thrive in more basic conditions, we hypothesized that compound pKa and pH environment play a role in OGG1 activity. Indeed, we observed that compounds **3**, **14** and TH10785 are more potent in catalyzing reactions that are closer to their individual pKa. **3** promoted an AP lyase activity in slightly acidic conditions, while **14** was more active at higher pH over 8. As observed earlier, TH10785 performed best around pH 7.5. Since, a number of processes during Glycosylase and AP lyase function require proton abstraction, we investigated protein stabilization by the compounds as well as a solvent effect using D₂O as solvent. While stabilization was indeed pH dependent and followed the general trend of compound pKa, the use of D₂O indicated significant slower incision events in the fluorophore-quencher assay. The question of whether pKa is the driver of the elimination reaction or favors protein-Schiff Base binding remains elusive. Given, that all structures used in this study bear multiple nitrogen atoms with a variety of pKa, we see the need to identify a minimum structure of organocatalytic switches. Modulating the pKa of a minimalist structure would then allow to assess whether active nitrogen pKa is an additional descriptor for the development of organocatalytic switches.

Another evolutionary selection that OGG1 underwent, is the selectivity for an 8-oxoG:cytosine pair as opposed to for example the selectivity of MUTYH for 8-oxoG:adenine. With the AP lyase activity stimulated, we thus asked the question whether OGG1 continues to discriminate against the other canonical nucleobases. Generating AP sites opposite adenine, cytosine, guanine and thymine and assessing the burst phase of the reaction of OGG1 with **3** and TH10785, we observed a continued selectivity for cytosine independent of incision mode. Still, incision events were markedly stimulated for all substrates used, enabling cleavage of all AP sites in double stranded DNA.

In an attempt to rationalize the observed SAR, we then assessed key molecules in the catalysis of OGG1 mutants. As before,^[10] we only saw a stimulation of mutants outside of the active site. This confirmed an

orthosteric binding of the small molecules, the exact orientation of which was further elucidated using co-crystal structures. All four obtained co-crystal structures confirmed the established SAR, with the small molecules engaging key amino acid residues Gly42 and Phe319. Especially, the thioguanine series showed excellent similarity to the placement of 8-oxoG during catalysis.

These properties prompted us to evaluate the effects of the compounds in cells. Since OGG1 is able to incise AP sites in the presence of organocatalytic switches as a new substrate in addition to the removal of 8-oxoG, we set out to assess the levels of both substrates after a burst in oxidative DNA damage. We determined the levels of 8-oxoG and AP sites using immunofluorescence using an anti-8-oxoG-antibody and quantification of AP sites through an aldehyde reactive probe and FACS, respectively. As a proxy of target engagement, we used DSF to prioritize one compound per series, *i.e.* **10** and **14**. We observed both reduced levels of 8-oxoG and AP sites using compound **10** confirming an acceleration of initiation of base excision repair. No such effect was observed for **14**, which was likely connected to the fact that the concentration used is close to the compounds AC₅₀. In addition, it may be possible that compounds are less active in certain cellular environments, depending on their individual pK_a. Future research will need to address the possibility with a chemical series, that allows for robust pK_a modulation, as mentioned above.

The presented molecules activate the canonical but rudimentary β -elimination activity of OGG1 from within the active site of the protein. Active site affinity and a reactive center in the form of a basic nitrogen are combined in one molecule, as evidenced by studies involving OGG1 mutants, substrate scope, generated products and enzymatic activity covering a range of pH environments. Co-crystal structures of a number of analogues further confirm the product-assisted hypothesis of Fromme *et al.* and paint a detailed picture of functional enhancement of enzymatic activity on Schiff bases.

In conclusion, we demonstrate that a chemical space beyond TH10785 exists, that increases the repair of OGG1. Importantly, we show that these OGG1 organocatalytic switches may act through a distinct mechanism of action and in contrast to TH10785 primarily stimulate the β -elimination during OGG1 catalysis. OGG1 organocatalytic switches are the first chemical entities that rewrite an enzymatic function in cells by partaking in the biochemical reaction, allowing for increased DNA damage repair. Considering the widespread implications of OGG1 function within a number of diseases, including neurodegeneration,^[1,2] obesity^[3,4] and inflammation,^[7,31] these small molecules are novel, powerful tools to unravel disease biology, and offer the potential for further development into promising drug candidates.^[37]

AUTHOR INFORMATION

Corresponding Author

* Maurice Michel: maurice.michel@ki.se

Science for Life Laboratory, Department of Oncology and Pathology, Karolinska Institutet and Center for Molecular Medicine, Karolinska Institutet and Karolinska Hospital.

Author Contributions

Chemical synthesis: ECH, NDDE, OW, FO, AD, MEA, KN, MV, JS, MK and MM. Biochemistry: ECH, NDDE, LM, AdP, PC, KZ, EW, AK, HD, ASJ, MdV and MM. Structural Biology: ERS, SK and PS. Computational Chemistry: EJH, NDDE and MM. Cell Biology: CBB, IA, ML and MM. Supervision: OW, ASJ, MS, PS, MdV, SKn, LS, TH and MM. Resources: TH, PS, MdV, CBB, LS, SKn and MM. Writing and Editing: ECH, NDDE, OW and MM. Conceptualization: ECH, NDDE and MM.

ACKNOWLEDGMENTS

We would like to thank the Chemical Biology Consortium Sweden (CBCS), the Protein science facility (PSF) at Karolinska and the Structural Genomics Consortium (SGC) at Karolinska and Goethe-Universität Frankfurt for support. We are thankful to Athina Pliakou, Mari Kullman Magnusson, Kristina Edfeldt, Therese Pham and Michael Sundström for administrative support. We thank MAXIV Laboratory (Sweden, proposal MX20200204), Diamond Light Source (United Kingdom, proposals MX15806 and MX21625), and their scientists from the BioMAX and I03 beamlines for their support during data collection.

FUNDING

This work was funded by the Swedish Research Council (2018–03406 PS), the Alfred Österlund foundation (PS), the Crafoord foundation (20190532 PS), the Helleday Foundation (FO, LM), the Swedish Cancer Society (CAN2021/1490 TH), the Åke-Olsson foundation for haematological research (2020-00306 MM), a Novo Nordisk Pioneer Innovator Grant (NNF23OC0085944 MM), Karolinska Institutet Research Foundation Grants (2020-02186 and 2022-01776 MM), a Childhood Cancer Research Postdoctoral grant (ML), the Åke Wiberg Foundation (M23-0043 MM), Grant PID2020-115978GB-I00 (MdV) funded by MCIN/AEI/10.13039/501100011033, a Health Research Fund, Carlos III Health Institute, co-funded by European Regional Development (FEDER) funds (PI20-00335 LSG) and the Research Talent Attraction Grants (2023-T1/SAL-GL-29292 CBB). This project has received funding from the Innovative Medicines Initiative 2 Joint Undertaking (JU) under grant agreement No 875510 (MM, EJH, EW, IA, ASJ, AK, SKn, FO, KZ, MK, NDE). The JU receives support from the European Union's Horizon 2020 research and innovation programme and EFPIA and Ontario Institute for Cancer Research, Royal Institution for the Advancement of Learning McGill University, Kungliga Tekniska Högskolan, Diamond Light Source Limited. This communication reflects the views of the authors and the JU is not liable for any use that may be made of the information contained herein.

CONFLICT OF INTEREST

OW and TH are listed as inventors on a U.S. patent no. WO2019166639 A1, covering OGG1 inhibitors. The patent is fully owned by a non-profit public foundation, the Helleday Foundation, and TH is a member of the foundation board. MS is an employee of Oxcia, a company developing OGG1 inhibitors. EW, OW, EJH, IA, ASJ, TH and MS are shareholders of Oxcia. The remaining authors declare no competing financial interests.

REFERENCES

- [1] S. Oka, J. Leon, K. Sakumi, N. Abolhassani, Z. Sheng, D. Tsuchimoto, F. M. LaFerla, Y. Nakabeppu, *Scientific Reports* **2021**, *11*, 5819.
- [2] J. Fukae, M. Takanashi, S. Kubo, K. Nishioka, Y. Nakabeppu, H. Mori, Y. Mizuno, N. Hattori, *Acta Neuropathol.* **2005**, *109*, 256–262.
- [3] S. S. B. Komakula, J. Tumova, D. Kumaraswamy, N. Burchat, V. Vartanian, H. Ye, A. Dobrzyn, R. S. Lloyd, H. Sampath, *Sci Rep* **2018**, *8*, 14886.
- [4] H. Sampath, V. Vartanian, M. R. Rollins, K. Sakumi, Y. Nakabeppu, R. S. Lloyd, *PLOS ONE* **2012**, *7*, e51697.
- [5] J. M. Baquero, C. Benítez-Buelga, V. Rajagopal, Z. Zhenjun, R. Torres-Ruiz, S. Müller, B. M. F. Hanna, O. Loseva, O. Wallner, M. Michel, S. Rodríguez-Perales, H. Gad, T. Visnes, T. Helleday, J. Benítez, A. Osorio, *Scientific Reports* **2021**, *11*, 3490.

- [6] T. Visnes, C. Benítez-Buelga, A. Cázares-Körner, K. Sanjiv, B. M. F. Hanna, O. Mortusewicz, V. Rajagopal, J. J. Albers, D. W. Hagey, T. Bekkhus, S. Eshtad, J. M. Baquero, G. Masuyer, O. Wallner, S. Müller, T. Pham, C. Göktürk, A. Rasti, S. Suman, R. Torres-Ruiz, A. Sarno, E. Wiita, E. J. Homan, S. Karsten, K. Marimuthu, M. Michel, T. Koolmeister, M. Scobie, O. Loseva, I. Almlöf, J. E. Unterlass, A. Pettke, J. Boström, M. Pandey, H. Gad, P. Herr, A.-S. Jemth, S. El Andaloussi, C. Kalderén, S. Rodriguez-Perales, J. Benítez, H. E. Krokan, M. Altun, P. Stenmark, U. W. Berglund, T. Helleday, *Nucleic Acids Research* **2020**, *48*, 12234–12251.
- [7] M. Hussain, X. Chu, B. Duan Sahbaz, S. Gray, K. Pekhale, J.-H. Park, D. L. Croteau, V. A. Bohr, *Free Radic Biol Med* **2023**, *203*, 34–44.
- [8] B. A. Baptiste, S. R. Katchur, E. M. Fivenson, D. L. Croteau, W. L. Rumsey, V. A. Bohr, *Free Radical Biology and Medicine* **2018**, *124*, 149–162.
- [9] G. Tian, S. R. Katchur, Y. Jiang, J. Briand, M. Schaber, C. Kretsoulas, B. Schwartz, S. Thrall, A. M. Davis, S. Duvall, B. A. Kaufman, W. L. Rumsey, *Sci Rep* **2022**, *12*, 14685.
- [10] M. Michel, C. Benítez-Buelga, P. A. Calvo, B. M. F. Hanna, O. Mortusewicz, G. Masuyer, J. Davies, O. Wallner, K. Sanjiv, J. J. Albers, S. Castañeda-Zegarra, A.-S. Jemth, T. Visnes, A. Sastre-Perona, A. N. Danda, E. J. Homan, K. Marimuthu, Z. Zhenjun, C. N. Chi, A. Sarno, E. Wiita, C. von Nicolai, A. J. Komor, V. Rajagopal, S. Müller, E. C. Hank, M. Varga, E. R. Scaletti, M. Pandey, S. Karsten, H. Haslene-Hox, S. Loevenich, P. Marttila, A. Rasti, K. Mamonov, F. Ortis, F. Schömberg, O. Loseva, J. Stewart, N. D'Arcy-Evans, T. Koolmeister, M. Henriksson, D. Michel, A. de Ory, L. Acero, O. Calvete, M. Scobie, C. Hertweck, I. Vilotijevic, C. Kalderén, A. Osorio, R. Perona, A. Stolz, P. Stenmark, U. W. Berglund, M. de Vega, T. Helleday, *Science* **2022**, *376*, 1471–1476.
- [11] J. C. Fromme, S. D. Bruner, W. Yang, M. Karplus, G. L. Verdine, *Nat Struct Mol Biol* **2003**, *10*, 204–211.
- [12] B. Dalhus, M. Forsbring, I. H. Helle, E. S. Vik, R. J. Forstrøm, P. H. Backe, I. Alseth, M. Bjørås, *Structure* **2011**, *19*, 117–127.
- [13] T. Visnes, M. Grube, B. M. Fekry Hanna, C. Benitez-Buelga, A. Cázares-Körner, T. Helleday, *DNA Repair* **2018**, DOI 10.1016/j.dnarep.2018.08.015.
- [14] J. W. Hill, T. K. Hazra, T. Izumi, S. Mitra, *Nucleic Acids Res* **2001**, *29*, 430–438.
- [15] V. S. Sidorenko, G. A. Nevinsky, D. O. Zharkov, *DNA Repair* **2007**, *6*, 317–328.
- [16] H. Sampath, R. S. Lloyd, *DNA Repair* **2019**, *81*, 102667.
- [17] C. Benítez-Buelga, T. Helleday, M. Michel, *Clinical and Translational Medicine* **2022**, *12*, e1035.
- [18] H. E. Krokan, M. Bjørås, *Cold Spring Harb Perspect Biol* **2013**, *5*, a012583.
- [19] M. Michel, E. J. Homan, E. Wiita, K. Pedersen, I. Almlöf, A.-L. Gustavsson, T. Lundbäck, T. Helleday, U. Warpman Berglund, *Front. Chem.* **2020**, *8*, DOI 10.3389/fchem.2020.00443.
- [20] M. Michel, T. Visnes, E. J. Homan, B. Seashore-Ludlow, M. Hedenström, E. Wiita, K. Vallin, C. B. J. Paulin, J. Zhang, O. Wallner, M. Scobie, A. Schmidt, A. Jenmalm-Jensen, U. Warpman Berglund, T. Helleday, *ACS Omega* **2019**, *4*, 11642–11656.
- [21] B. D. G. Page, N. C. K. Valerie, R. H. G. Wright, O. Wallner, R. Isaksson, M. Carter, S. G. Rudd, O. Loseva, A.-S. Jemth, I. Almlöf, J. Font-Mateu, S. Llona-Minguez, P. Baranczewski, F. Jeppsson, E. Homan, H. Almqvist, H. Axelsson, S. Regmi, A.-L. Gustavsson, T. Lundbäck, M. Scobie, K. Strömberg, P. Stenmark, M. Beato, T. Helleday, *Nature Communications* **2018**, *9*, 250.
- [22] H. Gad, T. Koolmeister, A.-S. Jemth, S. Eshtad, S. A. Jacques, C. E. Ström, L. M. Svensson, N. Schultz, T. Lundbäck, B. O. Einarsdottir, A. Saleh, C. Göktürk, P. Baranczewski, R. Svensson, R. P.-A. Berntsson, R. Gustafsson, K. Strömberg, K. Sanjiv, M.-C. Jacques-Cordonnier, M. Desroses, A.-L. Gustavsson, R. Olofsson, F. Johansson, E. J. Homan, O. Loseva, L. Bräutigam, L. Johansson, A. Höglund, A. Hagenkort, T. Pham, M. Altun, F. Z. Gaugaz, S. Vikingsson, B. Evers, M. Henriks-son, K. S. A. Vallin, O. A. Wallner, L. G. J. Hammarström, E. Wiita, I. Almlöf, C. Kalderén, H. Axelsson, T. Djureinovic, J. C. Puigvert, M. Häggblad, F. Jeppsson, U. Martens, C. Lundin, B.

- Lundgren, I. Granelli, A. J. Jensen, P. Artursson, J. A. Nilsson, P. Stenmark, M. Scobie, U. W. Berglund, T. Helleday, *Nature* **2014**, *508*, 215–221.
- [23] S. M. Zhang, M. Desroses, A. Hagenkört, N. C. K. Valerie, D. Rehling, M. Carter, O. Wallner, T. Koolmeister, A. Throup, A.-S. Jemth, I. Almlöf, O. Loseva, T. Lundbäck, H. Axelsson, S. Regmi, A. Sarno, A. Krämer, L. Pudielko, L. Bräutigam, A. Rasti, M. Göttmann, E. Wiita, J. Kutzner, T. Schaller, C. Kalderén, A. Cázares-Körner, B. D. G. Page, R. Krimpenfort, S. Eshtad, M. Altun, S. G. Rudd, S. Knapp, M. Scobie, E. J. Homan, U. W. Berglund, P. Stenmark, T. Helleday, *Nat Chem Biol* **2020**, *16*, 1120–1128.
- [24] O. Wallner, A. Cázares-Körner, E. R. Scaletti, G. Masuyer, T. Bekkhus, T. Visnes, K. Mamonov, F. Ortis, T. Lundbäck, M. Volkova, T. Koolmeister, E. Wiita, O. Loseva, M. Pandey, E. Homan, C. Benítez-Buelga, J. Davies, M. Scobie, U. W. Berglund, C. Kalderén, P. Stenmark, T. Helleday, M. Michel, *ChemMedChem* **n.d.**, *n/a*, DOI 10.1002/cmcd.202200310.
- [25] A. D. Bochevarov, E. Harder, T. F. Hughes, J. R. Greenwood, D. A. Braden, D. M. Philipp, D. Rinaldo, M. D. Halls, J. Zhang, R. A. Friesner, *International Journal of Quantum Chemistry* **2013**, *113*, 2110–2142.
- [26] S. D. Bruner, D. P. Norman, G. L. Verdine, *Nature* **2000**, *403*, 859–866.
- [27] J. Carreras-Puigvert, M. Zitnik, A.-S. Jemth, M. Carter, J. E. Unterlass, B. Hallström, O. Loseva, Z. Karem, J. M. Calderón-Montaño, C. Lindskog, P.-H. Edqvist, D. J. Matuszewski, H. A. Blal, R. P. A. Berntsson, M. Häggblad, U. Martens, M. Studham, B. Lundgren, C. Wählby, E. L. L. Sonnhammer, E. Lundberg, P. Stenmark, B. Zupan, T. Helleday, *Nature Communications* **2017**, *8*, 1541.
- [28] O. Fedorov, F. H. Niesen, S. Knapp, *Methods Mol Biol* **2012**, *795*, 109–118.
- [29] K. V. M. Huber, E. Salah, B. Radic, M. Gridling, J. M. Elkins, A. Stukalov, A.-S. Jemth, C. Göktürk, K. Sanjiv, K. Strömberg, T. Pham, U. W. Berglund, J. Colinge, K. L. Bennett, J. I. Loizou, T. Helleday, S. Knapp, G. Superti-Furga, *Nature* **2014**, *508*, 222–227.
- [30] K. Kubo, H. Ide, S. S. Wallace, Y. W. Kow, *Biochemistry* **1992**, *31*, 3703–3708.
- [31] T. Visnes, A. Cázares-Körner, W. Hao, O. Wallner, G. Masuyer, O. Loseva, O. Mortusewicz, E. Wiita, A. Sarno, A. Manoilov, J. Astorga-Wells, A.-S. Jemth, L. Pan, K. Sanjiv, S. Karsten, C. Gokturk, M. Grube, E. J. Homan, B. M. F. Hanna, C. B. J. Paulin, T. Pham, A. Rasti, U. W. Berglund, C. von Nicolai, C. Benitez-Buelga, T. Koolmeister, D. Ivanic, P. Iliev, M. Scobie, H. E. Krokan, P. Baranczewski, P. Artursson, M. Altun, A. J. Jensen, C. Kalderén, X. Ba, R. A. Zubarev, P. Stenmark, I. Boldogh, T. Helleday, *Science* **2018**, *362*, 834–839.
- [32] X. Ba, A. Bacsi, J. Luo, L. Aguilera-Aguirre, X. Zeng, Z. Radak, A. R. Brasier, I. Boldogh, *The Journal of Immunology* **2014**, *192*, 2384–2394.
- [33] K. Foote, M. Rienks, L. Schmidt, K. Theofilatos, Yasmin, M. Ozols, A. Eckersley, A. Shah, N. Figg, A. Finigan, K. O’Shaughnessy, I. Wilkinson, M. Mayr, M. Bennett, *Cardiovascular Research* **2024**, cvae091.
- [34] F. Karl, C. Liang, R. Böttcher-Loschinski, A. Stoll, C. Flamann, S. Richter, C. Lischer, S. Völkl, B. Jacobs, M. Böttcher, R. Jitschin, H. Bruns, T. Fischer, E. Holler, W. Rösler, T. Dandekar, A. Mackensen, D. Mougiakakos, *Blood* **2023**, *141*, 1626–1639.
- [35] S. Sowlati-Hashjin, S. D. Wetmore, *Phys. Chem. Chem. Phys.* **2015**, *17*, 24696–24706.
- [36] K. K. Bhakat, A. K. Mantha, S. Mitra, *Antioxidants & Redox Signaling* **2009**, *11*, 621–637.
- [37] S. Youhanna, A. M. Kemas, S. C. Wright, Y. Zhong, B. Klumpp, K. Klein, A. Motso, M. Michel, N. Ziegler, M. Shang, P. Sabatier, A. Kannt, H. Sheng, N. Oliva-Vilarnau, F. A. Büttner, B. Seashore-Ludlow, J. Schreiner, M. Windbergs, M. Cornillet, N. K. Björkström, A. J. Hülsmeier, T. Hornemann, J. V. Olsen, Y. Wang, R. Gramignoli, M. Sundström, V. M. Lauschke, *Advanced Science* **2024**, 2407572.

Nucleobase catalysts for the enzymatic activation of 8-oxoguanine DNA glycosylase 1

Emily C. Hank,^{1, #} Nicholas D. D'Arcy-Evans,¹ Emma Rose Scaletti,² Carlos Benítez-Buelga,^{3, 4} Olov Wallner,¹ Florian Ortis,¹ Kaixin Zhou,¹ Liuzhen Meng,¹ Alicia del Prado,⁵ Patricia Calvo,⁵ Ingrid Almlöf,¹ Elisée Wiita,¹ Karen Nierlin,¹ Sara Košenina,² Andreas Krämer,⁶ Mario Kehler,¹ Maeve Long,¹ Ann-Sofie Jemth,¹ Holly Dawson,¹ Josephine Stewart,¹ Adam Dickey,¹ Mikhael E. Astorga,¹ Marek Varga,¹ Evert J. Homan,¹ Martin Scobie,¹ Stefan Knapp,⁶ Leandro Sastre,^{3, 7} Pål Stenmark,^{2, 8} Miguel de Vega,⁵ Thomas Helleday,^{1, 9} Maurice Michel^{1, 10 *}

AUTHOR ADDRESS

1 Science for Life Laboratory, Department of Oncology-Pathology, Karolinska Institutet, Stockholm, Sweden

2 Department of Biochemistry and Biophysics, Stockholm University, Stockholm, Sweden

3 Instituto de Investigaciones Biomédicas Alberto Sols CSIC/UAM, Madrid, Spain

4 Molecular Genetics Unit, Instituto de Investigación de Enfermedades Raras (IIER), Instituto de Salud Carlos III (ISCIII), Madrid, Spain.

5 Centro de Biología Molecular 'Severo Ochoa' (CSIC-UAM), Madrid, Spain

6 Institute of Pharmaceutical Chemistry & Structural Genomics Consortium (SGC), Goethe University, Frankfurt, Germany

7 Centro de Investigación Biomédica en Red de Enfermedades Raras (CIBERER). Instituto de Salud Carlos III. C., Madrid, Spain

8 Department of Experimental Medical Science, Lund University, Lund, Sweden

9 Weston Park Cancer Centre and Division of Clinical Medicine, School of Medicine and Population Health, University of Sheffield, Sheffield, United Kingdom

10 Center for Molecular Medicine, Karolinska Institute and Karolinska Hospital, Stockholm, Sweden

Current Address: Department of Pharmacy, Ludwig-Maximilians-Universität Munich, Germany

Supporting Data

Scheme S1: Possible mode of action of OGG1 biochemistry:

Glycosylase activity: OGG1 searches DNA for 8oxoG residues. The enzyme establishes additional affinity to the substrate through H-bonding with Gly42 and π -stacking with Phe319. Lys249 attacks the anomeric position and removes the oxidized base, forming a Schiff Base in the process. The Schiff Base is a masked abasic site which is the reaction product of OGG1's glycosylase activity. OGG1 requires APE1 to be removed from the Schiff Base, a process which requires some time in cells. OGG1's roles in transcription are mediated by the stability of this complex.

Lyase activity: 8oxoG may catalyze a low number of incision events by proton abstraction on the α -carbon of the Schiff Base, an event followed by elimination of the 3' DNA strand, called β -elimination, resulting in formation of 3'-phosphate unsaturated aldehyde (3'-PUA). Due to the limited physicochemical properties of 8oxoG, incision event following this abstraction are slow *in vitro* and absent in cells. Previously, TH10785 was developed which exploits identical amino acid interactions and has a suitable pKa to rapidly abstract protons from the Schiff Base. The result is a rapid accumulation of 3'-PUA and further δ -elimination, yielding both free 3'- and 5'-phosphates of the now detached DNA strand. This study examines the chemical space of nucleobases capable of promoting either β - or β,δ -eliminations.

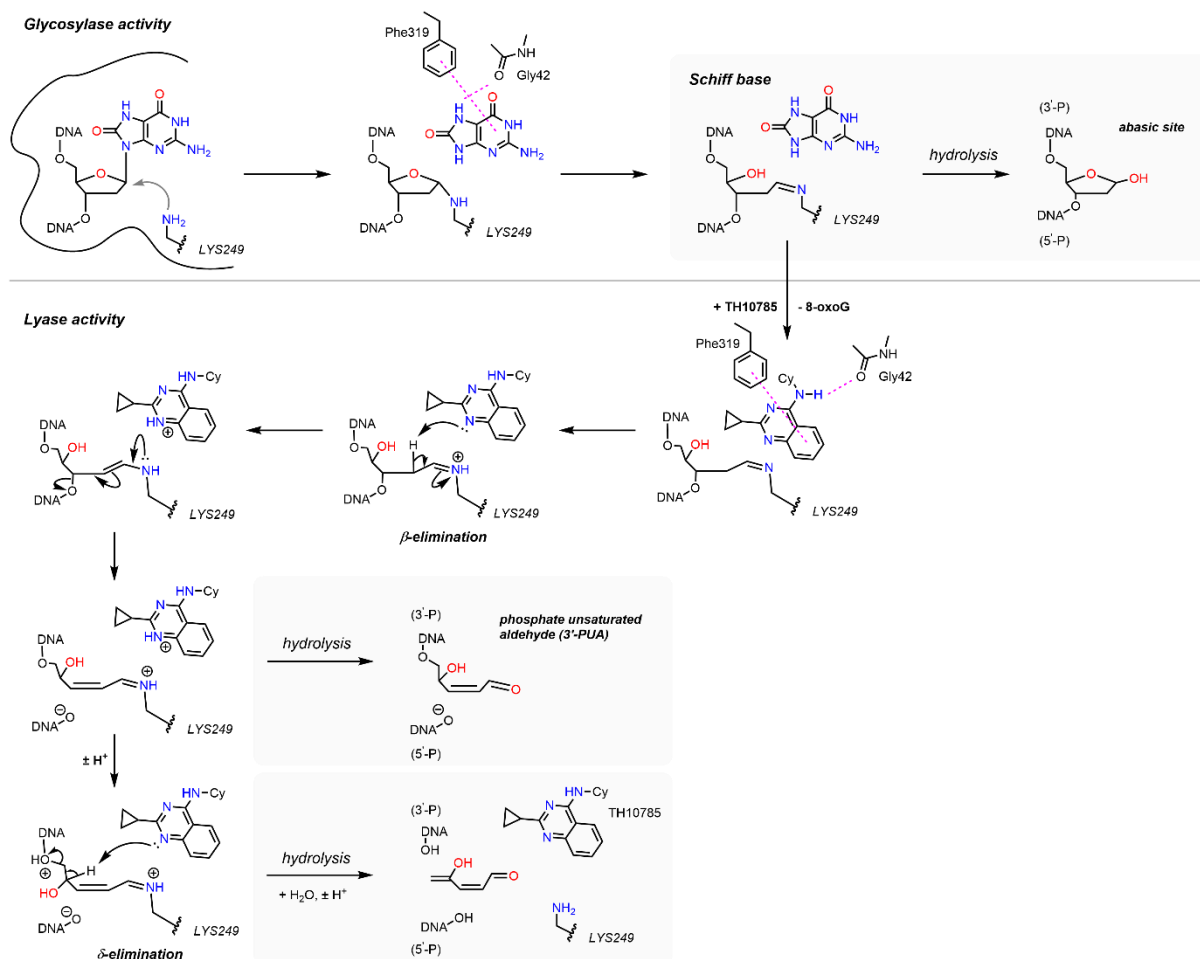
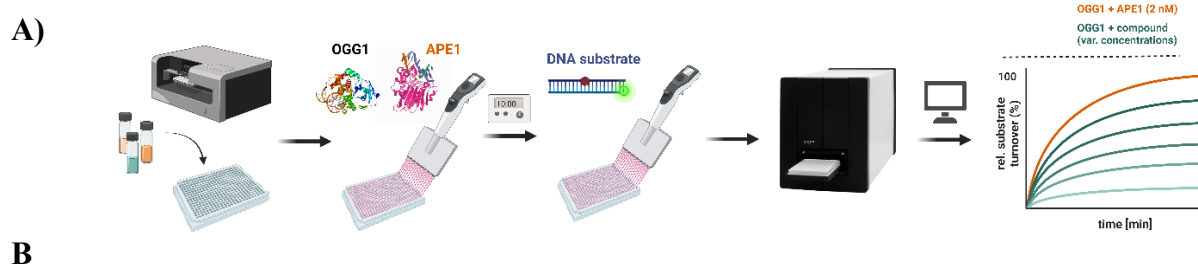
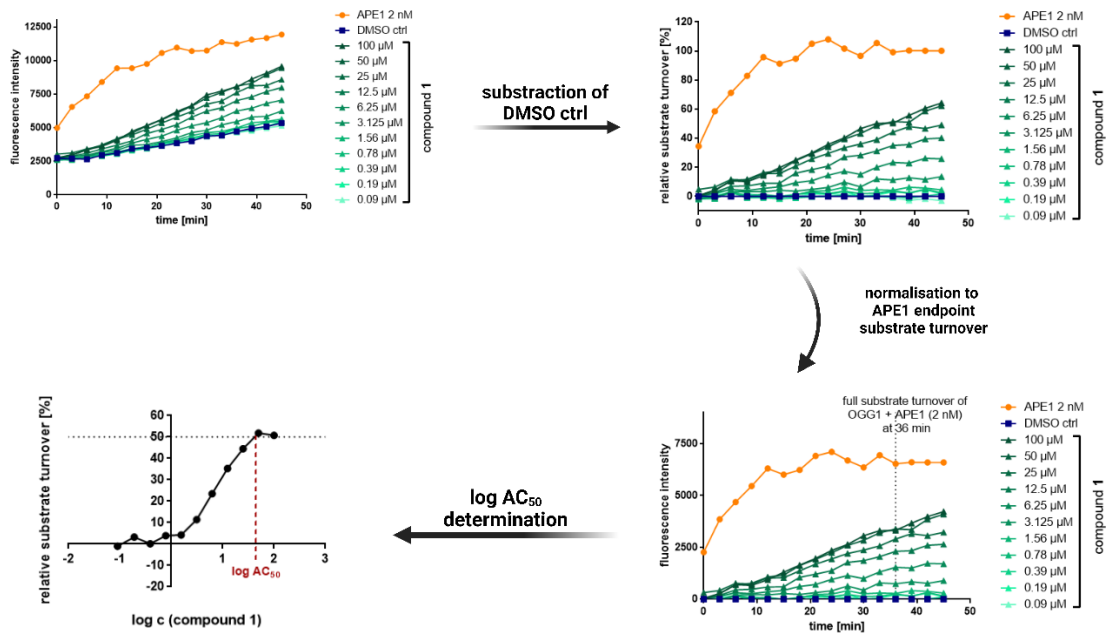


Figure S1: Biochemical assay and AC₅₀ calculation scheme and visualised raw data of the focused screen. A) Workflow of the biochemical assay as described in Materials and Methods. After the kinetic readout, fluorescence values for the DMSO control are subtracted from the fluorescence values of each compound concentration and the data is normalised to the full turnover fluorescence in the coupled APE (2 nM) control. Created in BioRender.com. B) Example of the raw data processing and AC₅₀ calculation for compound **1**. Created in BioRender.com. C) Assay data of the screened compounds at 100 μ M concentration presented as fluorescence intensity after background (DMSO control) subtraction, data at t = 0 min (start) and t = 36 min (endpoint, full turnover in the APE control), data are the mean \pm S.E.M., *n* = 2.





C

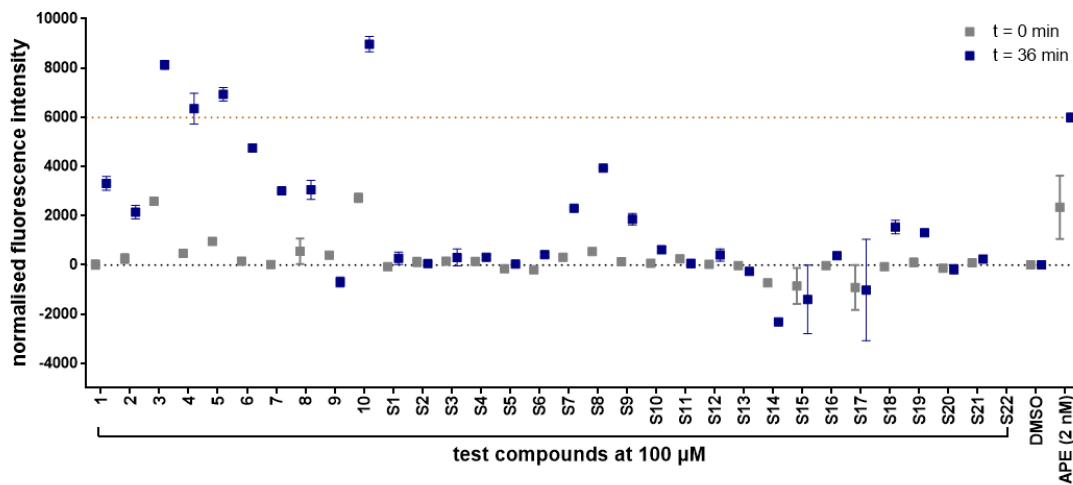
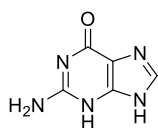
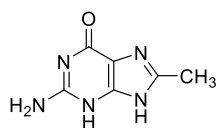


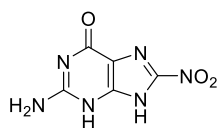
Figure S2: Extended results of a focused screen to identify OGG1 organocatalytic switches. Assay performed as described in Material and Method section. Compounds were screened at 100 μ M.

Guanines

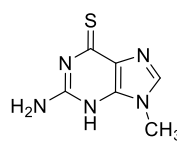
S1
guanine
inactive



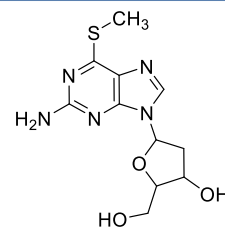
4
 AC_{50} 6 μ M



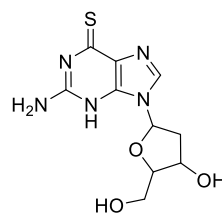
S2
inactive

N9-substitution

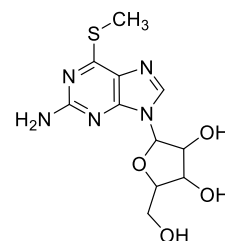
S3
inactive



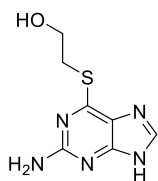
S4
inactive



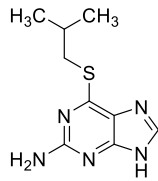
S5
inactive



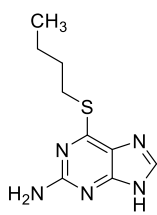
S6
inactive

6-modified thiapurines

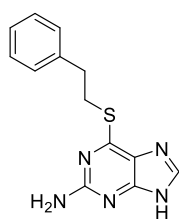
S7
 AC_{50} >100 μ M



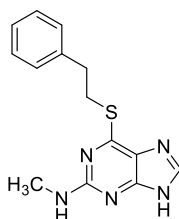
S8
 AC_{50} 51 μ M



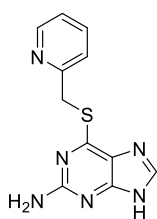
S9
 AC_{50} >100 μ M



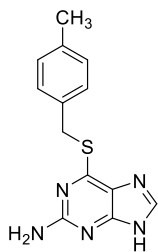
S10
inactive



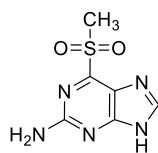
S11
inactive



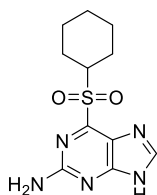
S12
inactive



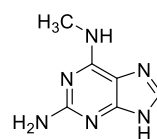
S13
inactive



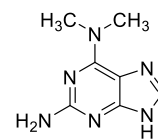
S14
inhibitor



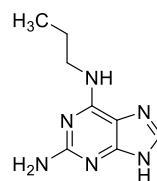
S15
inhibitor



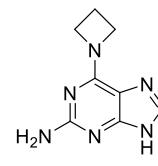
S16
inactive



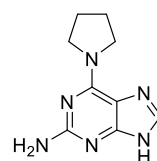
S17
inactive



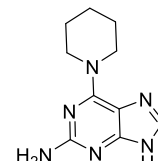
9
inactive



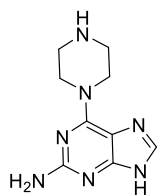
7
 AC_{50} 42 μ M



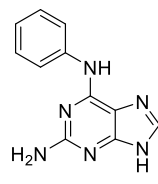
S18
 AC_{50} >100 μ M



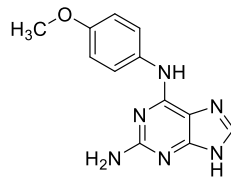
S19
 AC_{50} >100 μ M

6-N-substituted purines

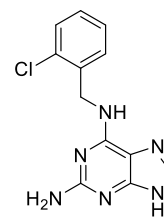
S20
inactive



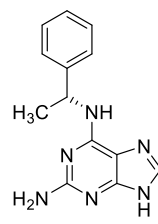
6
 AC_{50} 70 μ M



S21
inactive



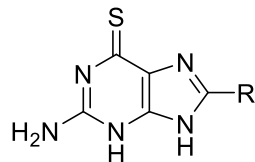
8
 AC_{50} 51 μ M



S22
inactive

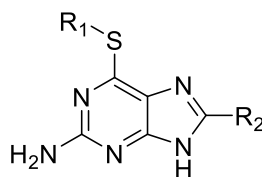
Table S1: Thioguanines are potent OGG1 organocatalytic switches. A) Investigation of effect of 8-substitution, B) Investigation of effect of combinations of 6- and 8-substitution; AC₅₀ in μM, CI95% confidence interval 95% in μM. Assay Details in Methods and Material.

A)



#	R	AC ₅₀ (CI 95)
1	-H	>100
3	-Me	0.32 (0.27 - 0.39)
10	-CH ₂ CH ₂ CH ₃	0.55 (0.26 - 1.2)
S23	-NH ₂	1.1 (0.68 - 1.9)
S24	-SMe	0.47 (0.19 - 1.2)
S25	-CH ₂ NH ₂	21.1 (17.6 – 25.3)
S26	- CH ₂ NHBoc	inactive

B)



#	R ¹	R ²	AC ₅₀ (CI 95)
S27	Me	H	>100
S28	-CH ₂ CH ₃	H	12.8 (11.2 – 14.8)
S29	<i>i</i> -Pr	H	14.3 (9.6 – 21.2)
S30	-CH ₂ CH ₂ CH ₃	H	20.5 (12.5 – 33.6)
S31	-CH ₂ CH=CH ₂	H	23.9 (15.7 – 36.4)
S32	Me, <i>N</i> -9 Me	H	Inactive
S33	Me	Me	3.1 (2.3 – 4.1)

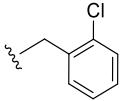
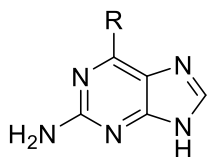
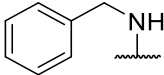
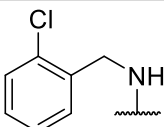
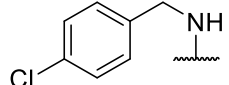
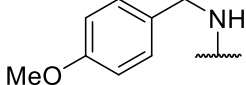
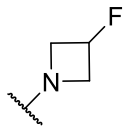
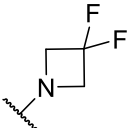
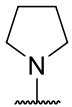
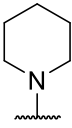
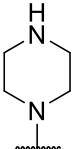
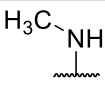
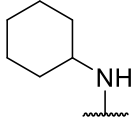
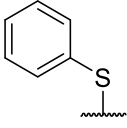
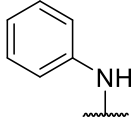
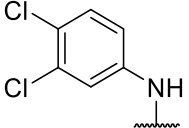
S34	Me	NH ₂	>100
S35	Me	-SMe	7.3 (3.6 – 15.2)
S14	-SO ₂ Me	H	Inactive
S15	-SO ₂ Cy	H	Inactive
S36	-SCy	H	>100
S37		H	>100
S38	Ph	H	Inactive
S39	(3,4-Dichloro)thiophenyl	H	>100

Table S2: Investigation of the 6-substitution in guanine. AC₅₀ in μM, CI95 confidence interval 95% in μM. Assay Details in Methods and Material.



#	R	AC ₅₀ (CI 95)
S40		> 100
8		>100
S41		>100
S21		>100

S42		59.2 (53.6 – 65.4)
S43		29.1 (13.2 – 64.1)
S18		> 100
S19		>100
S20		inactive
S16		inactive
13		>100
S38		inactive
6		62.2 (44.1 – 87.6)
11		12.5*

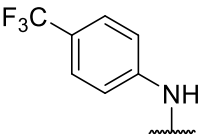
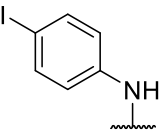
S44		inactive
S45		> 100

Figure S3: Fluorescence readout of the biochemical assay for OGG1 activation with compound 11 in different concentrations: The compound follows a bell-shaped activation profile and does not reach the half-maximal substrate turnover of APE1 in order to determine an AC50. Assay performed as described in Material and Method section.

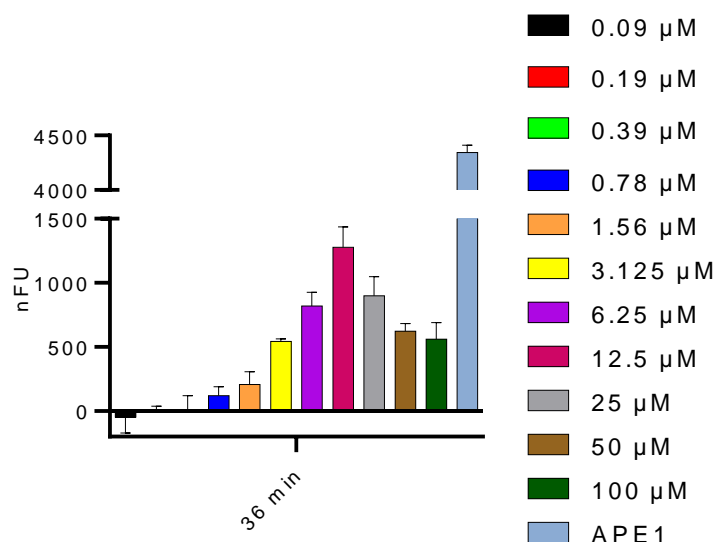
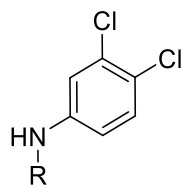


Table S3. 6-substituted pyrazolo-[3,4-*d*]-pyrimidine are organocatalytic switches of OGG1: A) Scaffolds other than guanine are investigated and reveal a fused pyrazolo ring to enhance potency of both guanine and adenine analogues; B) Matched-pair analysis of guanine and pyrazolo-[3,4-*d*]-pyrimidine derivatives confirm the superior performance of the latter scaffold; AC₅₀ in μM, CI95 confidence interval 95% in μM; * compound only reaches AC₃₅ following a bell-shape activity curve.

A)



	R	AC₅₀ (CI 95)
11		12.5*
12		13.1 (2.3 – 75.1)
S46		inactive
S47		6.2 (4.7 – 8.2)
S48		inactive
S49		inactive

B)

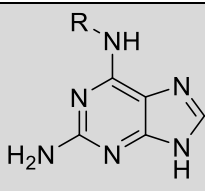
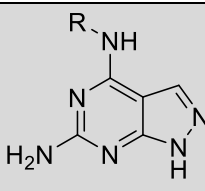
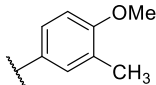
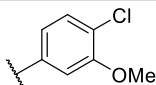
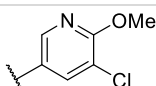
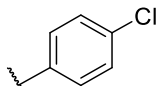
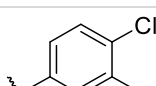
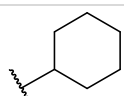
				
R	#	AC₅₀ (CI 95)	#	AC₅₀ (CI 95)
	S50	>100	S51	14.0 (11.4 – 17.3)
	S52	>100	S53	40.0 (23.7 – 67.5)
	S54	autofluorescence	15	28.2 (10.0–79.8)
	S55	>100	S56	5.4 (1.6 – 18.5)
	11	12.5*	12	13.1 (2.3-75.1)
	13	>100	14	11.7 (5.5 – 24.9)

Figure S4. Effect of the compounds on the AP-lyase activity of *h*OGG1 on 8-oxoG:C-containing DNA over a 2- and 4- minute (top) or 30- and 60-min (down) timespan respectively. The assay was performed as described in Materials and Methods using 2 nM of the indicated [³²P]5'-labeled 8-oxoG-containing substrate, in the presence of 10 nM *h*OGG1, 20 mM EDTA and either 10% DMSO or 6.25 μM for TH10785, **13** and **3**; 50 μM for TH5487. After incubation for the indicated times at 37°C, reactions were either stopped or further incubated 10 min in the presence of T4 PNK (+). Thereafter, samples were analyzed by 7M urea-20% PAGE and autoradiography. Position of products is indicated. DMSO and TH10785 serve as controls of β- and β,δ-elimination respectively.

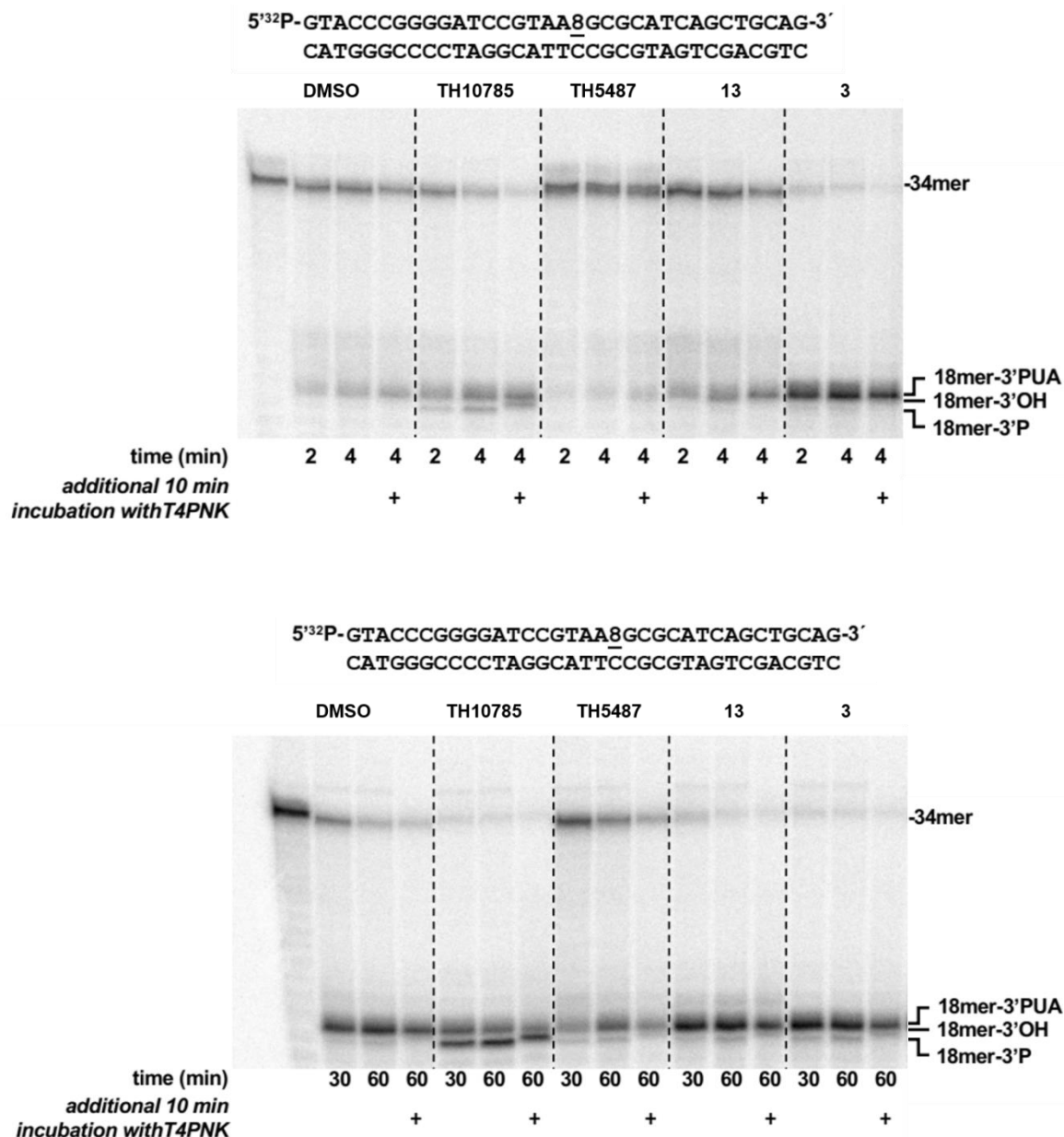


Table S4: Nano-DSF confirms OGG1 protein stability to be influenced by pH and compound binding: **A)** Light scattering was monitored to assess the degree of protein aggregation due to protein denaturation; **B)** OGG1 binder increase scattering in distinct pH environments; **C)** The melting temperature (T_m) of OGG1 in the presence of compound confirms OGG1 stabilization, indicating that the observed activity boost in Figure 2B can be partly attributed to protection against pH induced denaturation. Nano-DSF as performed in Materials and Methods. Protein was used at 25 μ M concentration and compound at 200 μ M.

A)	pH 6.7	pH 7.5	pH 7.7	pH 8.0	pH 8.3
Upper limit (Scattering, AU) for wtOGG1	88.5	87.4	88.7	91.6	90.1
Lower limit (Scattering, AU) for wtOGG1	85	87.4	85.5	88.7	89.0
Average (Scattering, AU) for wtOGG1	86.8	87.4	87.1	90.2	89.6

B)	pH 6.7	pH 7.5	pH 7.7	pH 8.0	pH 8.3
wtOGG1 + TH 10785 (AU)	102.0	100	117	116.0	106
wtOGG1 + 14 (AU)	85	86	87	87.5	90.0
wtOGG1 + 3 (AU)	87	89	91	90	85
wtOGG1 (AU)	86.8	87.5	87.1	90.1	89.6

C)	pH 6.7	pH 7.5	pH 7.7	pH 8.0	pH 8.3
T _m for wtOGG1 (°C)	48.2	46.8	48.4	47.2	46.4
T _m for wtOGG1 + TH10785 (°C)	55.0	55.6	56.4	55.8	55.8
T _m for wtOGG1 + 14 (°C)	49.5	50.3	50.3	52.1	51.6
T _m for wtOGG1 + 3 (°C)	51.5	51.4	50.6	49.8	49.9

Figure S5: Performing the incision assay in deuterated solvent confirms the role of proton transfer and nitrogen basicity in the action of organocatalytic switches. Assay was performed in water or deuterated water using 8-oxoA:C as substrate. Compounds were used at their best performing concentration and at three pH environments; a) pH 6.8; b) pH 7.5; c) pH 8.2. The general ratio of incision events remains similar compared to Figure 2B but is significantly reduced for the deuterated environment. Assay performed as described in Materials and Methods.

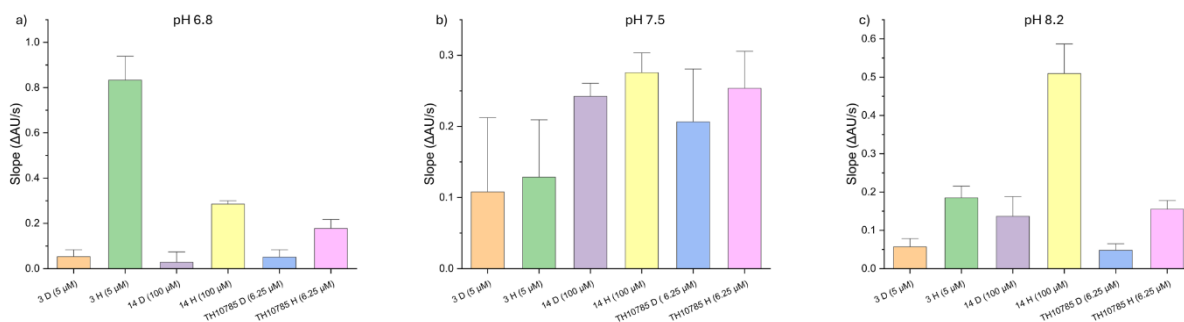


Figure S6: Saturation curves displaying the rate of substrate turnover for OGG1 with TH10785 and 3 against a number of AP site substrates in the fluorescence-based biochemical assay: Top) TH10785 activates OGG1 on AP sites opposite any canonical nucleobase; Bottom) 3 follows a similar pattern and all AP sites are more efficiently converted than 8-oxo substrates. v_0 of reaction measured within the initial linear slope of the reaction. Details described in Materials and Methods.

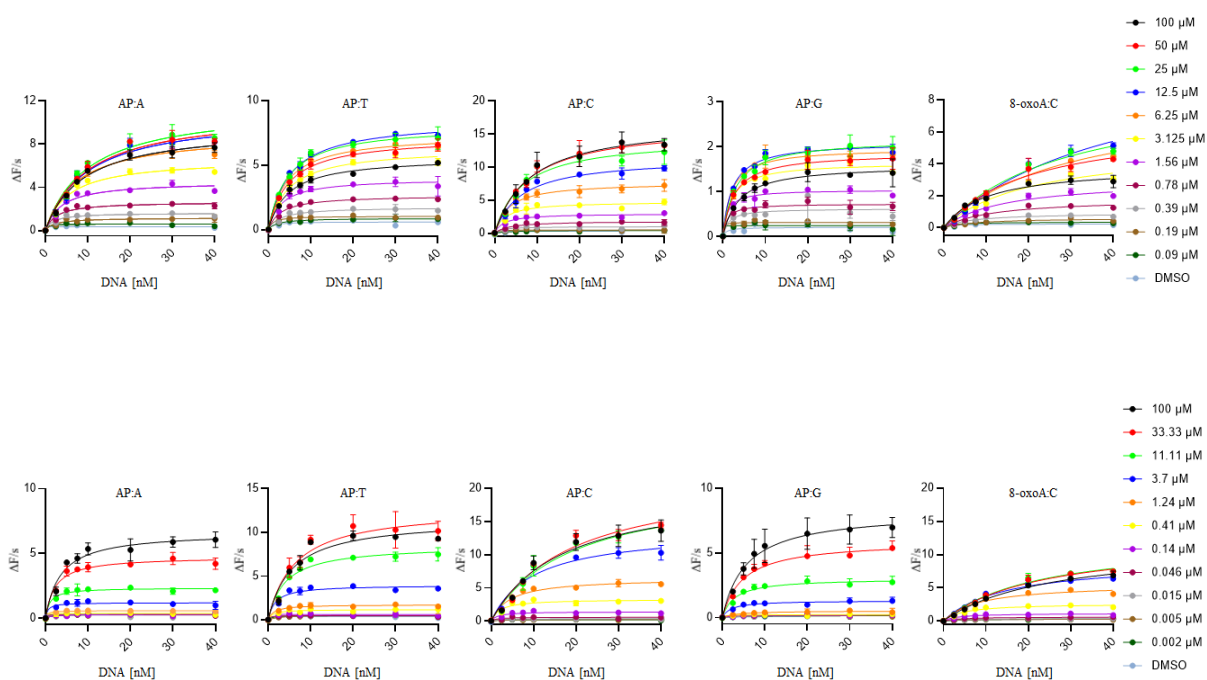


Figure S7. The recognition of ligands by mouse OGG1: Amino acids contributing to ligand binding are depicted as sticks; C atoms are coloured blue, O atoms red, N atoms dark blue and S atoms gold. The ligands 14 (A), 3 (B), 10 (C) and 15 (D) are presented as stick models; C atoms coloured yellow, N atoms coloured dark blue, O atoms coloured red, Cl atoms coloured green and S atoms coloured gold. Hydrogen

bond interactions are shown as dashed lines. Water molecules are shown as red spheres. The 2Fo-Fc electron density maps around the ligands are contoured at 1.0 σ (blue) and the Fo-Fc electron density maps are contoured at - 3.5 σ (red) and +3.5 σ (green).

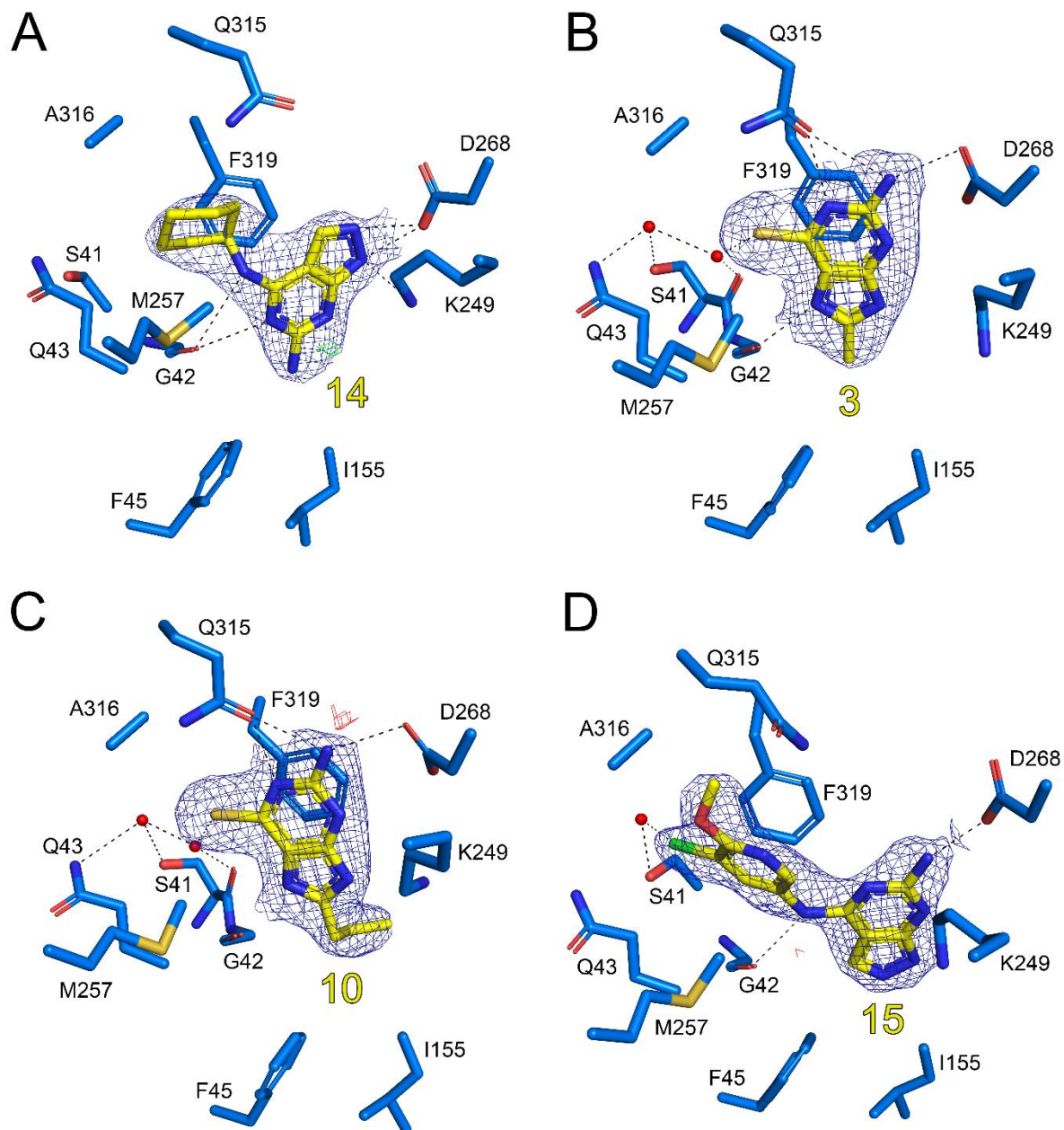


Table S5: X-ray crystallography data collection and refinement statistics

	mOGG1-14	mOGG1-3	mOGG1-10	mOGG1-15
Data collection				
PDB code	8BQ7	9F8U	9F8V	9F8Z
Station	MAXIV-BioMAX	DLS-I03	DLS-I03	DLS-I03
Space group	P2 ₁ 2 ₁ 2 ₁	P2 ₁ 2 ₁ 2 ₁	P2 ₁ 2 ₁ 2 ₁	P2 ₁ 2 ₁ 2 ₁
Cell dimensions:				
a, b, c (Å)	80.7, 82.1, 169.5	81.3, 81.7, 169.9	81.5, 81.6, 170.3	80.6, 82.3, 171.9
α , β , γ (°)	90, 90, 90	90, 90, 90	90, 90, 90	90, 90, 90
Resolution (Å)	72.9-2.6 (2.72-2.60)	58.7-2.5 (2.60-2.50)	58.9-2.4 (2.48-2.40)	85.9-2.50 (2.71-2.50)
Total reflections	474075 (58223)	552287 (63840)	603093 (52882)	427533 (23269)
Unique reflections	35462 (4247)	40082 (4445)	45246 (4343)	31051 (1553)
R_{merge}	14.0 (279.6)	7.5 (212.8)	8.6 (105.9)	11.8 (241.6)
R_{pim}	5.6 (112.1)	3.0 (83.4)	3.5 (45.9)	3.7 (91.8)
CC _{1/2} (%)	99.8 (58.9)	100 (59.7)	99.9 (77.4)	100 (70.5)
I/σ	11.4 (1.2)	19.8 (1.4)	16.9 (2.1)	13.9 (1.4)
Completeness	100 (100)	100 (100)	100 (100)	94.1 (71.2)
Redundancy	13.4 (13.7)	13.8 (14.4)	13.3 (12.2)	13.8 (15.0)
Refinement				
$R_{\text{work}}/R_{\text{free}}$ (%)	25.5/30.6	23.7/29.0	23.0/28.1	22.5/27.7
<i>B</i> -factors:				
Protein (all atoms) ^a	67.5/84.8/100.5	71.4/91.3/117.4	53.1/78.9/99.2	68.9/64.6/78.1
Ligand ^a	85.0/x/x	53.0/x/x	41.5/64.2/90.6	66.2/58.0/x
Water	64.9	67.5	49.5	41.1
R.m.s. deviations:				
Bond lengths (Å)	0.035	0.012	0.010	0.010
Bond angles (°)	1.18	0.98	1.43	1.27
Ramachandran statistics:				
Favoured (%)	99.9	99.8	99.2	99.5
Outliers (%)	0.1	0.2	0.8	0.5

Values in parentheses are for the highest-resolution shell. ^a Values for each monomer (A, B and C) of the asymmetric unit. An x indicates that a ligand is not bound in that specific monomer.

Table S6: Results from the DSF-based selectivity screening against a curated kinase library. The assay was performed as described in Materials and Methods using compounds **3**, **10**, **14** and TH10785 in a concentration of 10 μ M. n.d. = not determined.

Kinase	ΔT_m [K]				Reference		
	comp d3	compd 14	compd 10	TH1078 5	Reference substance	Δ Tm [K]	IC ₅₀ /K _D [nM]
MAP3K5	-0.1	3.5	-0.2	-0,2	Staurospo- rine	16	24
RSK1_b	-0.1	2.6	-0.6	n.d.	Staurospo- rine	3	0.1
BIKE	0.3	2.6	0.1	-0,1	Staurospo- rine	18	1
ULK3	-0.1	2.3	-0.3	-0,2	Staurospo- rine	17	1.5
GAK	0.3	2.1	-0.5	-1,3	Staurospo- rine	9	17
AAK1	-1.2	2.1	-1.6	0,0	Staurospo- rine	15	1.2
ABL1	0.1	2.0	0.3	0,1	Staurospo- rine	9	60

AURKB	0.4	1.9	1.6	n.d.	Staurospore rine	8	5
AurA	-0.8	1.9	-1.1	-0,1	Staurospore rine	17	1.5
CLK1	-0.5	1.7	-0.4	0,0	Staurospore rine	16	4
BMPR2	-0.2	1.7	0.1	0,3	Staurospore rine	3	670
TAF1	0.1	1.4	1.2	0,6	Bromospore rine	7	n.d.
DMPK1	0.1	1.3	1.0	0,0	Staurospore rine	9	22.7
CDK2	-1.6	1.2	-1.8	-0,3	Staurospore rine	15	1.3
MEK4	-0.8	1.1	-1.6	0,1	Staurospore rine	11	1
FLT1	-0.5	0.9	-0.8	-0,7	Staurospore rine	12	11
PCTAIRE1	-0.3	0.9	-0.3	0,6	Staurospore rine	9	14
PAK4	0.2	0.8	-0.2	2,4	Staurospore rine	12	6.3
MARK3	-0.6	0.8	-0.9	0,2	Staurospore rine	18	0.5
BRD4	0.1	0.7	0.3	0,5	JQ1	7	60

BRAF	0.3	0.7	0.2	0,1	Dabrafenib	27	0.7
MARK4	0.1	0.7	0.0	0,8	Staurospo- rine	14	0.5
PLK4	-0.3	0.7	-0.1	-0,1	Staurospo- rine	18	4
BMX	-0.5	0.6	-1.3	0,2	Staurospo- rine	7	170
ULK1	-0.5	0.6	-0.4	0,3	Staurospo- rine	12	n.d.
DYRK2	-0.5	0.5	-1.5	0,2	Staurospo- rine	7	280
CASK	-0.2	0.5	-0.4	-0,2	Staurospo- rine	5	19
CAMK1G	-0.7	0.5	-0.5	n.d.	Staurospo- rine	9	23
MAPK15	0.0	0.4	0.0	n.d.	Staurospo- rine	14	5.5
CHK2	-0.4	0.4	0.4	0,1	Staurospo- rine	17	0.1
NEK1	0.2	0.3	0.5	-0,5	-	-	-
MAP2K6	0.0	0.3	-0.2	-0,2	Staurospo- rine	11	1
MST1	-1.3	0.3	-2.9	n.d.	Staurospo- rine	16	1

SRC	-0.2	0.3	0.0	-0,2	Staurospo- rine	5	2.3
DAPK3	0.5	0.2	-0.7	0,4	Staurospo- rine	16	1
CAMK2B	-0.5	0.2	-1.2	0,6	Staurospo- rine	11	0.1
CLK3	-0.5	0.2	-0.7	-0,2	CLK-T3	15	110
MST2	-3.1	0.2	-4.4	1,2	Staurospo- rine	13	0.18
CAMK1D	-0.1	0.2	-0.4	0,2	Staurospo- rine	9	0.4
JNK1	-0.8	0.2	-1.0	-1,8	Staurospo- rine	8	220
MRCKa	0.0	0.2	-0.1	-0,7	Staurospo- rine	n.d.	10.3
EPHA7	-0.6	0.2	-0.4	-0,2	Staurospo- rine	11	30.4
EphA2	-0.7	0.2	-0.8	0,1	Staurospo- rine	7	53
p38d	0.3	0.2	-0.2	0,3	Dora- mapimod	n.d.	1
MELK	0.1	0.1	0.3	0,3	Staurospo- rine	13	0.7
SLK	-1.0	0.1	-1.7	0,1	Staurospo- rine	17	3.9

DRAK2	-1.7	0.1	-3.0	-1,2	Staurospo- rine	11	21
CK1d	0.4	0.1	0.1	0,2	PF-670462	9	8
Haspin	-0.9	0.1	-0.7	-0,4	Staurospo- rine	9	50
PIM3	-0.6	0.1	-1.9	0,2	Staurospo- rine	19	0.1
CDKL1	-0.6	0.1	-1.5	0,2	CEP-32496	7	n.d.
FGFR1	-0.1	0.1	-0.3	-0,2	Staurospo- rine	6	3.2
WNK1	-0.3	0.1	-0.5	0,0	-	5	n.d.
EPHA4	-1.1	0.0	-0.1	n.d.	Staurospo- rine	5	7.4
STLK3	-0.1	0.0	-0.3	0,2	Staurospo- rine	11	22
TTK	0.1	0.0	-0.7	-0,4	Staurospo- rine	9	61
JNK3	-0.7	0.0	-2.5	0,1	CEP-32496	9	n.d.
CK2a1	-0.1	0.0	-0.4	-0,3	Similtasertib	15	1
MAP2K1	-0.3	0.0	-0.7	0,1	Staurospo- rine	3	24
DAPK1	0.2	0.0	-0.6	-0,6	Staurospo- rine	9	4

MAPKAPK2	-0.6	0.0	-0.7	n.d.	Staurospore rine	4	196
PIM1	-0.7	-0.1	-1.0	n.d.	Staurospore rine	12	3
JNK2	-0.9	-0.1	-1.8	0,8	SBI-0069279	9	n.d.
CSNK1E	-0.1	-0.1	0.0		PF-670462	8	14
MSSK1	-0.4	-0.1	-0.3	-0,4	-	-	-
EPHB1	0.2	-0.1	-0.3	n.d.	Staurospore rine	6	25
GPRK5	-0.3	-0.1	-2.6	0,1	Staurospore rine	6	150
Erk2	0.0	-0.1	0.3	-0,2	GDC-0994	8	1
OSR1	-0.1	-0.1	-1.7	0,0	Staurospore rine	6	91
HIPK2	-0.9	-0.1	-0.9	n.d.	Staurospore rine	4	791
CK2a2	-0.2	-0.1	-0.6	0,1	Similtasertib	16	1
AKT3	-0.3	-0.1	0.1	0,0	Staurospore rine	7	5
CAMK2D	0.4	-0.2	-1.2	0,2	Staurospore rine	16	0.5
SRPK1	-0.6	-0.2	-1.0	-0,4	Staurospore rine	7	120

FGFR2	-0.2	-0.2	-0.2	-0,4	Staurospo- rine	8	3.3
FES	-1.1	-0.3	-1.5	0,1	Staurospo- rine	8	1.7
MYT1	-1.0	-0.3	-2.9	n.d.	Dasatinib	5	130
EPHA5	-0.8	-0.3	-0.9	0,3	Staurospo- rine	7	19
NEK7	-0.6	-0.3	-0.9	-0,2	-	-	-
PAK1	-1.6	-0.3	-2.1	-0,2	Staurospo- rine	7	0.3
VRK1	-0.7	-0.3	-0.6	-0,3	-	5	n.d.
p38a	-1.2	-0.3	-2.1	-0,2	Dora- mapimod	20	1
TIF1	-6.8	-0.3	-2.0	0,6	-	6	222
BRPF1	-1.0	-0.4	-3.0	n.d.	GSK6853	14	20
LOK	-2.5	-0.4	-2.7	n.d.	Staurospo- rine	24	0.03
DYRK1A	-1.4	-0.5	-2.3	n.d.	Staurospo- rine	10	4
NQO2	-0.4	-0.5	1.1	n.d.	Imatinib	n.d.	43
PHKg2	-1.5	-0.5	-2.0	-0,2	Staurospo- rine	21	0.1
CAMK4	-0.8	-0.6	-0.1	n.d.	Staurospo- rine	8	141

MER	-0.7	-0.6	-0.9	0,1	Staurospo- rine	6	6.4
DRAK1	-1.2	-0.7	-1.0	-0,3	Staurospo- rine	8	14
MST4	-2.1	-0.7	-1.5	0,3	Staurospo- rine	6	6.7
MAP2K7	0.1	-0.7	-0.3	n.d.	Staurospo- rine	7	440
NDR2	-1.0	-0.9	-1.8	0,2	Staurospo- rine	12	1.4
TLK1	-1.7	-1.0	-2.0	n.d.	Staurospo- rine	9	44
MST3	-3.1	-1.0	-2.5	-0,7	Staurospo- rine	6	120
DCAMKL1	-1.6	-1.0	-1.1	-1,4	Staurospo- rine	11	120
EPHB3	-2.1	-1.0	-1.2	0,2	Staurospo- rine	6	825
NEK2	-1.9	-1.1	-0.6	-0,4	Staurospo- rine	4	650
MSK1_b	-0.2	-1.1	1.0	n.d.	Staurospo- rine	16	5

Figure S8. Results from the DSF-based selectivity screening against a curated kinase library. The assay was performed as described in Materials and Methods using compounds **3**, **10**, **14** and TH10785 in a concentration of 10 μ M. Heatmap indicating stabilization or destabilization of the kinase set through compounds used, white = not determined.

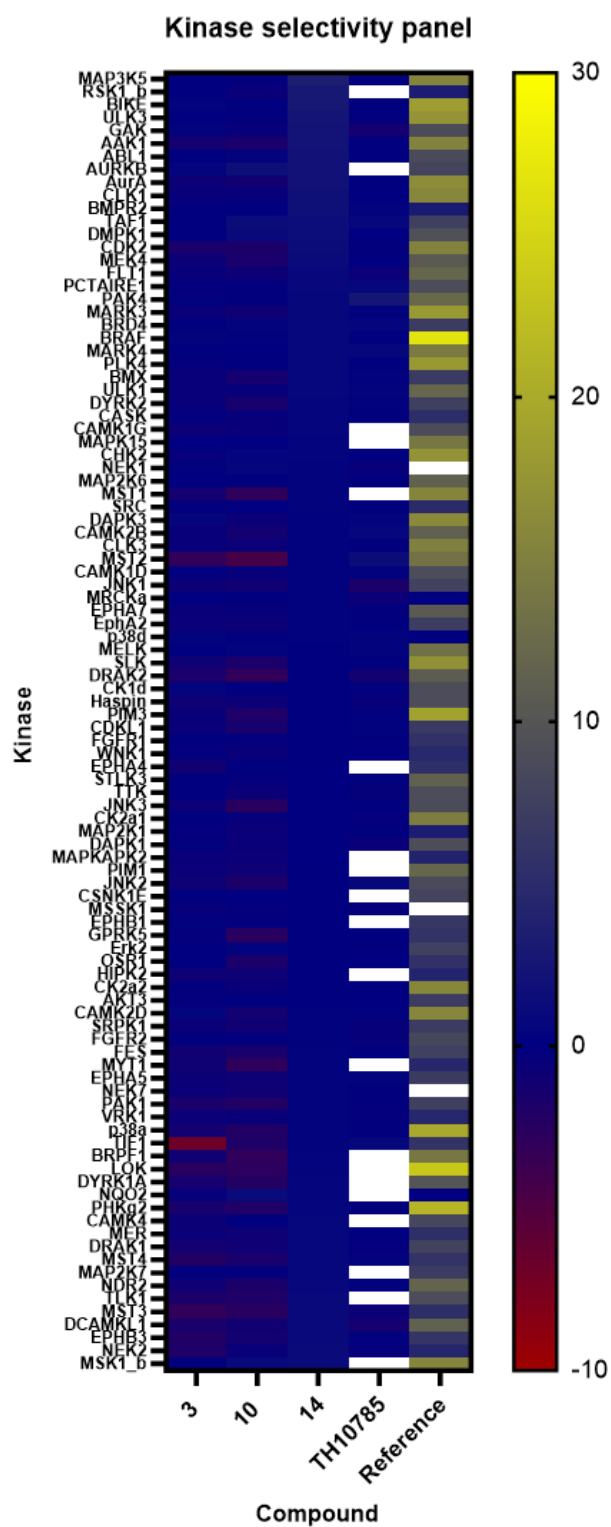


Table S7: Results from selectivity experiments on other DNA glycosylases and NUDIX protein family members. The assay was performed as described in Materials and Methods using compounds **3**,

10, 12 and 14 in a concentration of 99 μ M. X* is an AP site targeting PAINS (pan-assay interference compound), that stalls AP site.

entry	3	10	14	12	TH010785	reference	
Glycosylase or NUDIX	inhibition%					inhibition%	substance
APE1	-10.38	-8.07	-5.61	-8.81	3.26	92.99	X*
MPG	-38.05	-36.95	4.13	22.11	20.84	88.01	X*
NEIL1	-6.92	-5.09	-6.86	25.00	14.71	90.30	X*
NTHL1	-6.32	-14.56	-0.71	24.19	28.50	70.89	X*
NUDT5	-9.74	-15.86	-7.45	1.62	2.08	99.31	TH005427
NUDT15	5.23	-0.01	-5.55	3.80	3.38	96.48	TH001760
NUDT22	-16.15	-11.12	-7.97	-8.54	3.66	92.93	TH008525
SMUG1	-21.97	-17.81	-30.10	12.70	-15.36	76.37	X*
TDG	-5.51	-10.87	5.73	35.39	14.09	83.00	X*
UNG	-11.06	-13.72	5.42	39.24	48.6	94.93	X*

Figure S9: Results from selectivity experiments on other DNA glycosylases and NUDIX protein family members. The assay was performed as described in Materials and Methods using compounds 3, 10, 12 and 14 in a concentration of 99 μ M.

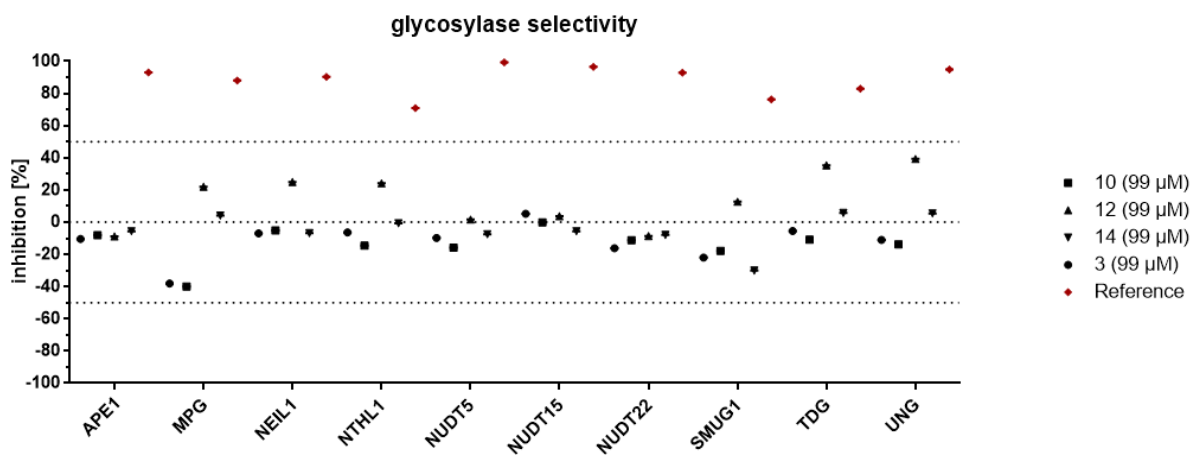
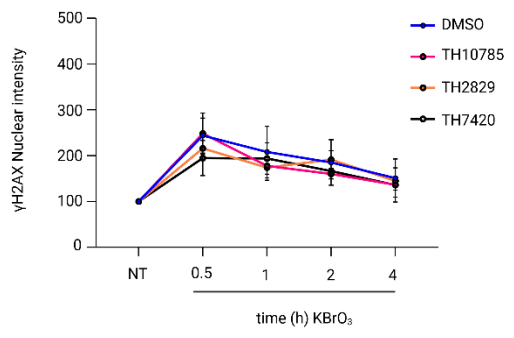


Table S8: Cell viability dose-response of compounds 3, 10, 12 and 14 in BJ-hTERT and BJ-hTERT SV40RAS cell lines. The assay was performed as described in Materials and Methods. TH000287C, an MTH1 inhibitor, served as reference.

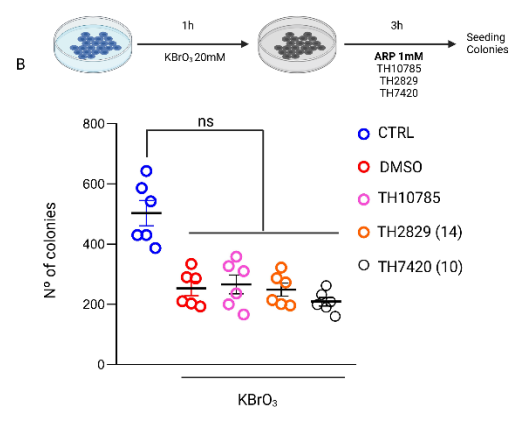
Entry		3	10	14	12	Reference: TH000287 C
IC50 [μ M]	BJ-hTERT	>100	>100	>100	57.7	6.27
	BJ-hTERT SV40RAS	>100	>100	>100	35.0	2.35

Figure S10: A) Quantification of nuclear γ H2AX levels across different time points in U2OS cells exposed to organocatalytic switches or DMSO, under oxidative stress conditions (20 mM of KBrO₃ for 1h). Each bar represents the mean \pm SEM. Data are the average of three independent experiments. For each experiment, 25 fields and around 1000 cells were captured per condition. Statistical significance was calculated using two-way ANOVA for multiple comparisons. Nonsignificant differences were found **B) Clonogenic survival of U2OS cells to KBrO₃ in the presence of activators.** The cancer cell line U2OS was first exposed to an acute dose of KBrO₃ (20mM for 1h) and incubated overnight in the presence of activators (10 μ M) or DMSO, and replaced with fresh media to allow the formation of colonies. After 10 days, colonies were counted. Data are average \pm SD values of three biological replicates of two independent experiments. Statistical significance was calculated using an unpaired two-tailed Student's t-test. ns, nonsignificant

A) A



B)



Materials and Methods

Biochemical assay (Fluorescence)

Enzymes were purified as below and the biochemical assay including materials used was based on the publication by Visnes *et al.*^[1] and “EUBOPEN” protocols (<https://www.eubopen.org/protocols-reagents>) and adapted where mentioned. OGG1 activation was monitored in a kinetic mode and a time resolved curve was obtained for each compound concentration in triplicates except where stated otherwise. Initial slopes were taken of the linear part of these curves to determine rates and kinetics. Fluorescence values of each compound concentration were normalised by the DMSO control values and calculated as % activation of the full turnover fluorescence of the APE (2 nM) control. The median activation concentration (AC₅₀) for each compound was calculated from the % activation of all tested concentrations and refers to the compound concentration which activates the reaction to 50% of the substrate turnover reached in the assay control coupled to APE1 (2 nM) as described before.^[2] In the screening, primary hits were defined as compounds with an AC₅₀ of below 100 µM. A schematic representation of the assay and AC₅₀ determination can be found in Figure S2.

Proteins and reagents

Enzymes (APE1, UNG2, TDG, SMUG1, MPG, NEIL1, NTHL1, NUDT15, NUDT22, NUDT5) and mutants were produced as reported previously.^[1-4] 8-oxoG-containing oligonucleotide (see sequence below) was radiolabelled at the 5' end with [γ ³²P]-ATP (Perkin-Elmer Life Sciences) and T4 polynucleotide kinase (T4PNK) from New England Biolabs.

Oligonucleotides

For PAGE analysis: Oligonucleotide 5'GTACCCGGGGATCCGTAA8GCGCATCAGCTGCAG (Integrated DNA Technologies), where 8 stands for 8oxodG, was 5'-labeled and further hybridized to the complementary oligonucleotide 5'-CAGCAGCTGATGCGCCTTACGGATCCCCGGGTAC in the presence of 60 mM Tris-HCl (pH 7.5) and 0.2 M NaCl by heating to 80 °C for 5 min before slowly cooling to room temperature overnight.

For standard biochemical assay: Complementary strands containing FAM and DAB were ordered from ATD BIO. Sequence were 5'-FAM-TCTG CCA XCA CTG CGT CGA CCT G-3' and 5'-CAG GTC GAC GCA GTG YTG GCA GT-Dab-3' where X is a lesion such as uracil, thymine glycol, 8-oxoA, AP-site analogue, inosine, hydroxymethyl cytosine and Y is the corresponding required complementary base.

hOGG1 activity assay on 8oxodG-containing substrates (PAGE)

To analyse the AP lyase activity of *hOGG1* on 8-oxoG containing substrates, 2 nM of the indicated 34 mer [³²P]5'-labeled 8oxoG-containing substrate was incubated with 10 nM *hOGG1* and either 10% DMSO or 6.25 μM for TH10785, **13** and **3**; 50 μM for TH5487 in the presence of 30 mM Hepes, pH 7.5, 4% glycerol and 20 mM EDTA. Samples were incubated at 37 °C for the indicated times. When specified, samples were further incubated 10 min in the presence of 0.2 U of T4PNK. The reaction products were stabilized by incubation with 30 mM of freshly prepared NaBH₄ and further incubation for 20 min on ice. DNA products were analyzed by 7 M urea-20% PAGE and autoradiography.

pKa prediction

pKa predictions were carried out within the Schrödinger Suite 2023-2 using the Epik module. States were predicted for aqueous conditions with a pH of 7 ± 2, tautomers were generated where applicable and the number of output structures was limited to 16. Position corresponding to basic positions able to abstract the α-proton are reported.

Crystallization

Purified mOGG1 (22 mg/mL) was pre-incubated with 6.25 mM ligand (TH2829, TH7399, TH7420 or TH13677) and crystallized via sitting drop vapor diffusion in conditions from the Morpheus Screen (Molecular Dimensions). This included 0.12 M Monosaccharides, 0.1 M bicine/Trizma base pH 8.5, 50 % GOL_P4K (mOGG1-**14** and mOGG1-**10**), 0.09 M NPS, 0.1 M imidazole/MES pH 6.5, 50 % MPD_P1K_P3350 (mOGG1-**3**) or 0.12 M Ethylene Glycols, 0.1 M sodium HEPES/MOPS pH 7.5, 50 % GOL_P4K (mOGG1-**15**) at 18 °C. Protein crystals were fished without additional cryoprotectant and flash frozen in liquid nitrogen.

Data collection, structure determination, and refinement

For the mOGG1-**14** complex, X-ray diffraction data was collected at BioMAX (Lund, Sweden) equipped with an EIGER X 16M detector. A complete dataset was collected on a single crystal at 100 K. The dataset was processed and scaled with DIALS^[5] and AIMLESS^[6] within the CCP4 suite^[7]. For the mOGG1-**3**, mOGG1-**10** and mOGG1-**15** complexes, X-ray diffraction data were collected at station I03 of the Diamond Light Source (Oxford, UK) equipped with a PILATUS-6M detector. Complete datasets were collected on single crystals at 100 K. The datasets were processed with DIALS^[5] or XDS^[8] and scaled with AIMLESS^[6] or STARANISO. Molecular replacement was performed in Phaser^[9] or MOLREP^[10] using

the structure of mouse OGG1 (PDB ID: 6G3Y) with all ligands and waters removed, as the search model. Several rounds of manual model building and refinement were performed using COOT^[11] and REFMAC5^[12] during which waters and ligands were incorporated into the structures.

NanoDSF

Buffer (HEPES 200 mM + NaCl 300 mM + Glycerol 30%) and pH solution was prepared for pH 6.7, 7.5, 7.7, 8 and 8.3. Protein solution was prepared at protein stock solution (42.5 μ M) + 9.3 μ L reaction buffer at desired pH. DMSO controls were included. The reaction solutions were taken up by capillary tubes and melted in a process with constant increment of 2.5°C from 0°C to 90°C in a Prometheus (Nano Temper Technologies). The scattering of protein from the melting process was plotted, as well as the first derivatives of the scatterings.

DSF-based selectivity screening against OGG1 and a curated kinase library

The assay was performed as previously described.^[13,14] Briefly, protein kinase domains at a concentration of 2 μ M were mixed with 10 μ M compound in a buffer containing 20 mM HEPES, pH 7.5, and 500 mM NaCl. Conditions for OGG1 were as reported previously.^[15] SYPRO Orange (5000 \times , Invitrogen) was added as a fluorescence probe (1 μ L per mL). Subsequently, temperature-dependent protein unfolding profiles were measured using the QuantStudio™ 5 Realtime PCR machine (Thermo Fisher). Excitation and emission filters were set to 465 nm and 590 nm, respectively. The temperature was raised with a step rate of 3°C per minute. Data points were analysed with the internal software (Thermal Shift Software™ Version 1.4, Thermo Fisher) using the Boltzmann equation to determine the inflection point of the transition curve.

Selectivity screen against other glycosylases and NUDIX enzymes

The compounds were tested at a concentration of 99 μ M in biochemical assays following a similar protocol as for the OGG1 biochemical readout, using the respective enzyme and the labelled enzyme substrate. Glycosylase inhibition was monitored in a kinetic mode and calculated in percent in relation to the DMSO control. The experiment was performed in duplicates for each compound. For NUDT5, NUDT15 and NUDT22, a malachite green assay was conducted, using a previously described protocol.^[16-18]

Resazurin cell viability assay with BJ-hTERT and BJ-hTERT SV40RAS cells for toxicity testing in a dose-response manner

Prior to cell-seeding, compounds **3**, **10**, **12** and **14** were dispensed in 384-well cell culture plates using an Echo acoustic liquid handler. Dose response curves were dispensed in duplicates from 100 μM to 0.09 μM . BJ-hTERT and BJ-hTERT SV40RAS cells were cultured in DMEM Glutamax + 10% FBS + 50U/50 $\mu\text{g}/\text{mL}$ Penicillin/Streptomycin and were seeded in the cell culture plates containing the nano-dispensed compounds to concentrations of 1200 cells/well (BJ-hTERT) and 600 cells/well (BJ-hTERT SV40RAS) using a Multidrop Combi reagent dispenser. After incubation for 72 hours at 37°C, Resazurin (59 $\mu\text{g}/\text{mL}$ in PBS/ 10 $\mu\text{L}/\text{well}$) was added and the plates were incubated for a further 4-7 hours at 37°C before performing a fluorescence readout on a Hidex Sense microplate reader.

Immunofluorescence analysis (γH2AX and 8-OxoG)

Cells were seeded on coverslips in 24-well plates (25,000 cells per well). After the treatments, cells were fixed with 3.7% PFA for 10 min. Permeabilization was performed by incubation with 0.5% Triton X-100 in PBS for 15 min. Cells were washed with PBS twice and blocked for 1 hour at room temperature with a blocking solution (3% BSA complemented with 0.1% Tween-20 in PBS). Cells were incubated overnight with the primary antibody in a blocking solution (γH2AX : 05-636; Millipore). Cells were washed three times with PBS-Tween 20 (0.1%) and incubated with a secondary antibody diluted in a blocking solution for 1 hour at room temperature in the dark. Cells were washed three times with PBS-Tween 20 (0.1%), and nuclei were stained with 0.5 $\mu\text{g}/\text{mL}$ DAPI. Coverslips were washed three times (10 min in PBS each time) and mounted. Image acquisition was performed with a Zeiss Axio Observer / Cell Observer. Coverslips were scanned, and 25 fields were acquired at 20X. The nuclear fluorescence signal of γH2AX was determined using Cell Profiler®.

Relative AP-site quantification by FACS

A total of 100,000 cells were seeded in a p35 petri dish. Cells were exposed to 40 mM of KBrO_3 for 1 hour in the presence of compounds or vehicle (DMSO). Afterward, fresh media containing compounds or DMSO was added. ARP (N-(aminooxyacetyl)-N'-(D-Biotinoyl) hydrazine (ref: A10550) was then added in a concentration of 1 mM, for a period of 3 hours. The cells were fixed and permeabilized using eBioscience™ Foxp3 / Transcription Factor Staining Buffer Set according to the manufacturer's instructions (00-5523-00). The cells were then incubated with Streptavidin-PE Conjugate antibody (1:500) or Vari Fluor 555-Streptavidin. Labeled cells were analyzed in a FACS Canto II cytometer and each condition was run in biological triplicates. FloJo software analysis was used to calculate the ARP-Streptavidin-FITC geometrical mean signal intensity. Graphs were plotted using Graphpad Prism.

Colony formation assays

The U2OS cell line was seeded and grew in 80% subconfluence in a p100. Cells were treated with 40 mM of KBrO₃ for 1 hour, or not (control). Cells were trypsinized, counted, and seeded in p35 plates at 400 cells per well and incubated overnight with TH10785, **14**, **10** or DMSO. After that, cells were allowed to grow in fresh media until colony size surpassed 50 cells in the control, followed by medium removal and the addition of 4% (w/v) methylene blue in methanol. Following washing with tap water and air drying, colonies with >50 cells were counted.

Statistics

Unless stated otherwise, all biochemical assays were performed in three independent replicates with triplicates in each experiment. In cell biology experiments, each bar represents the mean \pm SD. Data are the average of three biological replicates. Statistical significance was calculated using an unpaired two-tailed Student's t-test. ns, nonsignificant; *P < 0.05; **P < 0.01; ***P < 0.001. ****P < 0.0001

General Information Chemical Synthesis

All reagents and solvents were purchased from commercial vendors and used without further purification. Unless otherwise stated, reactions were performed without care to exclude air or moisture. Analytical thin-layer chromatography was performed on silica gel 60 Å F-254 plates (E. Merck) and visualized under a UV lamp. Flash column chromatography was performed in a Biotage® SP1 MPLC system using Fisher Chemical silica gel 60 Å. ¹H and ¹³C NMR spectra were recorded on Bruker DRX-400 MHz or Bruker Ascend 400 MHz spectrometers. Chemical shifts are expressed in parts per million (ppm) and referenced to the residual solvent peak (¹H: δ 7.26 for CDCl₃, δ 2.50 for DMSO-*d*₆, δ 3.31 for methanol-*d*₄; ¹³C: δ 29.84 for CDCl₃, δ 39.52 for DMSO-*d*₆, δ 49.00 for methanol-*d*₄). Analytical LC-MS were performed either on an Agilent MSD mass spectrometer connected to an Agilent 1100 system or an Agilent 1260 infinity II with a G6125B mass spectrometer. Columns used were ACE 3 C8 (50 x 3.0 mm); H₂O (+ 0.1% TFA) and MeCN were used as mobile phases at a flow rate of 1 mL/min, or Xterra MSC18 (50 x 3.0 mm) column where H₂O (10 mM NH₄HCO₃; pH = 10) and MeCN were used as mobile phases at a flow rate of 1 mL/min. For LC-MS, detection was made by UV and MS (ESI+). Preparative LC was performed on a Gilson system using Waters C18 OBD 5 μm column (30 x 75 mm) with water buffer (50 mM NH₄HCO₃ at pH 10) and MeCN as mobile phases using a flow rate of 45 mL/min or ACE 5 C8 (100 x 21.2 mm) column with water buffer (0.1 % TFA) and MeCN as mobile phases using a flow rate of 30 mL/min. All final compounds were assessed to be >95% pure by LC-MS analysis. Compounds in our nucleobase/nucleoside/nucleotide and prior art screening set were not resynthesized and no characterization was performed. Compounds available through NCI DTP were not resynthesized and no characterization was performed. High-resolution mass spectra (HRMS) were measured with EI or ESI ionization. A chromatographic purification was performed before each measurement. The Thermo Q-Exactive plus device for ESI-mass spectra was coupled to a binary UHPLC system. For EI-measurement, a GC-system was coupled to the Thermo Q-Exactive GC device.

General procedure A for the nucleophilic substitution with anilines or pyridine-3-amines

In a 10 mL reaction tube, the appropriate chloride and 1 – 2 equiv. of the corresponding aniline or pyridine-3-amine were dissolved in 1 – 2 mL of 2,2,2-trifluoroethanol (TFE). To the stirred solution, 1 – 2 equiv. of trifluoroacetic acid (TFA) were added dropwise. The reaction tube was flushed with N₂ and the reaction mixture was stirred at 80 °C for 2 – 48 h. After completion, the reaction was quenched with the respective amount of *N,N*-diisopropylethylamine (DIPEA; 1 equiv. per 1 equiv. of TFA), the solvent was removed under reduced pressure and the product was purified as stated in the descriptions below.

General procedure B for the nucleophilic substitution with amines

In a 10 mL reaction tube, the appropriate chloride and 1 – 2 equiv. of the corresponding amine were dissolved in 1-2 mL of N,N-dimethylformamide (DMF). To the stirred solution, 1 – 2 equiv. of DIPEA were added and the reaction mixture was stirred at 80 – 100 °C for 12 – 48 h. After completion, the solvent was removed under reduced pressure, and the product was purified as stated in the description below.

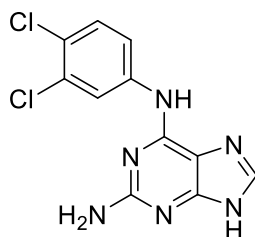
General procedure C for the nucleophilic substitution with thiols

In a 10 mL reaction tube, the appropriate chloride and 1 – 2 equiv. of the thiol were dissolved in 1 – 2 mL of DMF. 1 – 2 equiv. of K₂CO₃ were added, the tube was flushed with N₂, and the reaction mixture was stirred at 80 – 100 °C for 12 – 48 h. After completion, the remaining solids were filtered off, the solvent was evaporated under reduced pressure and the residue was purified as stated in the description below.

General procedure D for the alkylation of 2-amino-6-chloropurine.

Step 1: A mixture of the corresponding carboxylic acid (1.5 mmol), 4-dimethylaminopyridine (DMAP; 1.8 mg, 0.015 mmol), N-hydroxyphthalimide (240 mg, 1.5 mmol), and diisopropylcarbodiimide (0.23 mL, 1.5 mmol) were dissolved in DMSO (2.0 mL). N₂ was then bubbled through the solution for 2 – 3 min. The vial was closed, and the mixture was stirred at 20 °C for 16 h. The mixture was used in the next step without purification.

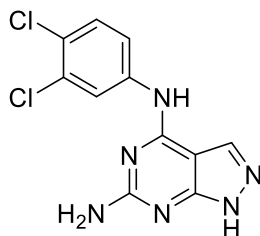
Step 2: In a 10 mL vial, 2-amino-6-chloropurine (170 mg, 1.0 mmol), 4CzIPN (7.9 mg, 0.010 mmol), and TFA (0.076 mL, 1.0 mmol) were dissolved in DMSO (2.0 mL), then the DMSO solution of the corresponding phthalimide carboxylate from step 1 was added. After this, N₂ was violently bubbled through the mixture for 5 min. The vial was sealed and illuminated (365 nm, 50 W) for 16 h under stirring. The reaction mixture was poured into aq. NaHCO₃ (10 mL) and was subsequently extracted with DCM (10 mL × 3). The combined organics were concentrated and purified by silica gel chromatography.



(11): N6-(3,4-dichlorophenyl)-9H-purin-2,6-diamine

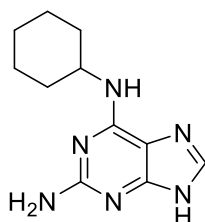
The compound was synthesised according to General procedure A from 2-amino-6-chloro-9H-purine (20 mg, 0.12 mmol) and 3-methoxyaniline (20 mg, 0.12 mmol). Recrystallisation from methanol yielded the product as a white solid (27 mg, 75%). LCMS [M+H]⁺ 295. ¹H-NMR (400 MHz, DMSO-*d*₆) δ 8.39 (d, *J* = 2.5 Hz, 1H), 8.06 (dd, *J* =

8.9, 2.6 Hz, 1H), 7.48 (d, $J = 8.9$ Hz, 1H), 7.31 (s, 1H), 7.18 (s, 1H), 7.05 (s, 1H). ^{13}C NMR (151 MHz, $\text{DMSO-}d_6 + 4\% \text{H}_2\text{SO}_4$) δ 154.3, 150.2, 148.6, 142.4, 138.4, 131.4, 130.8, 126.2, 122.3, 121.2, 106.2. HRMS (ESI⁺): m/z calculated 295.0260 for $\text{C}_{11}\text{H}_9\text{N}_6\text{Cl}_2$, found 295.0259 ($[\text{M}+\text{H}]^+$).



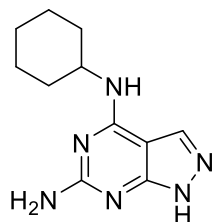
(12): *N4-(3,4-dichlorophenyl)-1H-pyrazolo[3,4-d]pyrimidin-4,6-diamine*

The compound was synthesised according to General procedure A from 4-chloro-1H-pyrazolo[3,4-d]pyrimidin-6-amine (17 mg, 0.10 mmol) and 3,4-dichloroaniline (22 mg, 0.14 mmol). Recrystallisation from methanol yielded the product as a yellowish solid (8 mg, 27%). LCMS $[\text{M}+\text{H}]^+$ 295. ^1H -NMR (400 MHz, $\text{DMSO-}d_6$) δ 8.34 (s, 1H), 7.99 (d, $J = 9.5$ Hz, 1H), 7.64 (d, $J = 8.9$ Hz, 2H). ^{13}C NMR (151 MHz, $\text{DMSO-}d_6 + 4\% \text{H}_2\text{SO}_4$) δ 156.7, 156.2, 149.4, 138.1, 131.2, 130.6, 128.5, 126.7, 123.5, 122.2, 97.4. HRMS (ESI⁺): m/z calculated 295.0260 for $\text{C}_{11}\text{H}_9\text{N}_6\text{Cl}_2$, found 295.0258 ($[\text{M}+\text{H}]^+$).



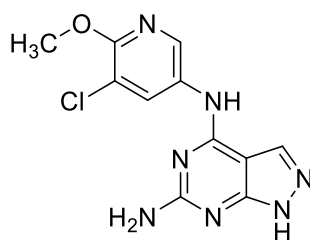
(13): *N6-cyclohexyl-9H-purin-2,6-diamine*

The compound was synthesised according to General procedure B from 2-amino-6-chloro-9H-purine (20 mg, 0.12 mmol) and cyclohexylamine (23 μL , 0.20 mmol). Purification by preparative HPLC (0.1% TFA in water/ acetonitrile) yielded the product as a white solid (6 mg, 14%). LCMS $[\text{M}+\text{H}]^+$ 233. ^1H -NMR (400 MHz, $\text{DMSO-}d_6$) δ 8.51 (s, 1H), 8.13 (s, 1H), 7.49 (s, 1H), 4.06 (s, 1H), 1.97 – 1.87 (m, 1H), 1.82 – 1.71 (m, 3H), 1.66 – 1.58 (m, 1H), 1.39 – 1.17 (m, 6H). ^{13}C NMR (151 MHz, $\text{DMSO-}d_6 + 4\% \text{H}_2\text{SO}_4$) δ 154.1, 151.4, 147.3, 141.7, 105.3, 49.8, 32.2, 25.3, 24.8. HRMS (ESI⁺): m/z calculated 233.1509 for $\text{C}_{11}\text{H}_{16}\text{N}_6$, found 233.1500 ($[\text{M}+\text{H}]^+$).



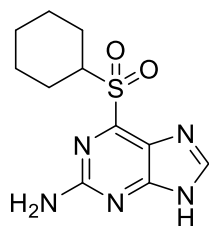
(14): *N4-cyclohexyl-1H-pyrazolo[3,4-d]pyrimidin-4,6-diamine*

The compound was synthesised according to General procedure B from 4-chloro-1*H*-pyrazolo[3,4-*d*]pyrimidin-6-amine (18 mg, 0.10 mmol) and cyclohexylamine (23 μ L, 0.20 mmol). Purification by preparative HPLC (50 mM NH_4HCO_3 pH 10/ acetonitrile) yielded the product as a white solid (3 mg, 14%). LCMS $[\text{M}+\text{H}]^+$ 233. $^1\text{H-NMR}$ (400 MHz, CDCl_3) δ 7.68 (s, 1H), 2.02 – 1.92 (m, 3H), 1.76 – 1.68 (m, 3H), 1.66 – 1.58 (m, 2H), 1.38 – 1.13 (m, 3H). $^{13}\text{C NMR}$ (151 MHz, $\text{DMSO-}d_6$ + 4% H_2SO_4) δ 157.3, 156.3, 149.4, 128.2, 96.7, 50.0, 32.1, 25.3, 25.1. HRMS (ESI $^+$): m/z calculated 233.1509 for $\text{C}_{11}\text{H}_{16}\text{N}_6$, found 233.1523 ($[\text{M}+\text{H}]^+$).



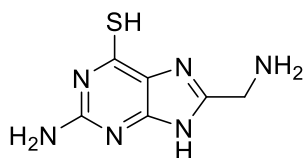
(15) *N4-(5-chloro-6-methoxy-pyridin-3-yl)-1H-pyrazolo[3,4-d]pyrimidine-4,6-diamine*

The compound was synthesised according to General procedure A from 4-chloro-1*H*-pyrazolo[3,4-*d*]pyrimidin-6-amine (18 mg, 0.10 mmol) and 5-chloro-6-methoxy-pyridin-3-amine (23 mg, 0.14 mmol). Purification by preparative HPLC (50 mM NH_4HCO_3 pH 10/ acetonitrile) yielded the product as a white solid (16 mg, 56%). LCMS $[\text{M}+\text{H}]^+$ 292. $^1\text{H-NMR}$ (400 MHz, $\text{DMSO-}d_6$) δ 12.63 (s, 1H), 9.65 (s, 1H), 8.72 (d, $J = 2.4$ Hz, 1H), 8.40 (d, $J = 2.4$ Hz, 1H), 7.95 (s, 2H), 6.38 (s, 1H), 3.93 (s, 3H). $^{13}\text{C NMR}$ (176 MHz, $\text{DMSO-}d_6$) δ 161.9, 157.6, 154.2, 153.9, 136.4, 132.2, 131.9, 131.2, 115.8, 95.3, 54.0. HRMS (ESI $^+$): m/z calculated 292.0708 for $\text{C}_{11}\text{H}_{10}\text{ClN}_7\text{O}$, found 292.0711 ($[\text{M}+\text{H}]^+$).



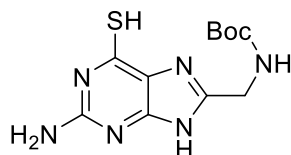
(S15) 6-(Cyclohexylsulfonyl)-9H-purin-2-amine

A mixture of 6-(cyclohexylthio)-9H-purin-2-amine (0.10 mmol) and mCPBA (0.20 mmol) was stirred in DCM (2.0 mL) for 3 hours at room temperature. The reaction mixture was then purified by silica gel chromatography using a gradient of MeOH (0 – 15%) in DCM which afforded 4 mg (14%) of the title compound. LCMS $[M+H]^+$ 282. 1H -NMR (400 MHz, DMSO- d_6) δ 11.95 (br. s., 3H), 8.45 (s, 1H), 6.09 – 8.10 (m, 1H), 3.75 (tt, $J = 3.3, 11.9$ Hz, 1H), 1.88 – 1.96 (m, 2H), 1.75 – 1.85 (m, 2H), 1.58 – 1.67 (m, 1H), 1.47 (dd, $J = 2.9, 12.2$ Hz, 1H), 1.40 (dd, $J = 3.1, 12.2$ Hz, 1H), 1.09 – 1.32 (m, 3H). ^{13}C NMR (176 MHz, DMSO- d_6) δ 159.85, 157.40, 152.31, 143.67, 121.93, 59.68, 24.84, 24.40, 24.11. HRMS (ESI $^+$): m/z calculated 282.1019 for $C_{11}H_{15}N_5O_2S$ found 282.1017 ($[M+H]^+$).



(S25) 2-Amino-8-(aminomethyl)-6,9-dihydro-3H-purine-6-thione

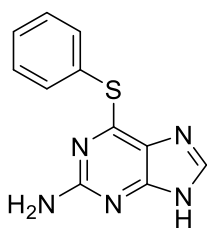
Tert-butyl N-[(2-amino-6-sulfanylidene-6,9-dihydro-3H-purin-8-yl)methyl]carbamate (**S26**, 25 mg, 0.084 mmol) was suspended in DCM (1 mL), then TFA (1 mL) was added. After 1 hours the solvents were evaporated and the crude compound was triturated using EtOH. The title compound was collected by filtration, no further purification was done. Yield 12 mg (72%). LCMS $[M+H]^+$ 197. 1H -NMR (400 MHz, DMSO- d_6) δ 12.05 (br. s., 1H), 8.53 (br. s., 3H), 6.70 (br. s., 2H), 4.16 (br. s., 2H). ^{13}C NMR (176 MHz, DMSO - d_6) δ 158.26, 158.08, 153.25, 118.02, 116.32, 36.27. HRMS (ESI $^+$): m/z calculated 197.0604 for $C_6H_8N_6S$ found 197.0610 ($[M+H]^+$).



(S26): *Tert-butyl N-[(2-amino-6-sulfanylidene-6,9-dihydro-3H-purin-8-yl)methyl]carbamate*

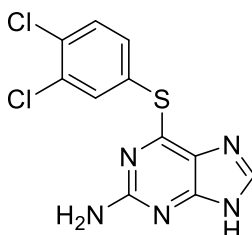
Step 1. *tert-butyl N-[(2-amino-6-chloro-9H-purin-8-yl)methyl]carbamate* was synthesized according to General procedure D from *N*-Boc glycine which afforded 100 mg (33%). LCMS $[M+H]^+$ 299. 1H -NMR (400 MHz, $DMSO-d_6$) δ 12.70 (s, 1H), 7.35 (br. s., 1H), 6.70 (s, 2H), 4.25 (d, $J = 5.6$ Hz, 2H), 1.41 (s, 9H).

Step 2: A mixture of *tert-butyl N-[(2-amino-6-chloro-9H-purin-8-yl)methyl]carbamate* (45 mg, 0.15 mmol), thiourea (45 mg, 0.60 mmol), and formic acid (0.015 mL, 0.39 mmol) was stirred in EtOH (1.0 mL) at reflux for 3 h. After cooling, the precipitate was collected by filtration and washed with aq. ethanolic solution (70 %). No further purification was done. Yield 25 mg (56%). LCMS $[M+H]^+$ 297. 1H -NMR (400 MHz, $DMSO-d_6$) δ 12.42 (br. s., 1H), 11.81 (br. s., 1H), 7.27 (br. s., 1H), 6.63 (br. s., 1H), 6.45 (br. s., 1H), 4.12 – 4.27 (m, 2H), 1.39 (br. s., 9H). HRMS (ESI⁺): m/z calculated 297.1128 for $C_{11}H_{16}N_6O_2S$ found 297.1149 ($[M+H]^+$).



(S38) *6-(phenylthio)-9H-purin-2-amine*

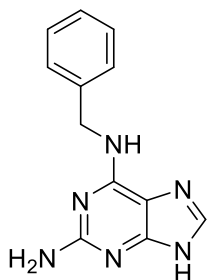
The title compound was synthesized according to Huang, *et. al.* Tetrahedron 2007, 63, 5323–5327.



(S39) *6-(3,4-dichlorophenyl)sulfanyl-9H-purin-2-amine*

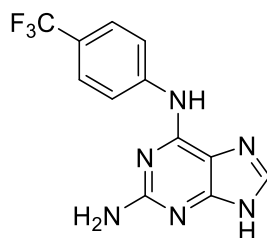
The compound was synthesised according to General procedure C from 2-amino-6-chloro-9H-purine (84 mg, 0.50 mmol) and 3,4-dichlorothiophenol (90 mg, 0.50 mmol). Purification on silica (DCM/MeOH

gradient method) yielded the product as a white solid (21 mg, 13%). LCMS $[M+H]^+$ 312. $^1\text{H-NMR}$ (400 MHz, $\text{DMSO-}d_6$) δ 12.61 (s, 1H), 7.96 (s, 1H), 7.88 (d, $J = 2.1$ Hz, 1H), 7.70 (d, $J = 8.4$ Hz, 1H), 7.59 (dd, $J = 8.4, 2.1$ Hz, 1H), 6.30 (s, 2H). $^{13}\text{C NMR}$ (151 MHz, $\text{DMSO-}d_6$) δ 159.74, 156.50, 152.56, 139.71, 135.85, 134.91, 131.86, 131.39, 130.92, 129.19, 123.53. HRMS (ESI+): m/z calculated 311.9872 for $\text{C}_{11}\text{H}_7\text{Cl}_2\text{N}_5\text{S}$ found 311.9870 ($[M+H]^+$).



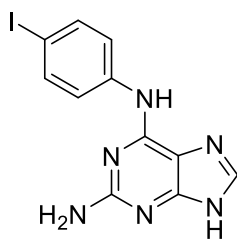
(S40) *N6-benzyl-9H-purin-2,6-diamine*

The compound was synthesised according to General procedure B from 2-amino-6-chloro-9H-purine (34 mg, 0.20 mmol) and benzylamine (55 μL , 0.40 mmol). Purification by preparative HPLC (0.1% TFA in water/ acetonitrile) yielded the product as a white solid (13 mg, 19%). LCMS $[M+H]^+$ 241. $^1\text{H-NMR}$ (400 MHz, $\text{Methanol-}d_4$) δ 8.03 (s, 1H), 7.43 – 7.39 (m, 2H), 7.38 – 7.33 (m, 2H), 7.32 – 7.27 (m, 1H), 4.82 (s, 2H). $^{13}\text{C NMR}$ (176 MHz, $\text{DMSO-}d_6$) δ 160.16, 140.70, 135.24, 128.67, 128.61, 128.33, 128.08, 127.26, 126.44, 42.55. HRMS (ESI+): m/z calculated 241.1196 for $\text{C}_{12}\text{H}_{12}\text{N}_6$ found 241.1182 ($[M+H]^+$).



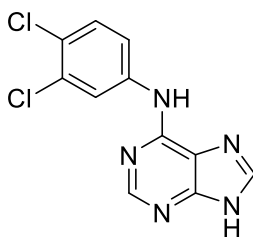
(S44) *N6-[4-(trifluoromethyl)phenyl]-9H-purin-2,6-diamine*

The compound was synthesised according to General procedure A from 2-amino-6-chloro-9H-purine (20 mg, 0.12 mmol) and 4-trifluoromethylaniline hydrochloride (25 mg, 0.13 mmol). Purification by preparative HPLC (0.1% TFA in water/acetonitrile) yielded the product as a white solid (19 mg, 53%). LCMS $[M+H]^+$ 295. $^1\text{H-NMR}$ (400 MHz, $\text{DMSO-}d_6$) δ 11.45 (s, 1H), 8.38 (s, 1H), 8.23 (d, $J = 8.3$ Hz, 2H), 7.73 (d, $J = 8.1$ Hz, 2H). $^{13}\text{C-NMR}$ (176 MHz, $\text{DMSO-}d_6$) δ 154.45, 150.04, 148.88, 141.98, 126.61, 125.96, 125.94, 125.06, 124.11, 123.52, 120.75. HRMS (ESI+): m/z calculated 295.0914 for $\text{C}_{12}\text{H}_9\text{F}_3\text{N}_6$ found 295.0917 ($[M+H]^+$).



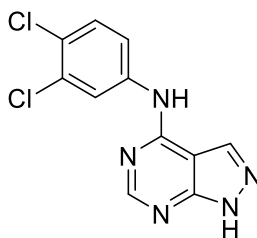
(S45): *N6-(4-iodophenyl)-9H-purin-2,6-diamine*

The compound was synthesised according to General procedure A from 2-amino-6-chloro-9*H*-purine (26 mg, 0.16 mmol) and 4-iodoaniline (45 mg, 0.20 mmol). Recrystallisation from methanol yielded the product as a white solid (19 mg, 25%). LCMS $[M+H]^+$ 353. 1H -NMR (400 MHz, DMSO- d_6) δ 12.44 (br. s., 1H), 9.61 (br. s., 1H), 7.79 – 8.00 (m, 3H), 7.60 (d, $J = 8.5$ Hz, 2H), 6.21 (br. s., 2H). ^{13}C NMR (151 MHz, DMSO- d_6 + 4% H_2SO_4) δ 154.4, 150.5, 148.6, 142.7, 138.3, 138.0, 124.0, 106.4, 89.3. HRMS (ESI+): m/z calculated 351.9928 for $C_{11}H_9IN_6$ found 353.0016 ($[M+H]^+$).



(S46) *N-(3,4-dichlorophenyl)-9H-purin-6-amine*

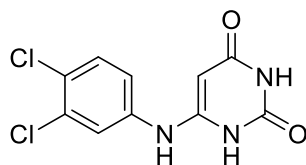
The title compound was synthesized according to Grotzfeld, Robert M.; Patel, Hitesh K.; Mehta, Shamal A.; Milanov, Zdravko V.; Lai, Andiliy G.; et al United States, US20050153989.



(S47) *N-(3,4-dichlorophenyl)-1H-pyrazolo[3,4-d]pyrimidin-4-amine*

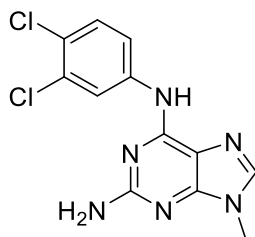
The title compound was synthesized from 4-chloro-1*H*-pyrazolo[3,4-*d*]pyrimidine (16 mg, 0.10 mmol) and 3,4-dichloroaniline (23 mg, 0.14 mmol) according to General procedure A affording 10 mg (35%). LCMS $[M+H]^+$ 281. 1H -NMR (400 MHz, DMSO- d_6) δ 13.76 (br. s., 1H), 10.23 (s, 1H), 8.49 (s, 1H), 8.39

(d, $J = 2.4$ Hz, 1H), 8.33 (s, 1H), 7.83 (dd, $J = 2.4, 8.8$ Hz, 1H), 7.67 (d, $J = 8.8$ Hz, 1H). ^{13}C NMR (176 MHz, DMSO- d_6) δ 155.02, 154.67, 153.75, 139.64, 132.28, 130.85, 130.54, 124.27, 121.61, 120.43, 100.82. HRMS (ESI+): m/z calculated 280.0149 for $\text{C}_{11}\text{H}_8\text{N}_5\text{Cl}_2$, found 280.0151 ($[\text{M}+\text{H}]^+$).



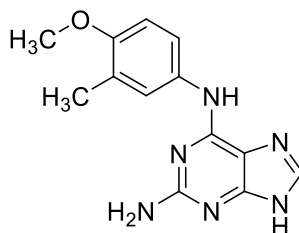
(S48) 6-((3,4-dichlorophenyl)amino)pyrimidine-2,4(1H,3H)-dione

The title compound was synthesized according to J.M. Wilson, *et. al.*, Bioorg. Med. Chem. 15 (1) (2007) 77-86.



(S49) N6-(3,4-dichlorophenyl)-9-methyl-9H-purine-2,6-diamine

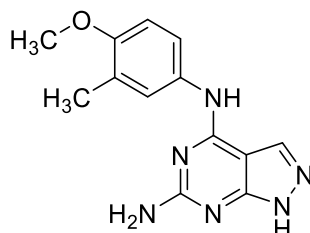
The title compound was synthesized from 6-chloro-9-methyl-9H-purin-2-amine (18 mg, 0.10 mmol) and 3,4-dichloroaniline (23 mg, 0.14 mmol) according to General procedure A. Purification by preparative HPLC (50 mM NH_4HCO_3 pH 10/ acetonitrile) yielded the product as a white solid (33%). ^1H -NMR (400 MHz, DMSO- d_6) δ 9.72 (s, 1H), 8.38 (d, $J = 2.1$ Hz, 1H), 8.07 (dd, $J = 2.3, 8.9$ Hz, 1H), 7.85 (s, 1H), 7.47 (d, $J = 8.9$ Hz, 1H), 6.28 (br. s., 2H), 3.60 (s, 3H). ^{13}C NMR (151 MHz, DMSO- d_6 + 4% H_2SO_4) δ 155.9, 151.5, 145.3, 139.9, 138.4, 131.2, 130.7, 126.0, 123.1, 121.9, 110.2, 31.2. HRMS (ESI+): m/z calculated 309.0417 for $\text{C}_{12}\text{H}_{10}\text{Cl}_2\text{N}_6$, found 309.0426 ($[\text{M}+\text{H}]^+$).



(S50) N6-(4-methoxy-3-methylphenyl)-9H-purin-2,6-diamine

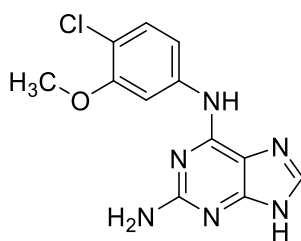
The compound was synthesised according to General procedure A from 2-amino-6-chloro-9H-purine (18 mg, 0.11 mmol) and 4-methoxy-3-methylaniline (16 mg, 0.12 mmol). Purification by preparative HPLC (50 mM NH_4HCO_3

pH 10/ acetonitrile) yielded the product as a white solid (12 mg, 40%). LCMS $[M+H]^+$ 271. 1H NMR (400 MHz, DMSO- d_6) δ 12.20 (br. s., 1H), 8.97 (s, 1H), 7.68 – 7.79 (m, 3H), 6.83 (d, J = 8.5 Hz, 1H), 5.88 (br. s., 2H), 3.76 (s, 3H), 2.16 (s, 3H). ^{13}C NMR (151 MHz, DMSO- d_6 + 4% H_2SO_4) δ 155.1, 154.0, 150.3, 148.0, 142.4, 130.3, 126.4, 124.9, 121.1, 110.7, 106.0, 55.8, 16.5. HRMS (ESI+): m/z calculated 271.1302 for $C_{13}H_{14}N_6O$, found 271.1331 ($[M+H]^+$).



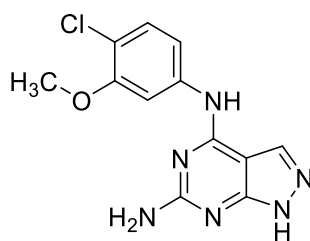
(S51) *N4-(4-methoxy-3-methylphenyl)-1H-pyrazolo[3,4-d]pyrimidin-4,6-diamine*

The compound was synthesised according to General procedure A from 4-chloro-1H-pyrazolo[3,4-d]pyrimidin-6-amine (17 mg, 0.10 mmol) and 4-methoxy-3-methylaniline (23 mg, 0.17 mmol). Purification by preparative HPLC (50 mM NH_4HCO_3 pH 10/ acetonitrile) yielded the product as a white solid (8 mg, 31%). LCMS $[M+H]^+$ 271. 1H -NMR (400 MHz, DMSO- d_6) δ 12.51 (s, 1H), 9.23 (s, 1H), 7.78 (s, 1H), 7.62 – 7.56 (m, 2H), 6.88 (d, J = 8.8 Hz, 1H), 6.14 (s, 2H), 3.78 (s, 3H), 2.17 (s, 3H). ^{13}C -NMR (101 MHz, DMSO- d_6) δ 156.6, 156.5 (overlap), 155.3, 149.4, 130.5, 128.4, 126.2, 125.5, 121.9, 110.6, 97.5, 55.9, 16.6. HRMS (ESI+): m/z calculated 271.1302 for $C_{13}H_{15}N_6O$, found 271.1300 ($[M+H]^+$).



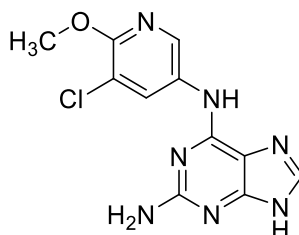
(S52) *N6-(4-chloro-3-methoxyphenyl)-9H-purin-2,6-diamine*

The compound was synthesised according to General procedure A from 19.7 mg 2-amino-6-chloro-9H-purine (20 mg, 0.12 mmol) and 4-chloro-3-methoxyaniline (21 mg, 0.14 mmol). Recrystallisation from methanol yielded the product as a white solid (33 mg, 95%). LCMS $[M+H]^+$ 291. 1H -NMR (400 MHz, DMSO- d_6) δ 7.93 (s, 1H), 7.57 (dd, J = 8.7, 2.4 Hz, 1H), 7.32 (d, J = 8.6 Hz, 1H), 7.29 (s, 1H), 7.16 (s, 1H), 7.03 (s, 1H), 3.88 (s, 3H). ^{13}C NMR (151 MHz, DMSO- d_6 + 4% H_2SO_4) δ 154.7, 154.2, 150.2, 148.4, 142.3, 138.3, 129.9, 116.6, 114.0, 106.1, 56.4. HRMS (ESI+): m/z calculated 291.0756 for $C_{12}H_{12}N_6OCl$, found 291.0754 ($[M+H]^+$).



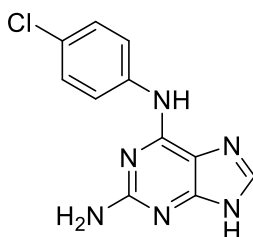
(S53): *N4-(4-chloro-3-methoxyphenyl)-1H-pyrazolo[3,4-d]pyrimidin-4,6-diamine*

The compound was synthesised according to General procedure A from 4-chloro-1H-pyrazolo[3,4-d]pyrimidin-6-amine (18 mg, 0.10 mmol) and 4-chloro-3-methoxyaniline (25 mg, 0.16 mmol). Recrystallisation from methanol yielded the product as a yellowish solid (11 mg, 37%). LCMS $[M+H]^+$ 291. $^1\text{H-NMR}$ (400 MHz, $\text{DMSO-}d_6$) δ 11.27 (s, 1H), 8.81 (s, 1H), 8.13 – 7.70 (m, 2H), 7.56 – 7.35 (m, 2H), 6.52 (s, 1H), 3.91 (s, 3H). $^{13}\text{C-NMR}$ (101 MHz, $\text{DMSO-}d_6$) δ 156.9, 156.7, 154.8, 149.7, 138.4, 130.0, 128.8, 117.3, 115.4, 107.6, 97.8, 56.7. HRMS (ESI+): m/z calculated 291.0756 for $\text{C}_{12}\text{H}_{12}\text{N}_6\text{OCl}$, found 291.0755 ($[M+H]^+$).



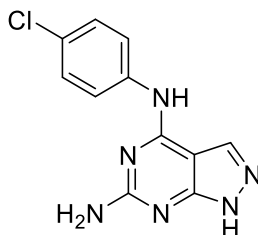
(S54): *N6-(5-chloro-6-methoxypyridin-3-yl)-9H-purine-2,6-diamine*

The compound was synthesised according to General procedure A from 2-amino-6-chloro-9H-purine (22 mg, 0.13 mmol) and 5-chloro-6-methoxy-pyridin-3-amine (20 mg, 0.13 mmol). Recrystallisation from methanol yielded the product as a white solid (20 mg, 53%). LCMS $[M+H]^+$ 292. $^1\text{H-NMR}$ (400 MHz, $\text{DMSO-}d_6$) δ 8.79 (d, $J = 2.5$ Hz, 1H), 8.42 (d, $J = 2.4$ Hz, 1H), 8.05 (s, 1H), 6.78 (s, 2H), 3.93 (s, 3H). ^{13}C NMR (151 MHz, $\text{DMSO-}d_6 + 4\% \text{H}_2\text{SO}_4$) δ 155.5, 154.1, 150.3, 148.1, 142.2, 137.7, 132.1, 129.8, 116.4, 106.3, 54.4. HRMS (ESI+): m/z calculated 292.0708 for $\text{C}_{11}\text{H}_{10}\text{ClN}_7\text{O}$, found 292.0714 ($[M+H]^+$).



(S55): *N6-(4-chlorophenyl)-9H-purin-2,6-diamine*

The compound was synthesised according to General procedure A from 2-amino-6-chloro-9*H*-purine (21 mg, 0.12 mmol) and 4-chloroaniline (17 mg, 0.13 mmol). Recrystallisation from methanol yielded the product as a white solid (24 mg, 76%). LCMS $[M+H]^+$ 261. 1H -NMR (400 MHz, DMSO- d_6) δ 12.42 (s, 1H), 9.58 (s, 1H), 8.06 (d, $J = 9.0$ Hz, 2H), 7.86 (s, 1H), 7.30 (d, $J = 9.0$ Hz, 2H), 6.15 (s, 2H). ^{13}C NMR (176 MHz, DMSO- d_6) δ 159.18, 152.57, 151.52, 139.33, 137.10, 128.12, 125.37, 121.51, 112.41. HRMS (ESI+): m/z calculated 261.0650 for $C_{11}H_9ClN_6$, found 261.0662 ($[M+H]^+$).

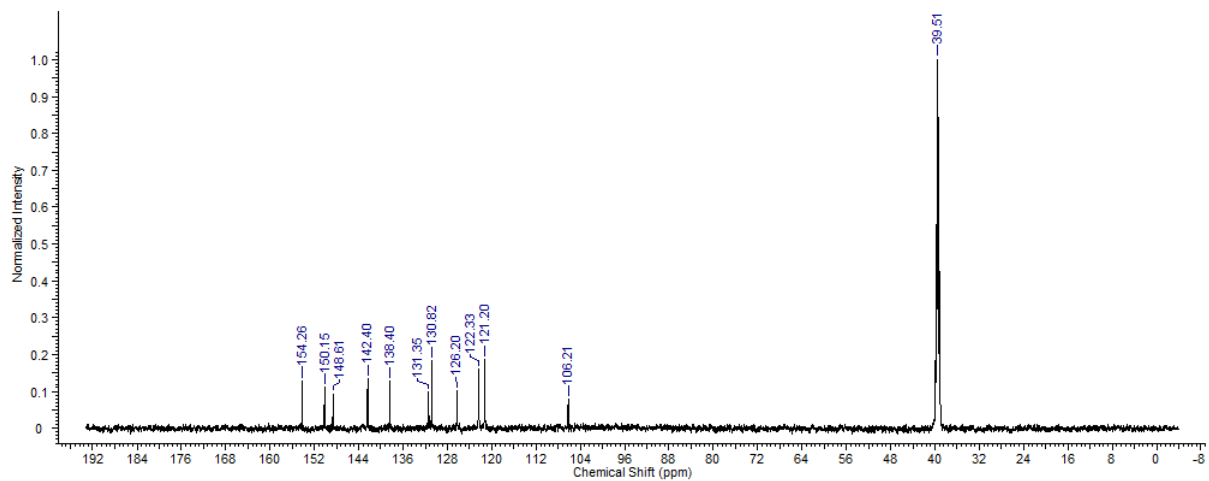
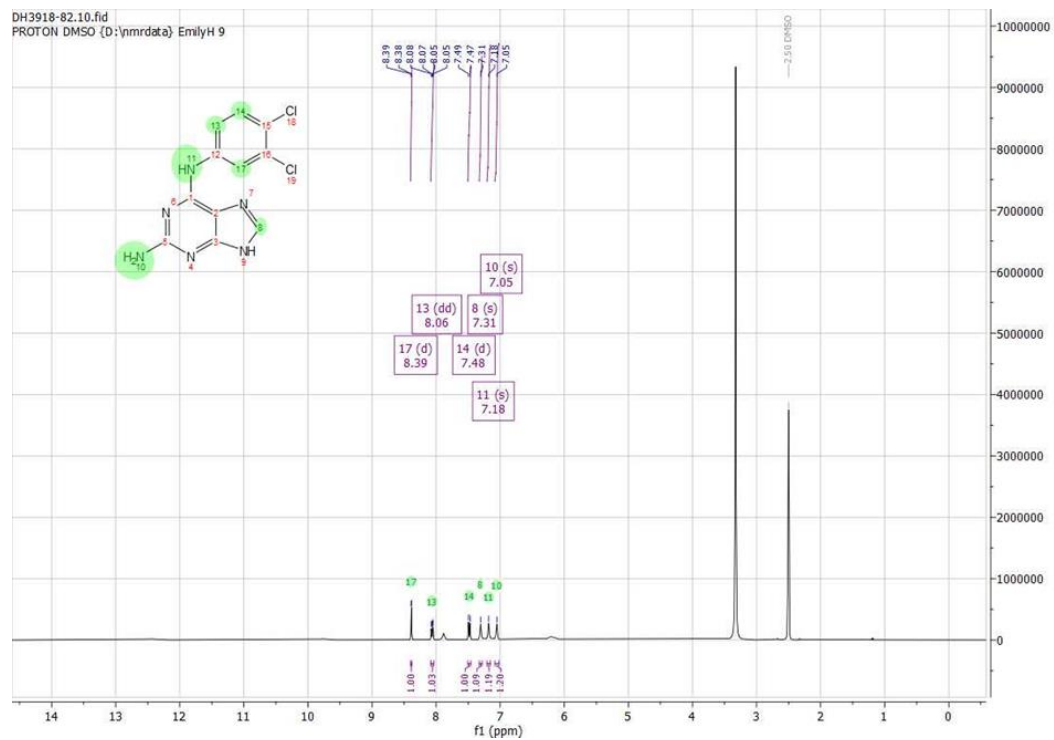


(S56): *N4-(4-chlorophenyl)-1H-pyrazolo[3,4-d]pyrimidin-4,6-diamine*

The compound was synthesised according to General procedure A from 4-chloro-1*H*-pyrazolo[3,4-*d*]pyrimidin-6-amine (18 mg, 0.11 mmol) and 4-chloroaniline (16 mg, 0.12 mmol). Recrystallisation from methanol yielded the product as a yellow solid (8 mg, 28%). LCMS $[M+H]^+$ 261. 1H -NMR (400 MHz, DMSO- d_6) δ 12.65 (s, 1H), 9.63 (s, 1H), 8.02 – 7.94 (m, 3H), 7.40 – 7.31 (m, 2H), 6.35 (s, 2H). ^{13}C -NMR (101 MHz, DMSO- d_6) δ 156.9, 156.7, 149.6, 137.4, 129.2, 129.0, 124.4, 97.7. HRMS (ESI+): m/z calculated 261.0650 for $C_{11}H_{10}N_6Cl$, found 261.0647 ($[M+H]^+$).

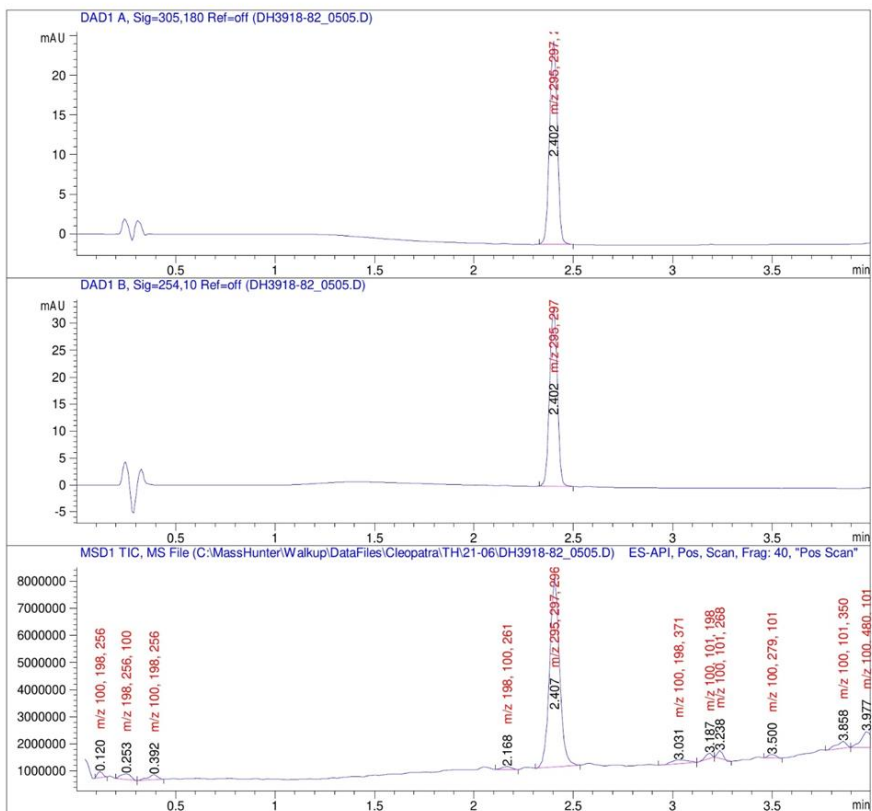
NMR Spectra and LC-UV purity:

Compound (**11**):

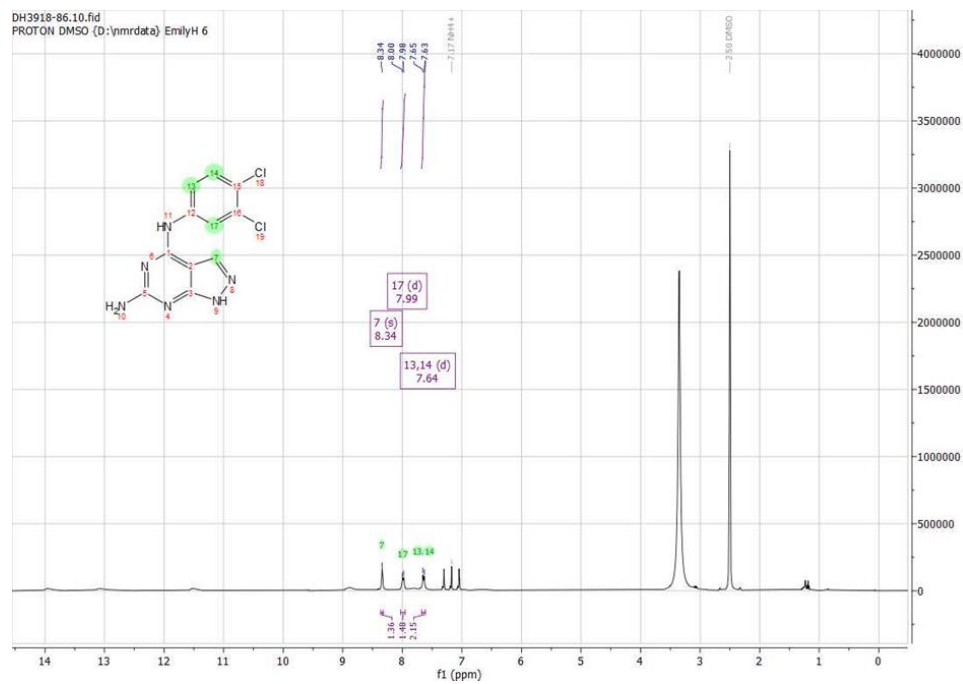


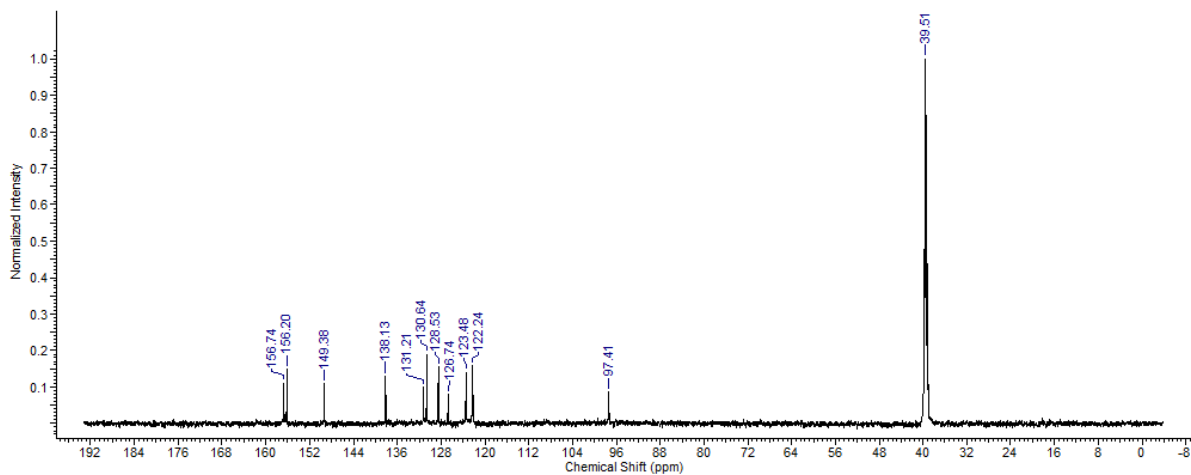
Method Info : X-bridge C18, 50x3.0 mm, 3.5u, 10-97% MeCN 3min,1mL/min, B: MeCN C: NH4HCO3

Sample Info : Walkup method: 'X1097-3'
Target:



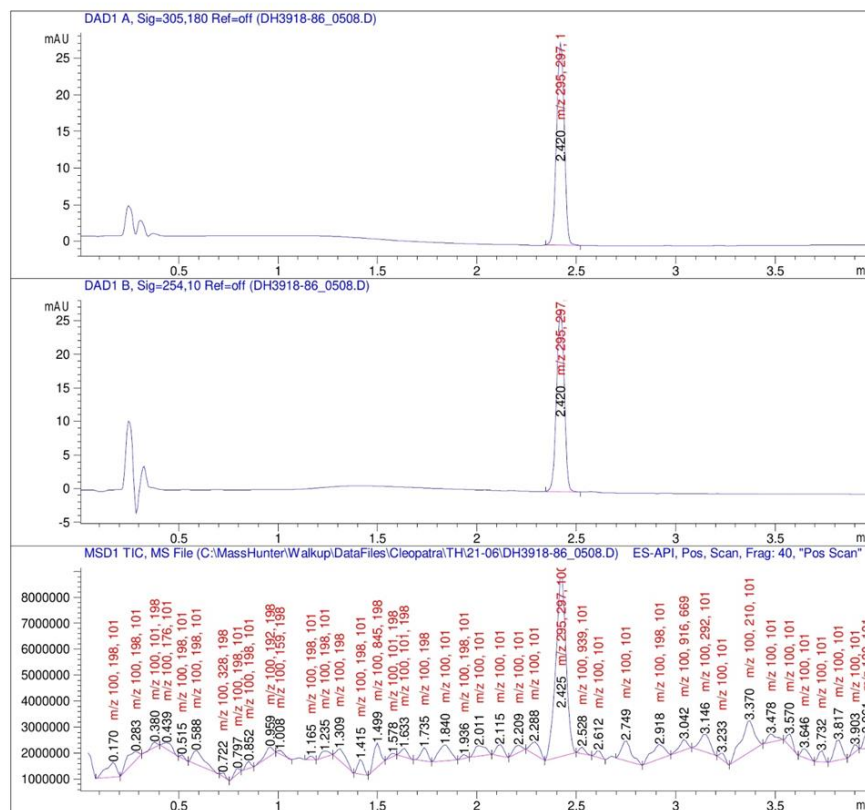
Compound (12):



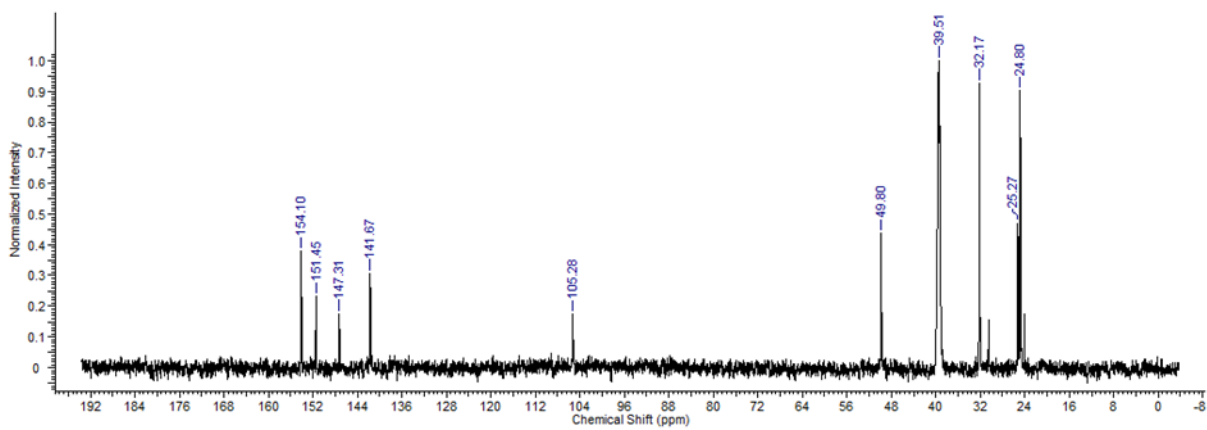
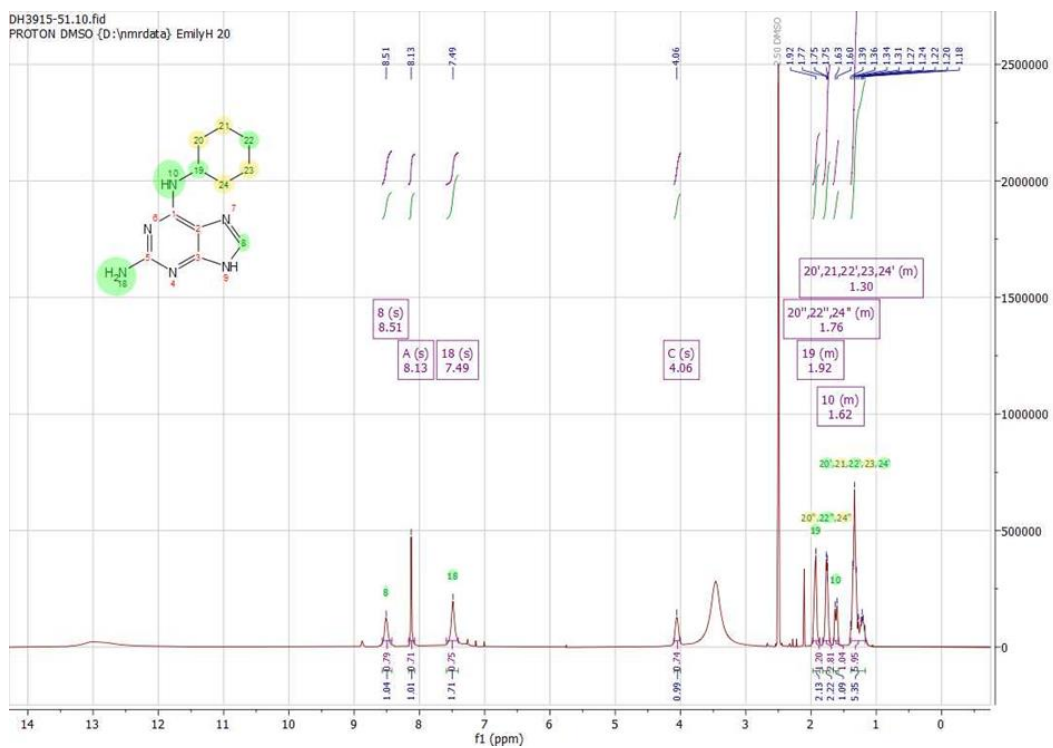


Method Info : X-bridge C18, 50x3.0 mm, 3.5u, 10-97% MeCN 3min,1ml/min, B: MeCN C: NH4HCO3

Sample Info : Walkup method: 'X1097-3'
Target:

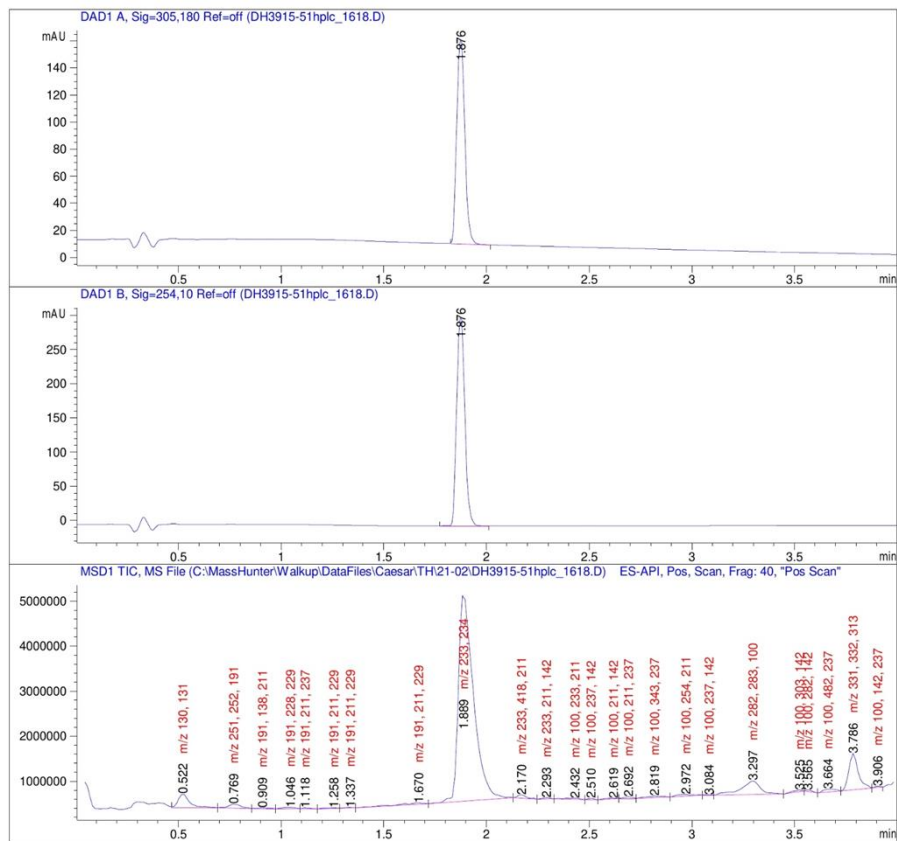


Compound (13):

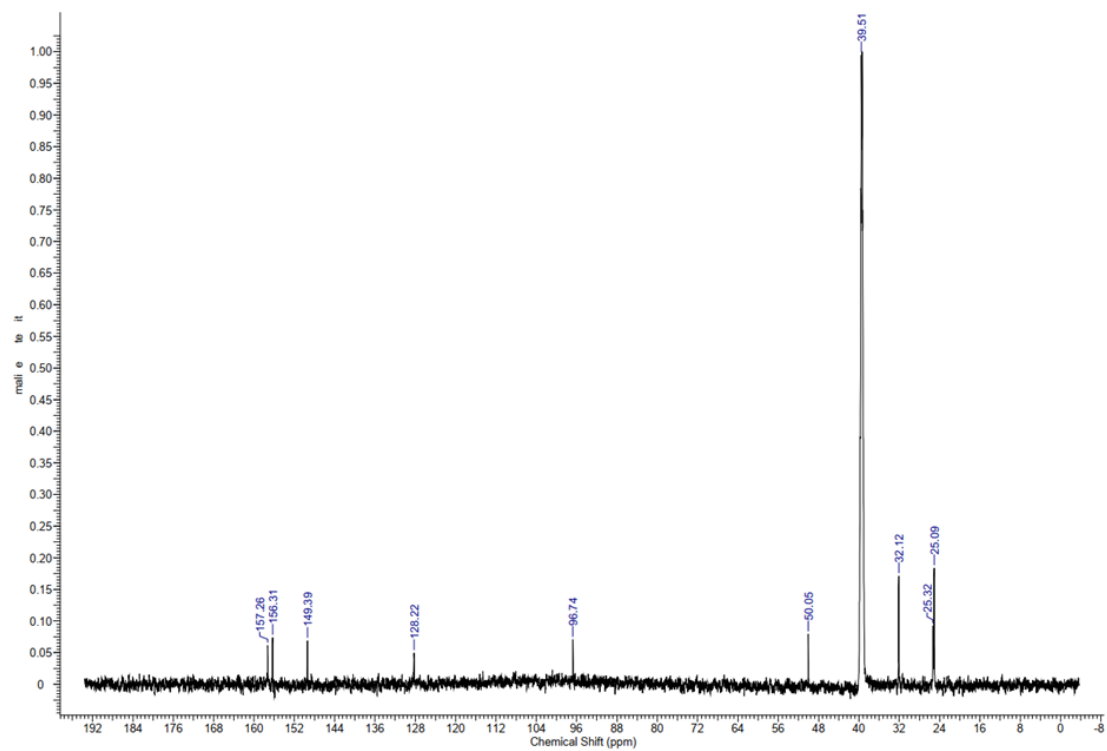
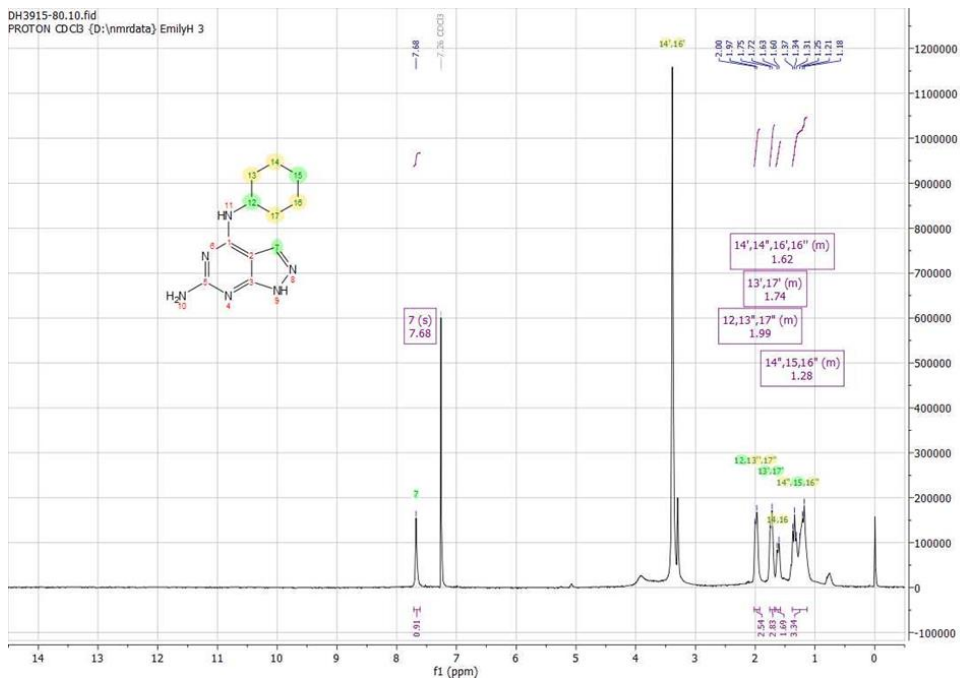


Method Info : ACE C8, 50x3mm, 3 μ , 10-97% MeCN, 3min; 1ml/min, A: water 0.1% TFA B MeCN

Sample Info : Walkup method: 'A1097-3'
Target:

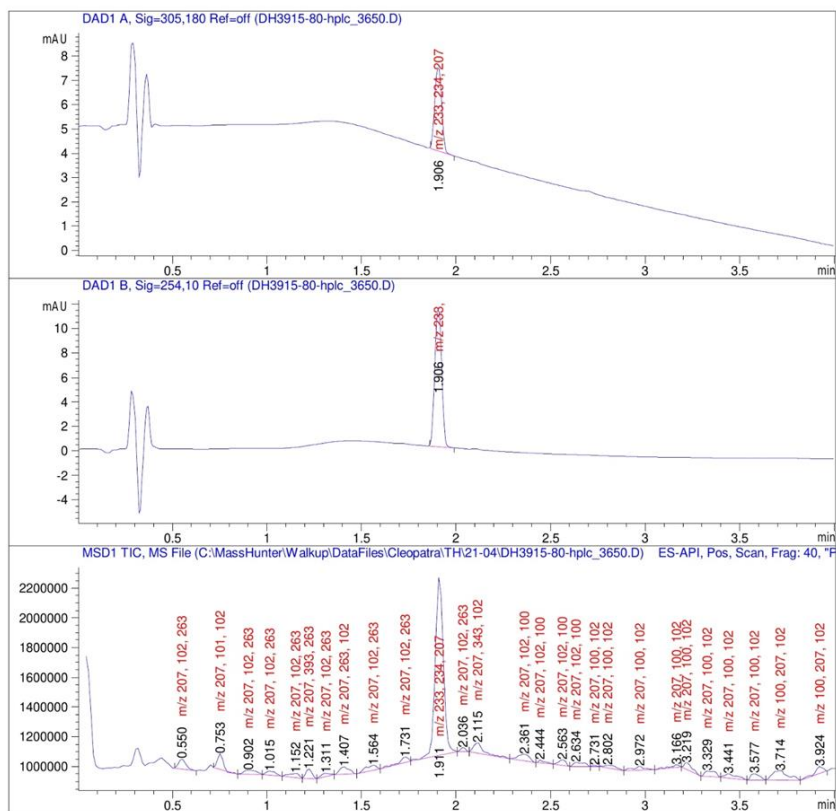


Compound (14):

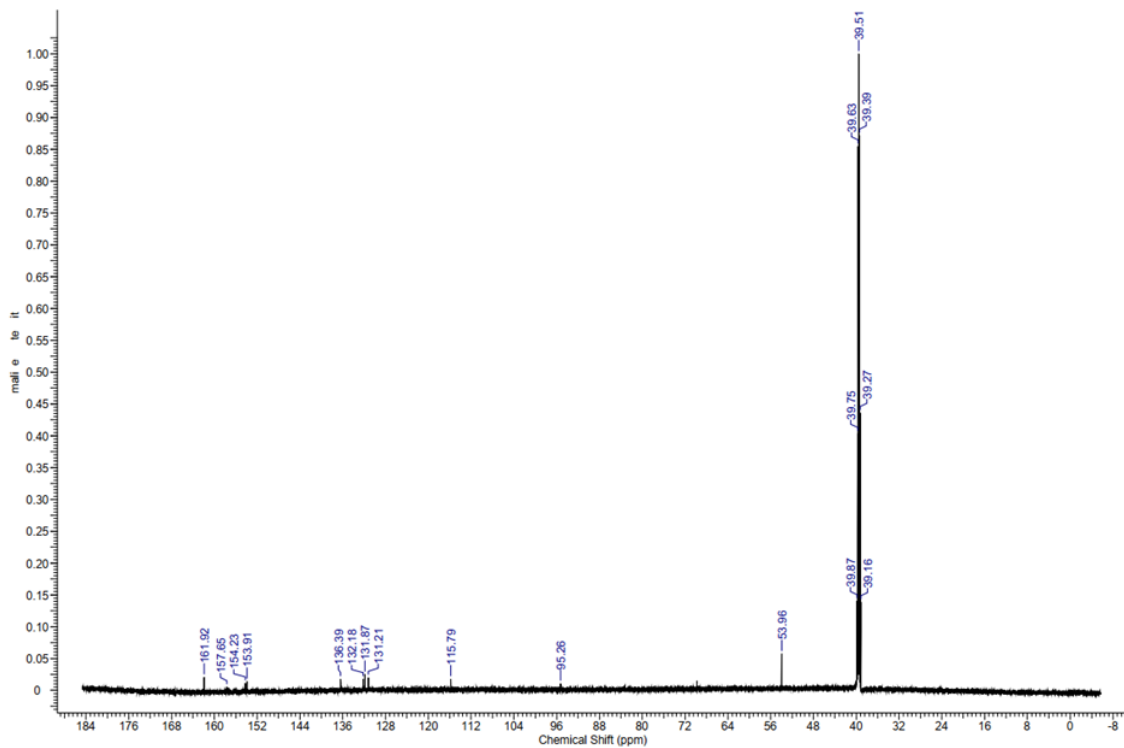
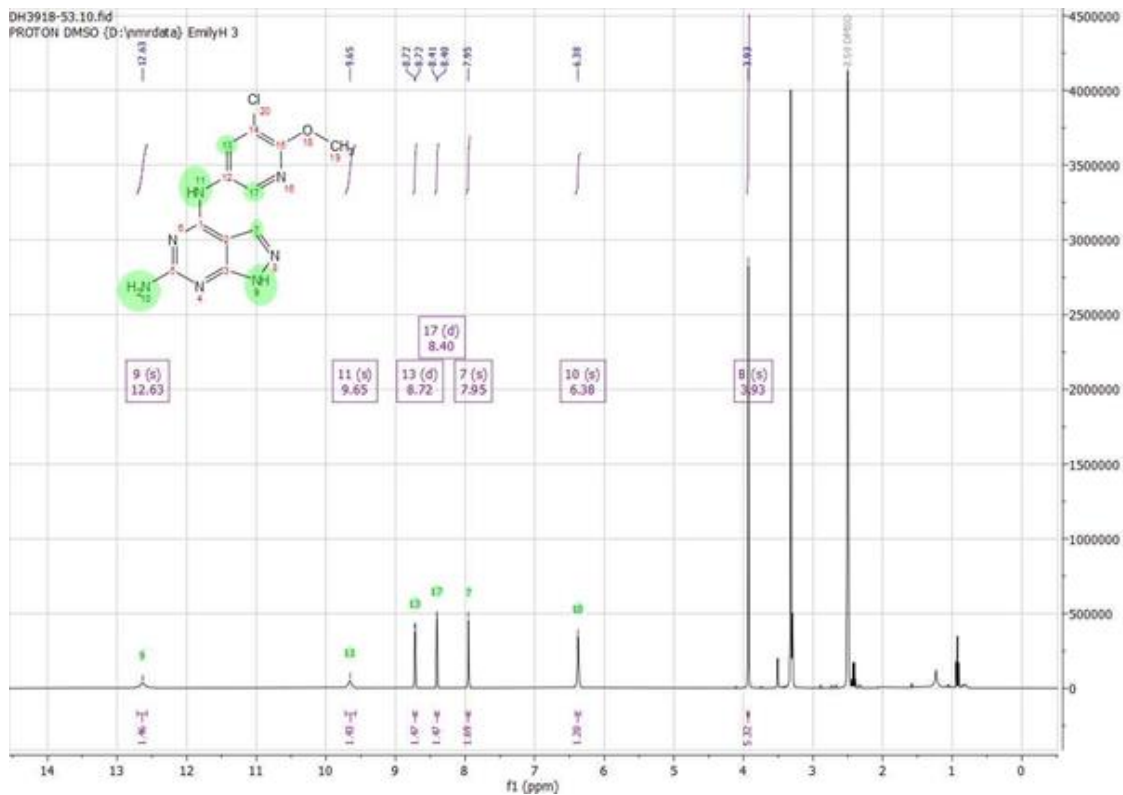


Method Info : ACE C8, 50x3mm, 3 μ , 10-97% MeCN, 3min; 1ml/min, A: 0.1% TFA, B:MeCN.

Sample Info : Walkup method: 'A1097-3'
Target:

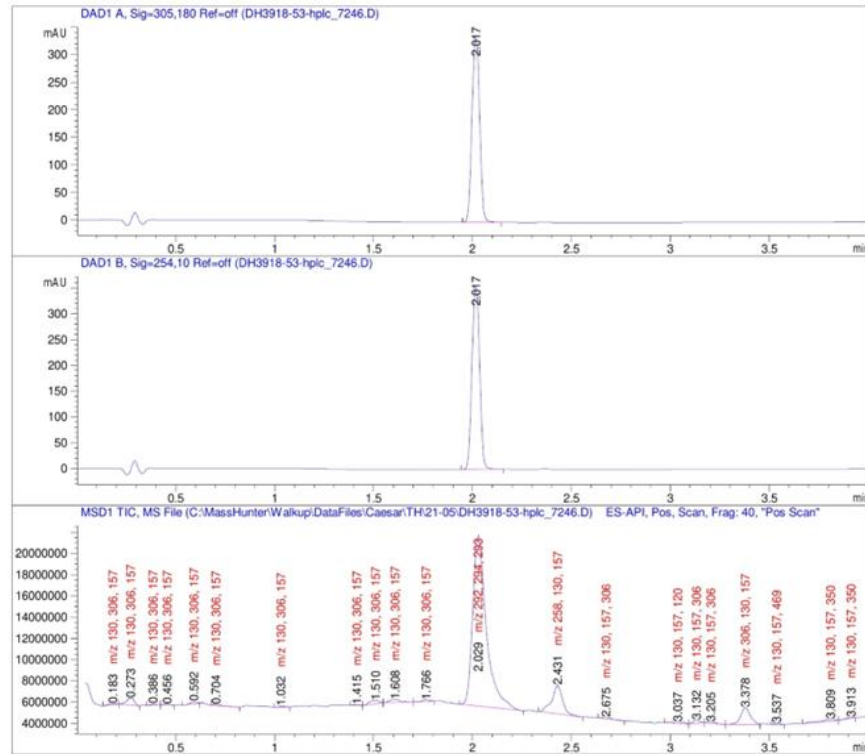


Compound (15):

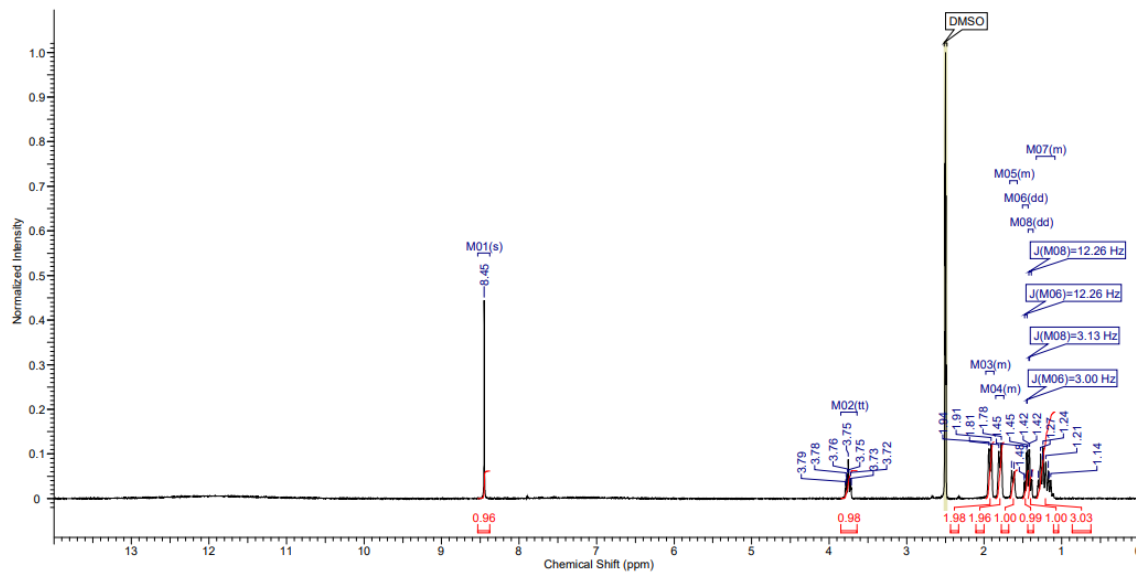


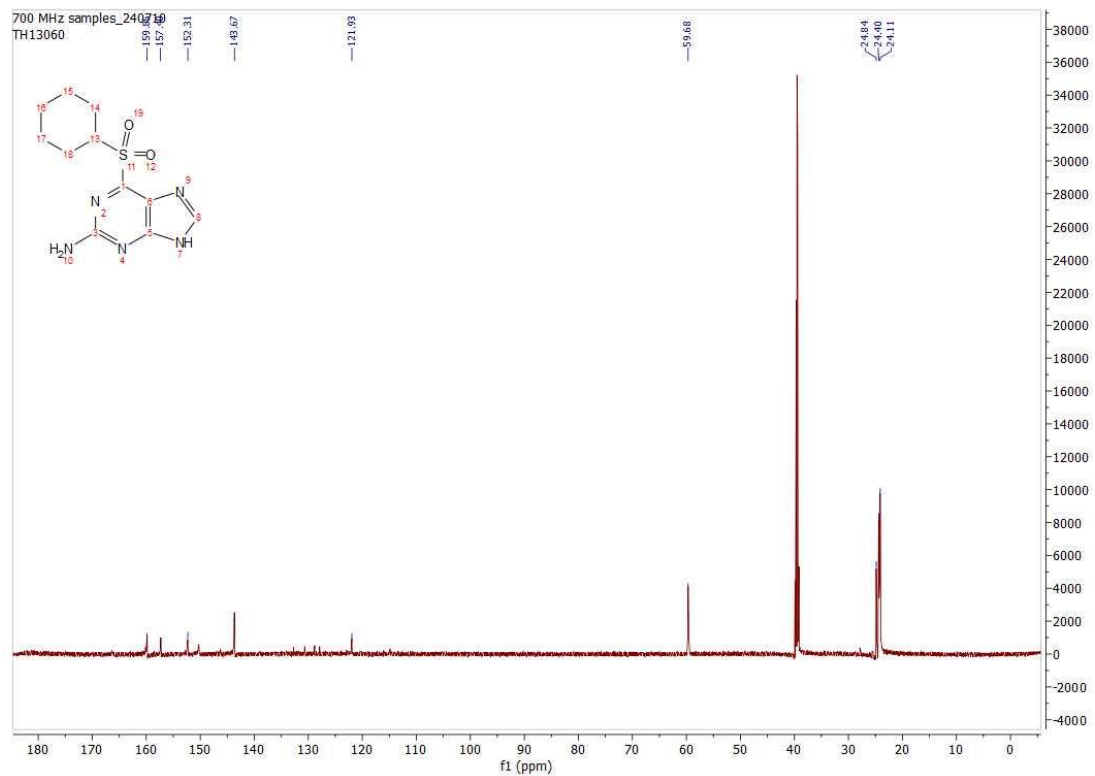
Method Info : X-bridge C18, 50x3.0 mm, 3.5u, 10-97% MeCN 1.5min,1mL/min, B: MeCN C: NH4HC03

Sample Info : Walkup method: 'X1097'
Target:



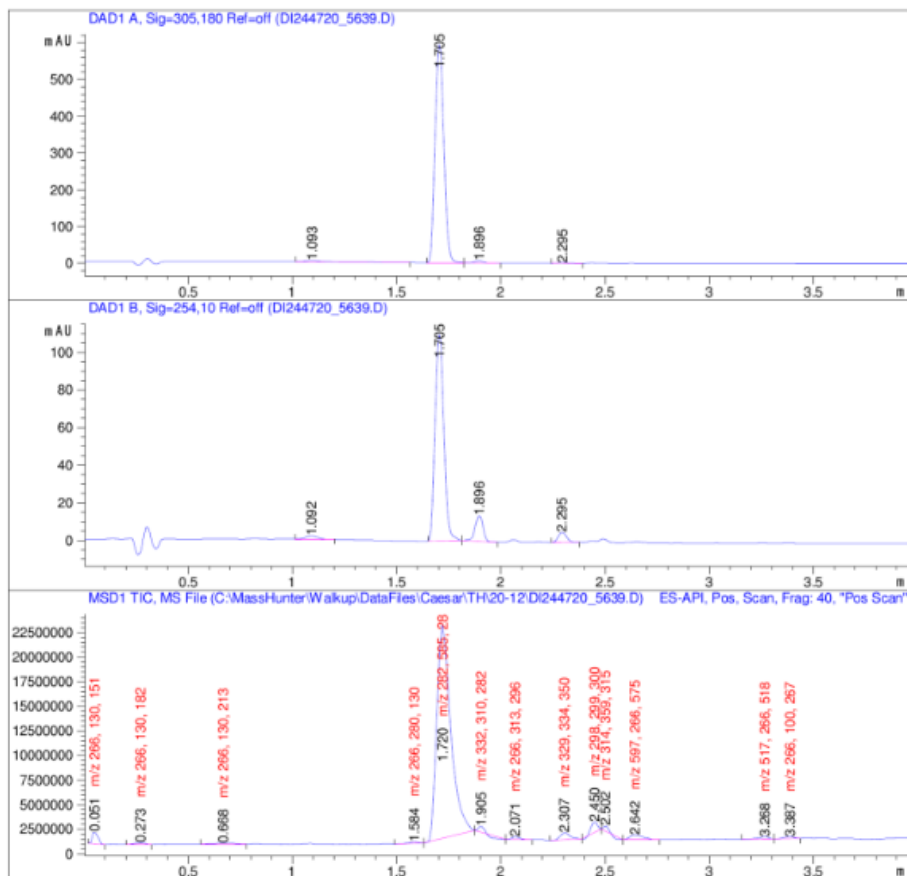
Compound (S15):



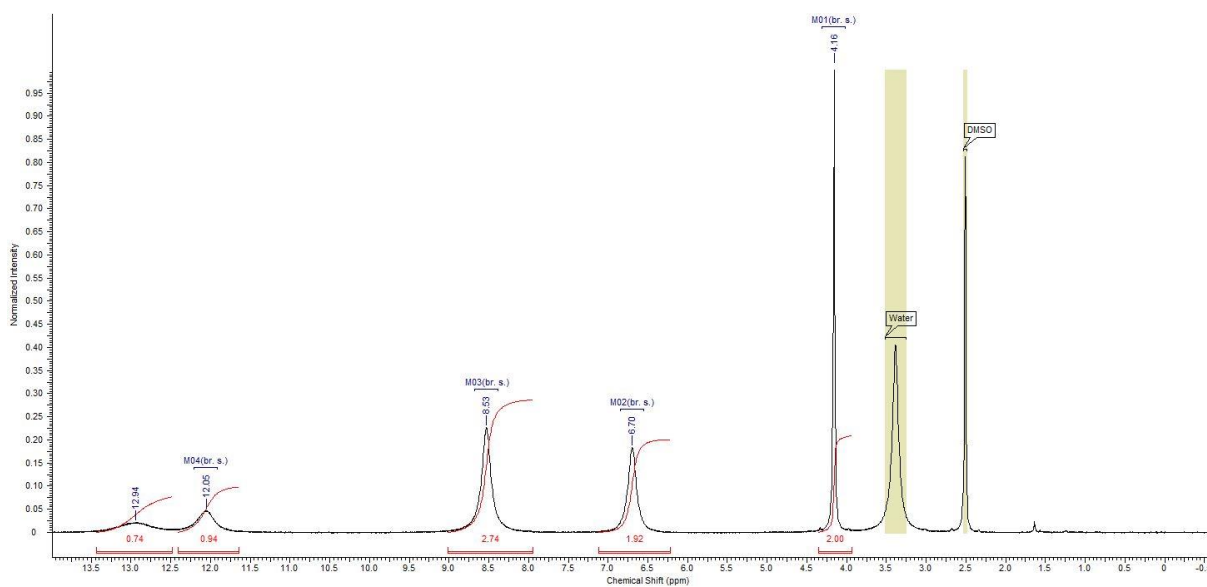


Method Info : X-bridge C18, 50x3.0 mm, 3.5u, 5-60% MeCN 3min,1ml/min, B: MeCN C: NH4HCO3

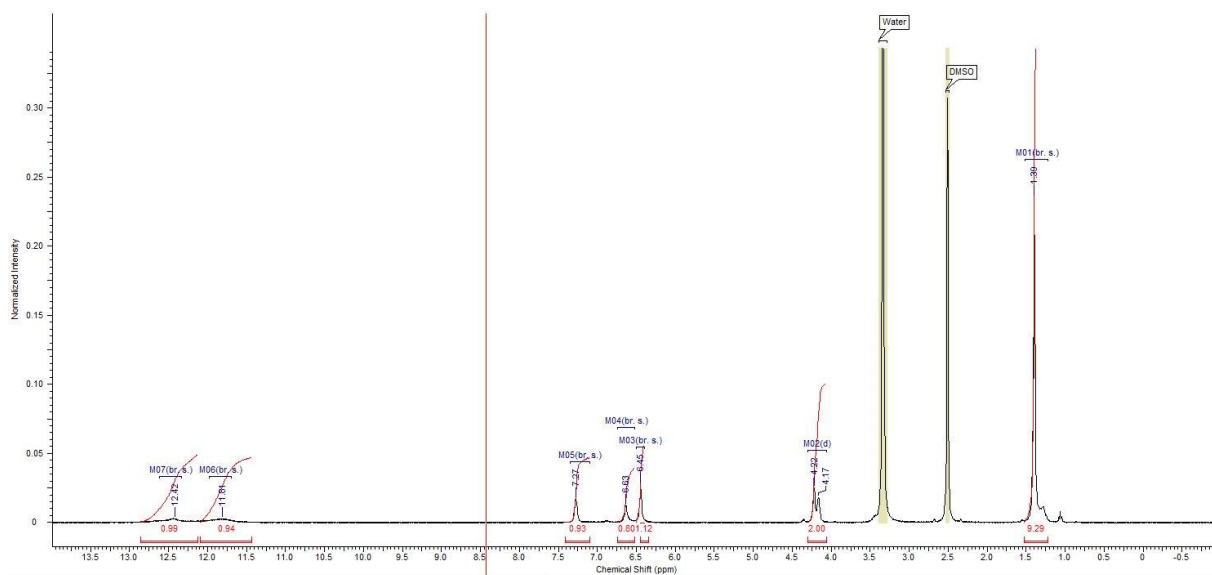
Sample Info : Walkup method: 'X0560-3'
Target:



Compound (S25):



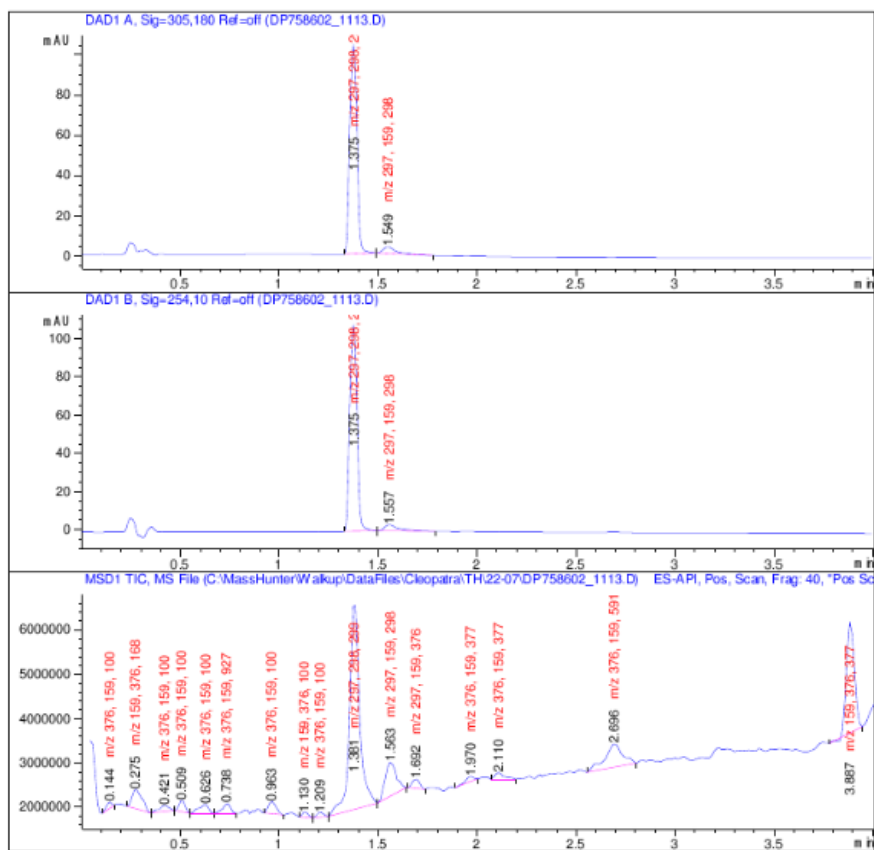
Compound (S26):



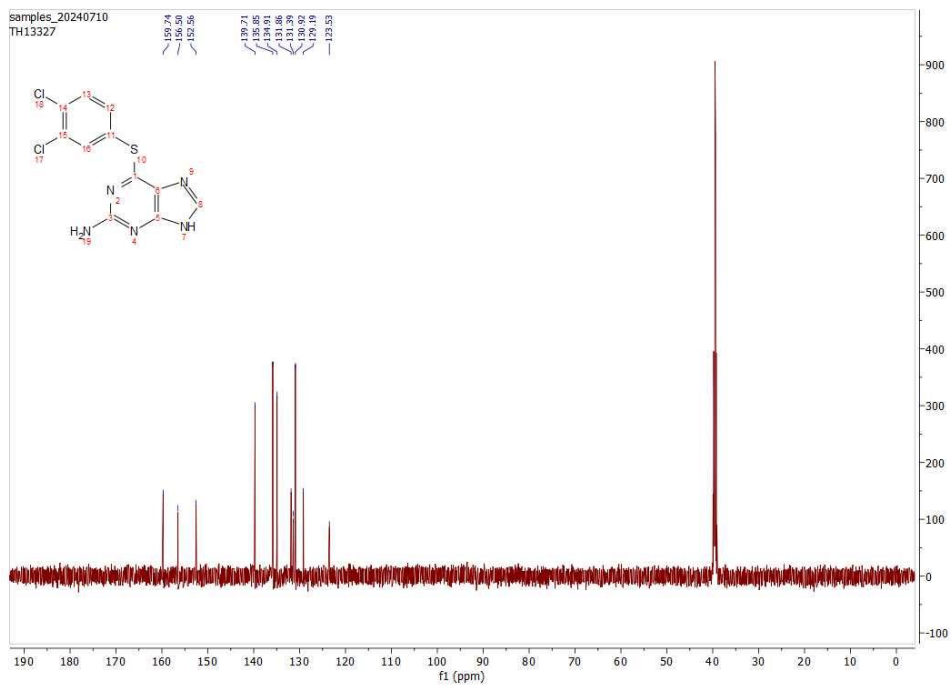
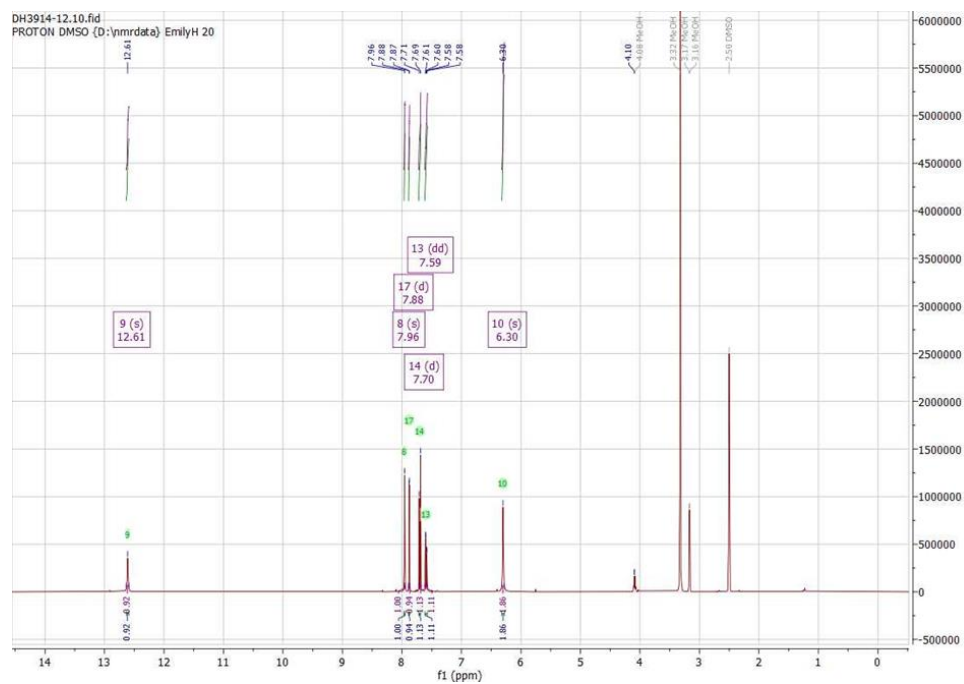
Method Info : X-bridge C18, 50x3.0 mm, 3.5u, 5-60% MeCN 3min, 1ml/min, B: MeCN C: NH4HCO3

Sample Info : Walkup method: 'X0560-3'

Target:

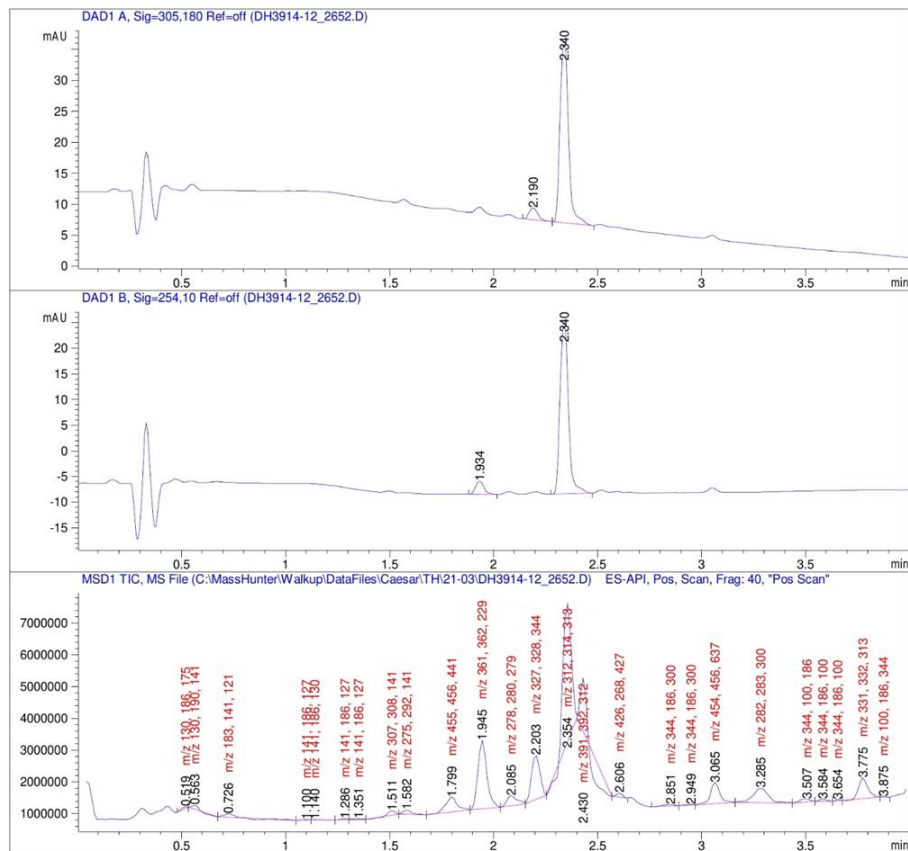


Compound (S39):

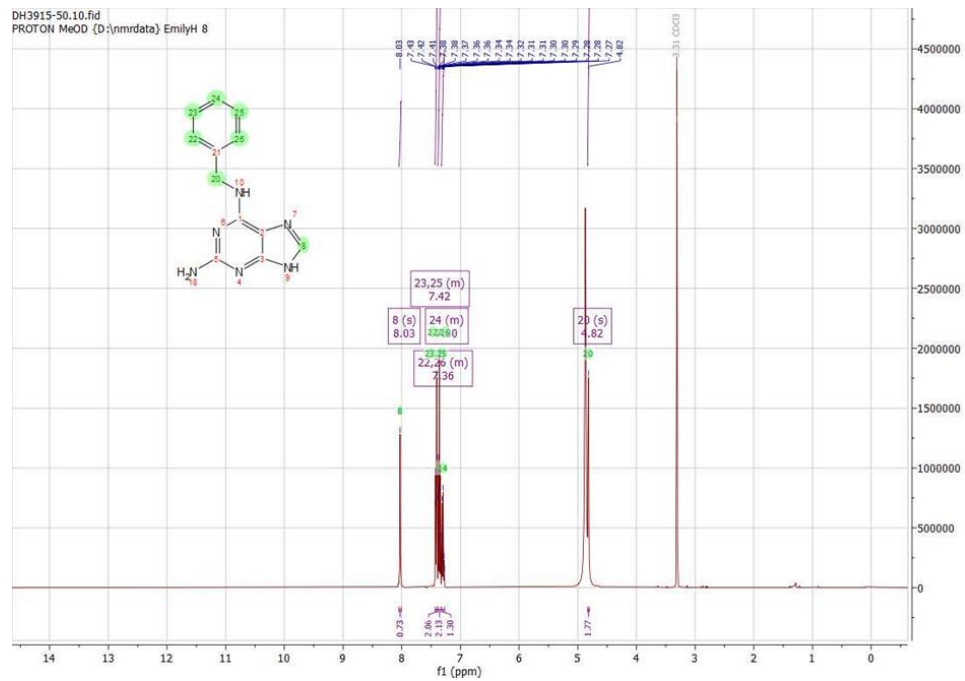


Method Info : ACE C8, 50x3mm, 3μ, 10-97% MeCN, 3min; 1mL/min, A: water 0.1% TFA B MeCN

Sample Info : Walkup method: 'A1097-3'
Target:

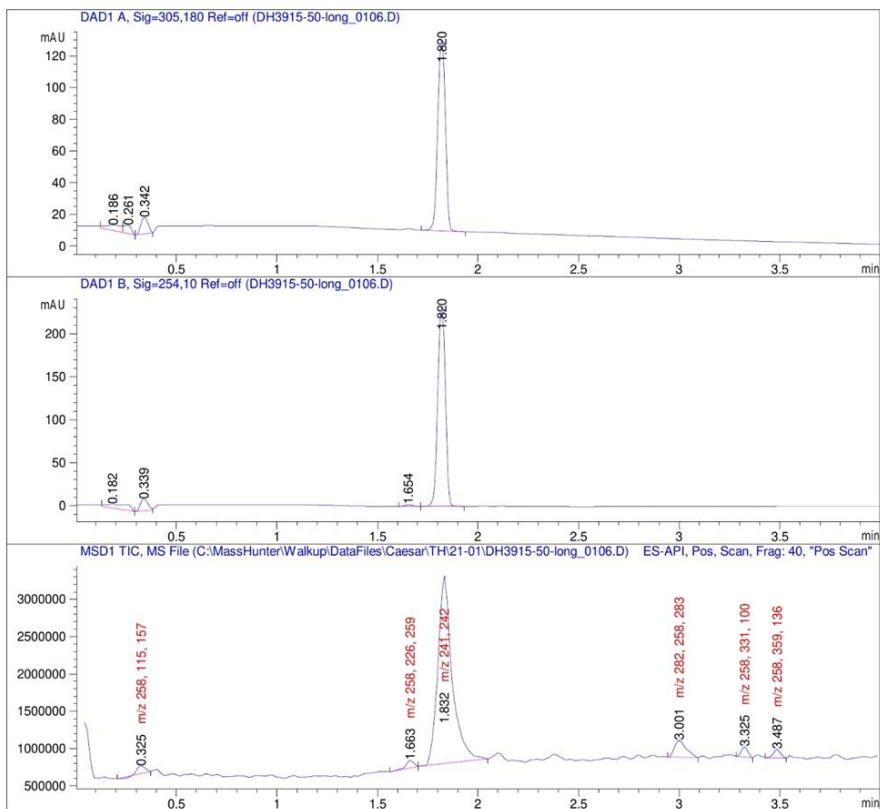


Compound (S40):

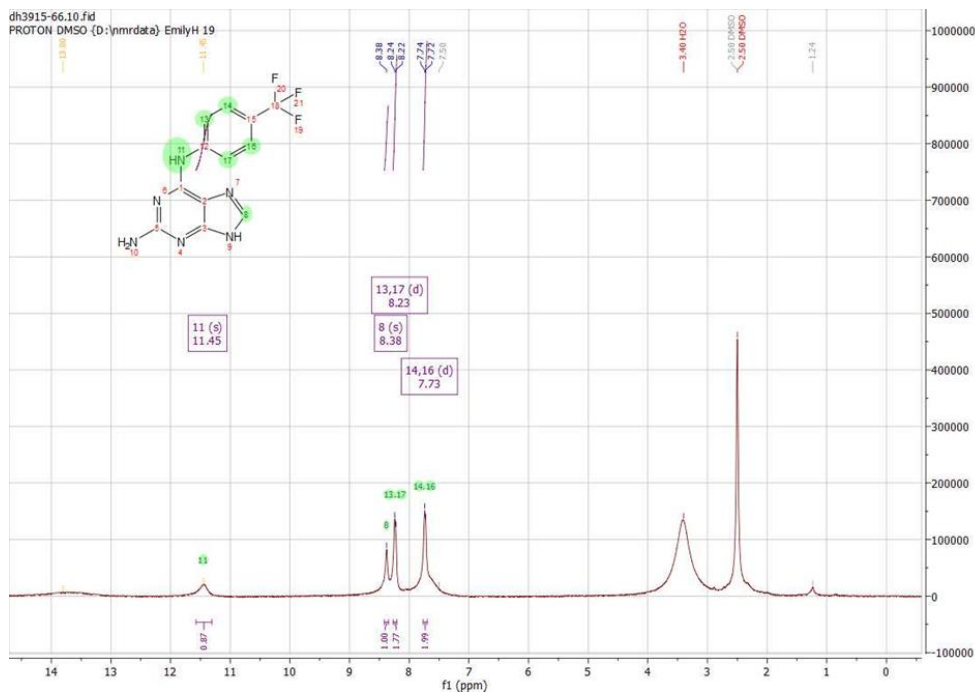


Method Info : ACE Phenyl, 50x3mm, 3 μ , 10-97% MeCN, 3min; 1mL/min, A: 0.1% TFA, B: MeCN.

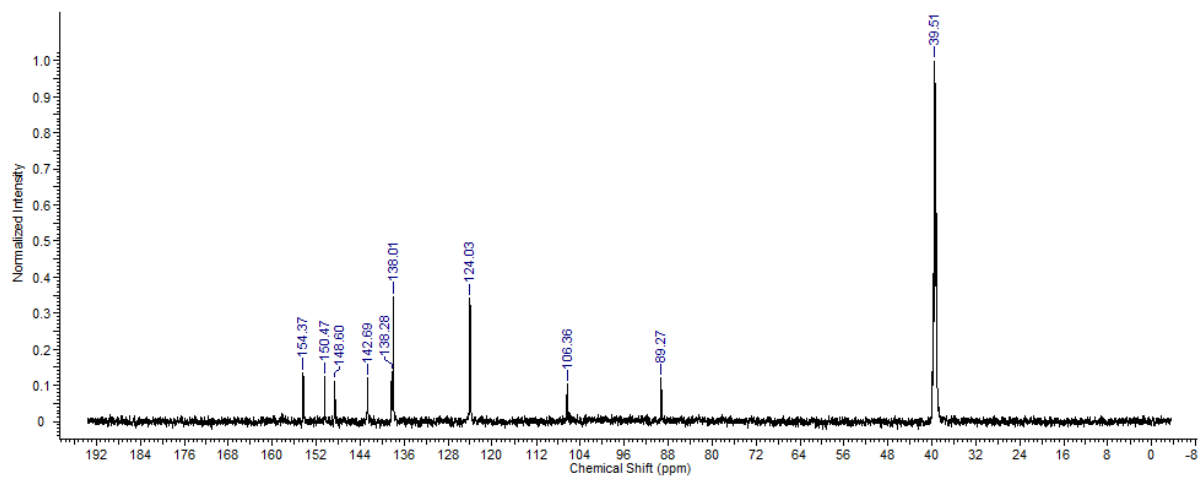
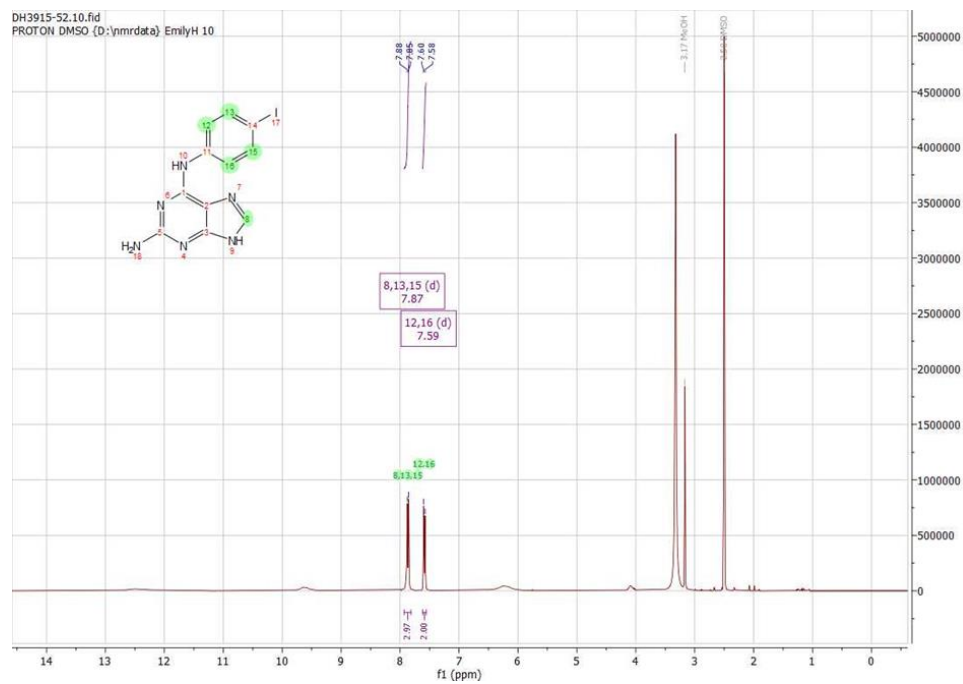
Sample Info : Walkup method: 'Ph1097-3'
Target:



Compound (S44):

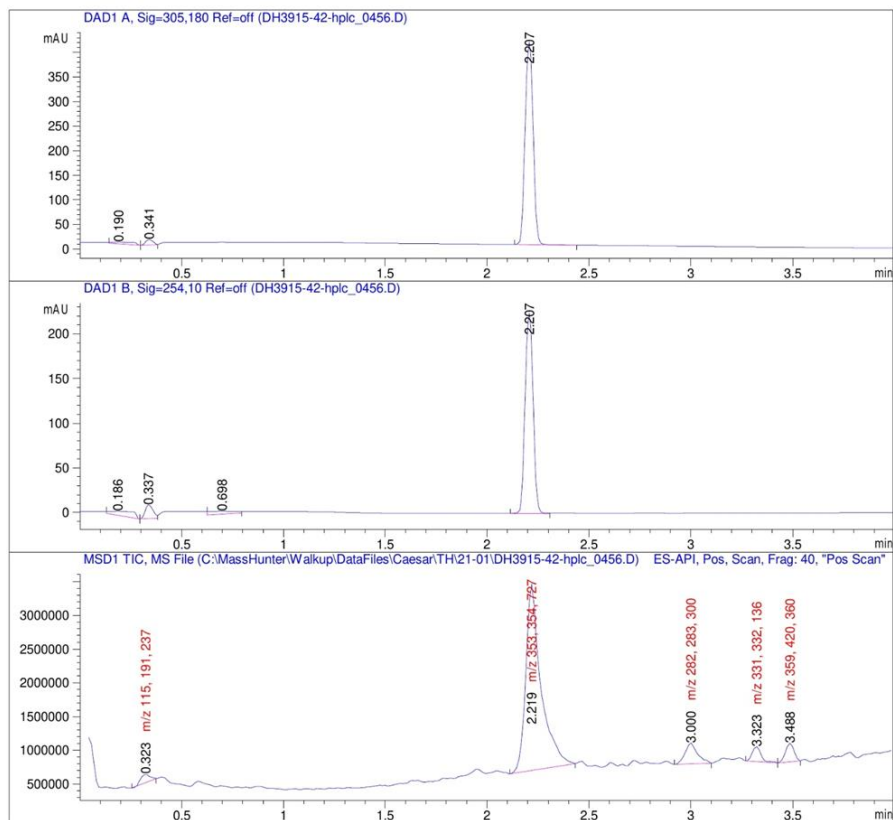


Compound (S45):

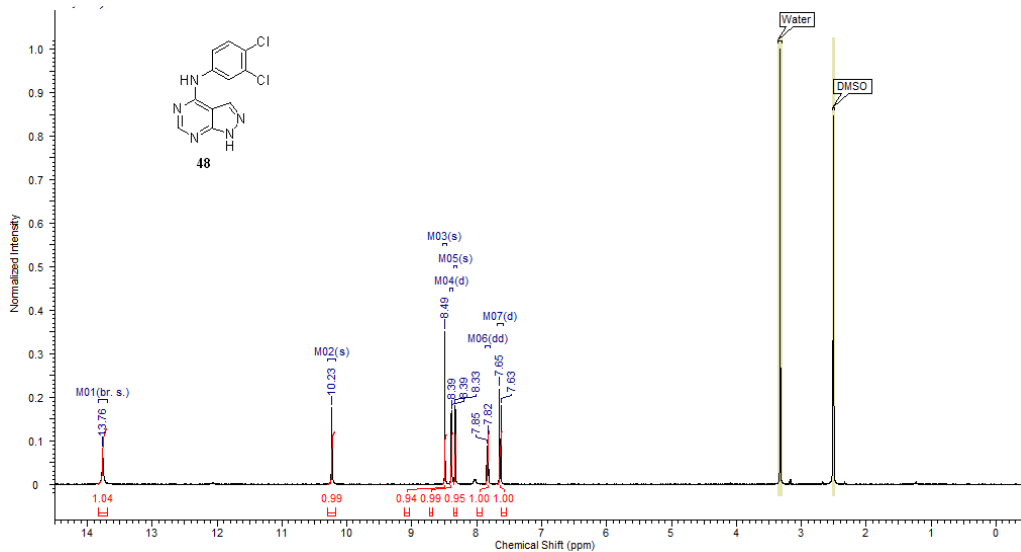


Method Info : ACE Phenyl, 50x3mm, 3 μ , 10-97% MeCN, 3min; 1mL/min, A: 0.1% TFA, B: MeCN.

Sample Info : Walkup method: 'Ph1097-3'
Target:

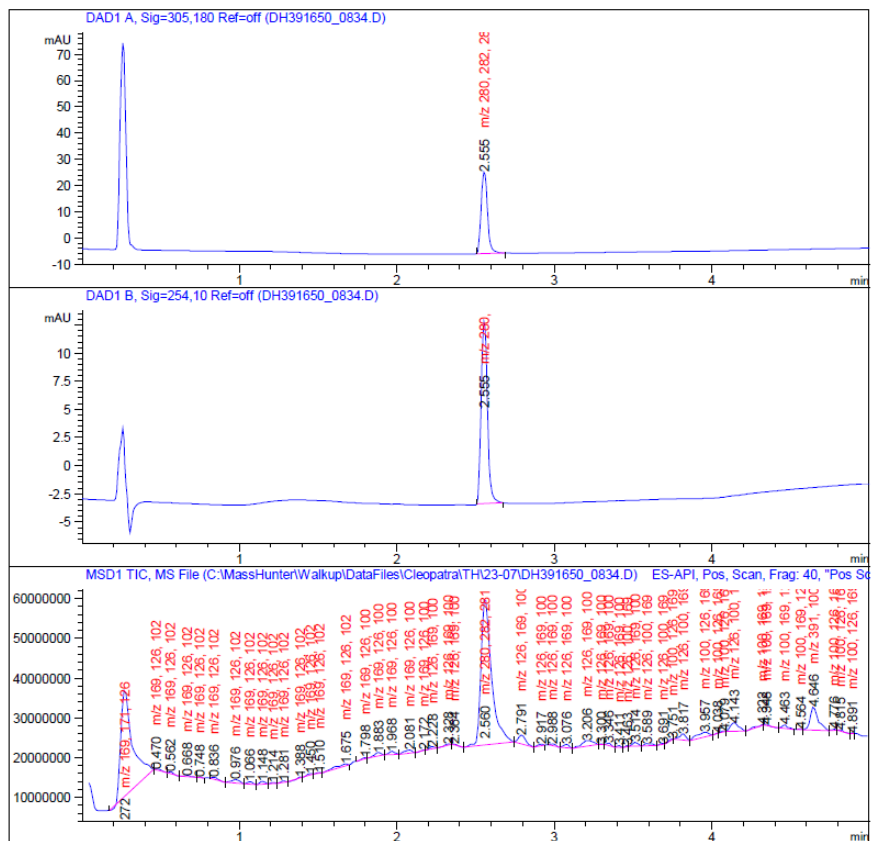


Compound (S46):

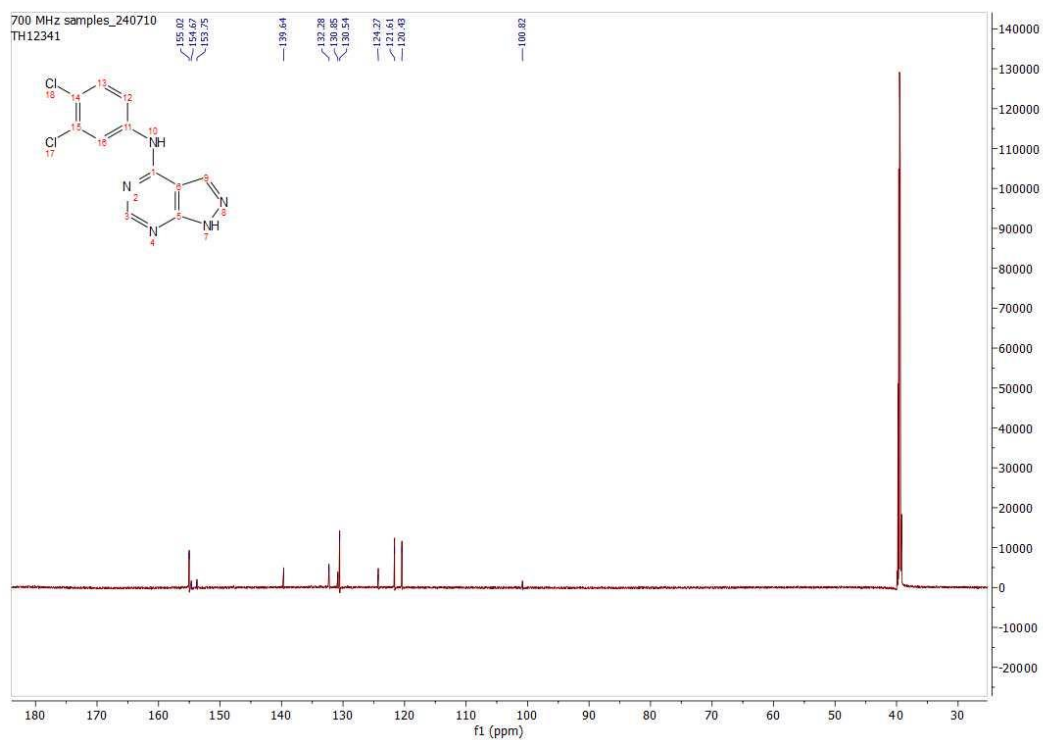
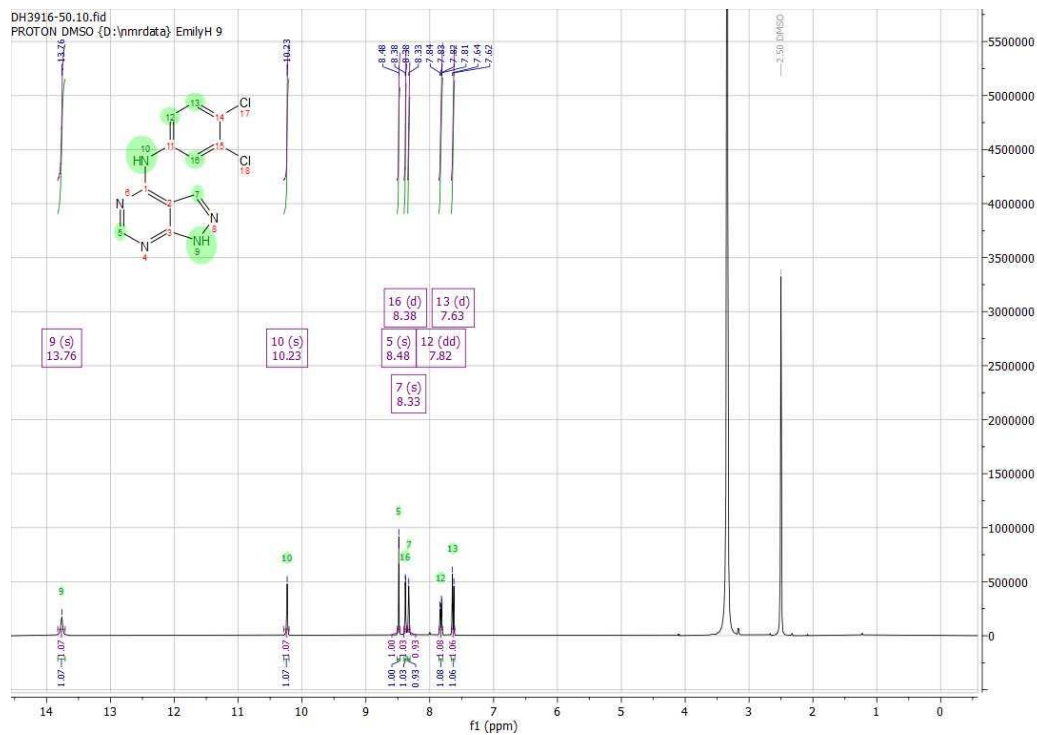


Method Info : X-bridge C18, 50x3.0 mm, 3.5u, 10-97% MeCN 3min,1ml/min, B: MeCN C: NH4HCO3

Sample Info : Walkup method: 'X1097-3'
Target:

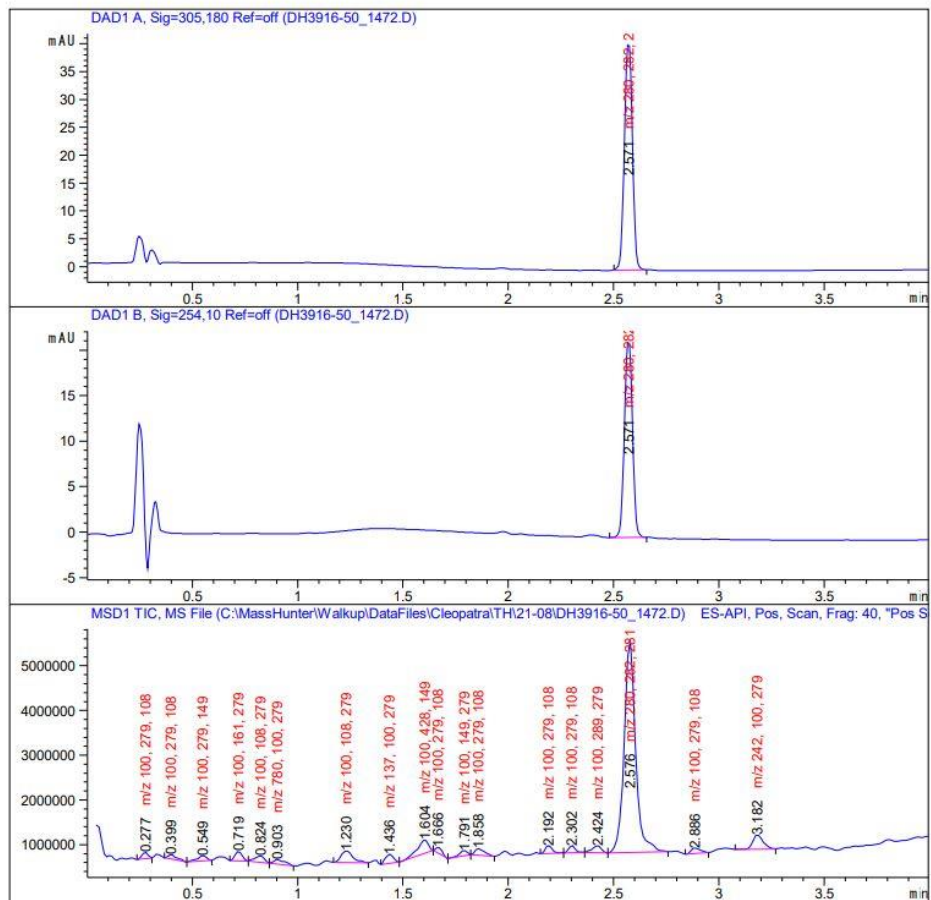


Compound (S47):

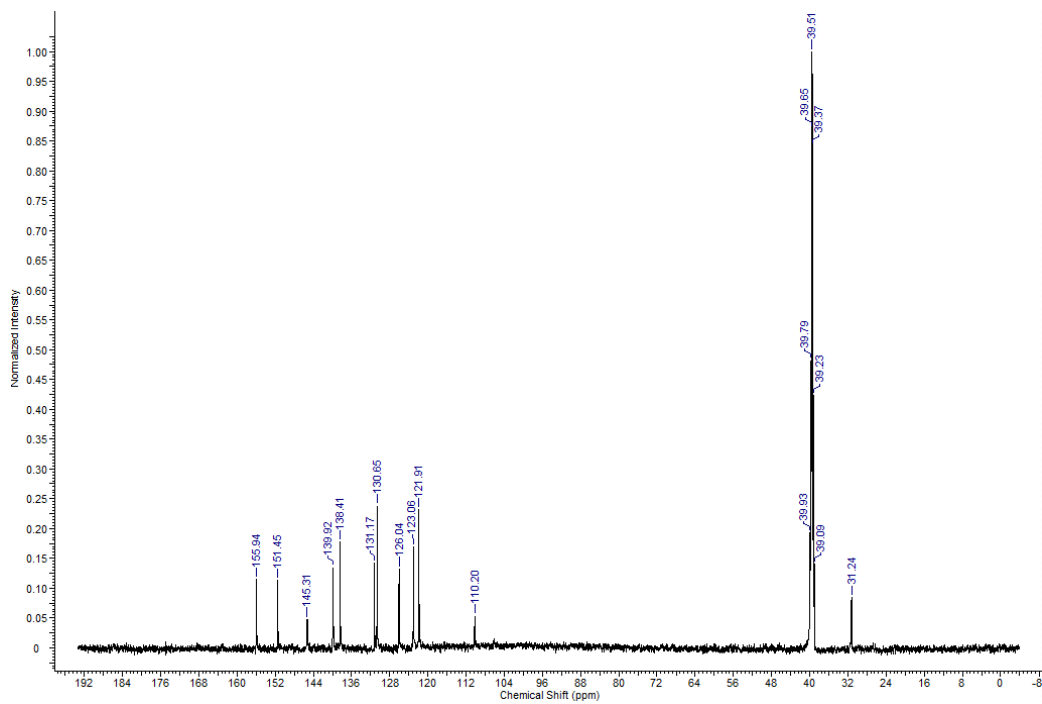
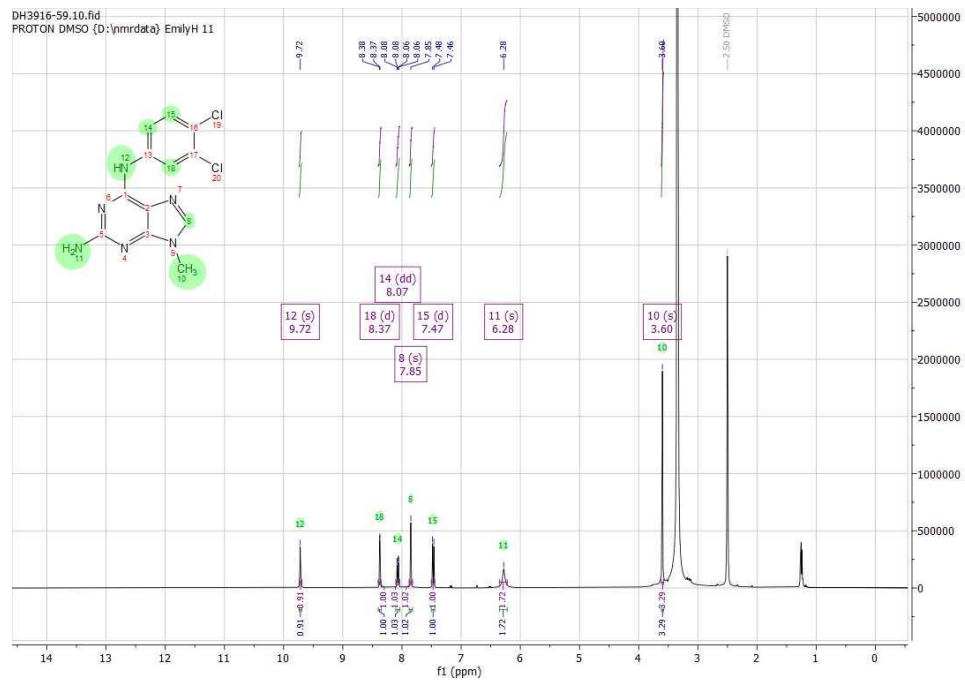


Method Info : X-bridge C18, 50x3.0 mm, 3.5u, 10-97% MeCN 3min,1ml/min, B: MeCN C: NH4HCO3

Sample Info : Walkup method: 'X1097-3'
Target:

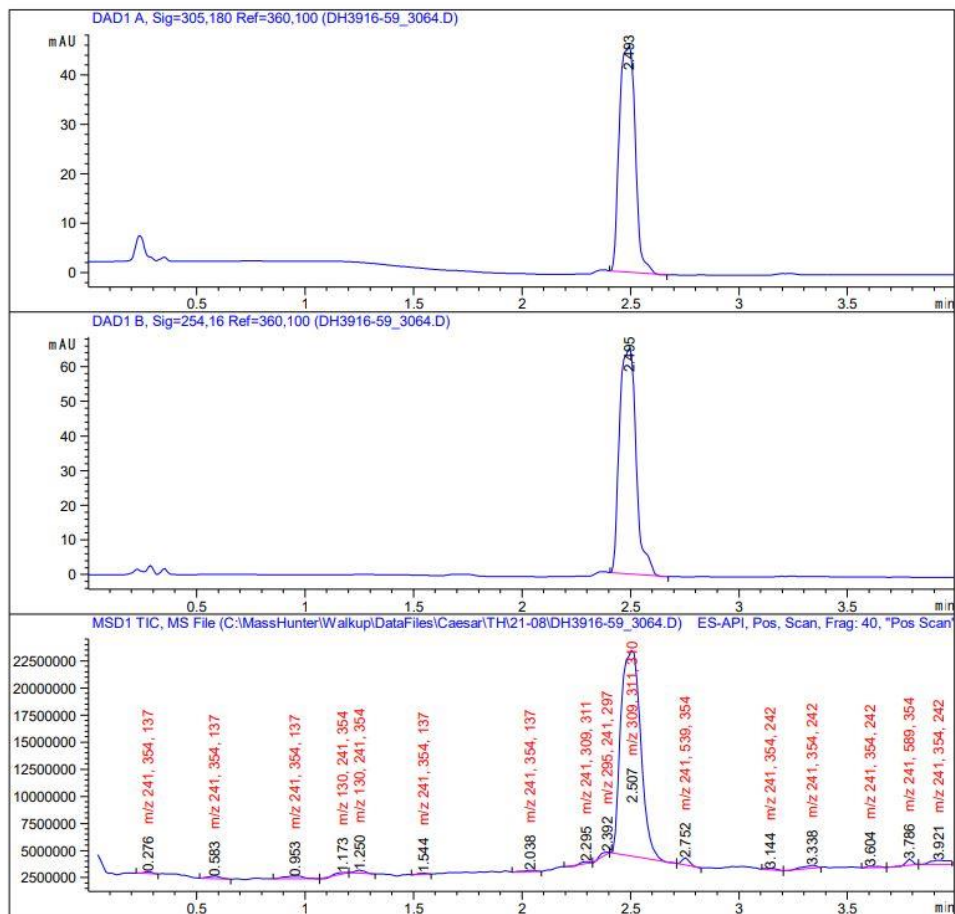


Compound (S49):

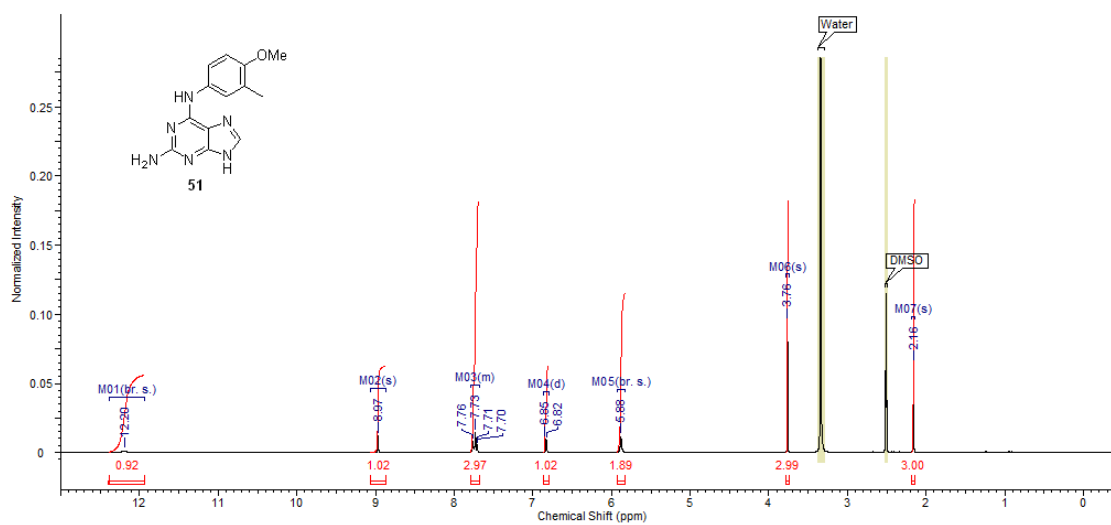


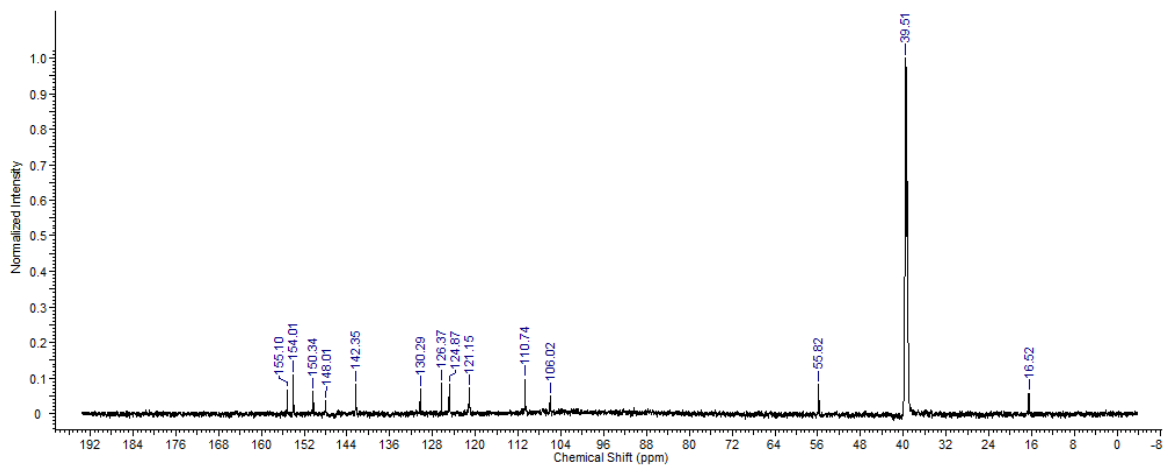
Method Info : X-bridge C18, 50x3.0 mm, 3.5u, 10-97% MeCN 3min,1ml/min, B: MeCN C: NH4HCO3

Sample Info : Walkup method: 'X1097-3'
Target:



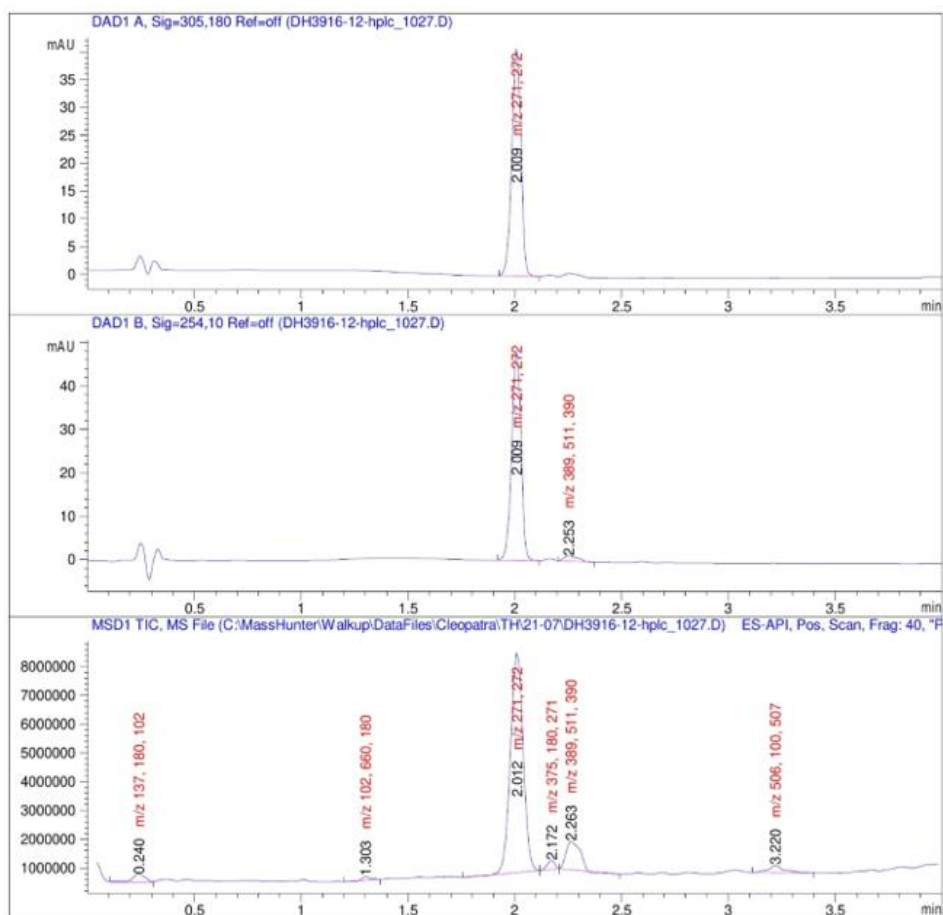
Compound (S50):



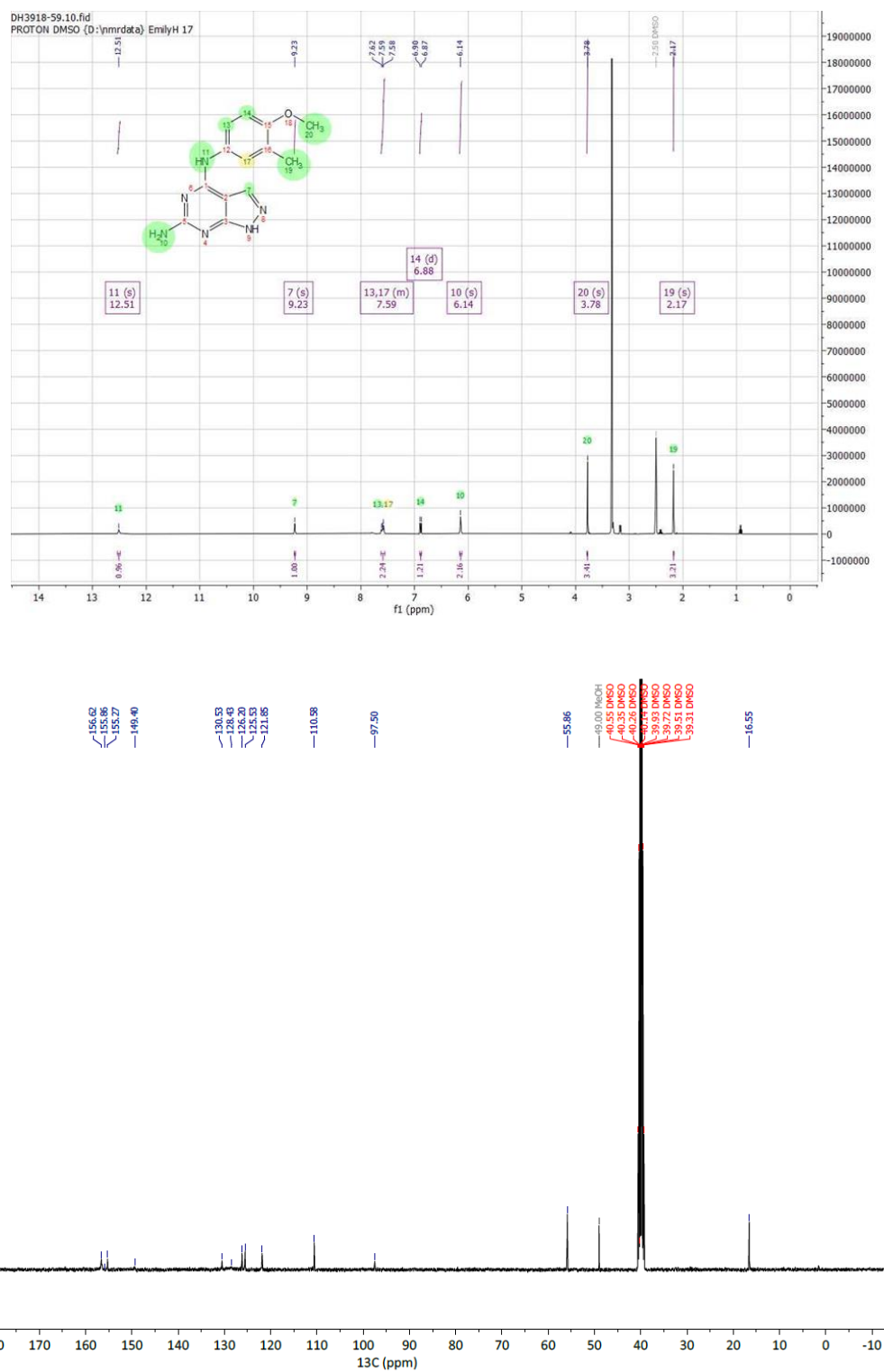


Method Info : X-bridge C18, 50x3.0 mm, 3.5u, 10-97% MeCN 3min, 1ml/min, B: MeCN C: NH4HCO3

Sample Info : Walkup method: 'X1097-3'
Target:

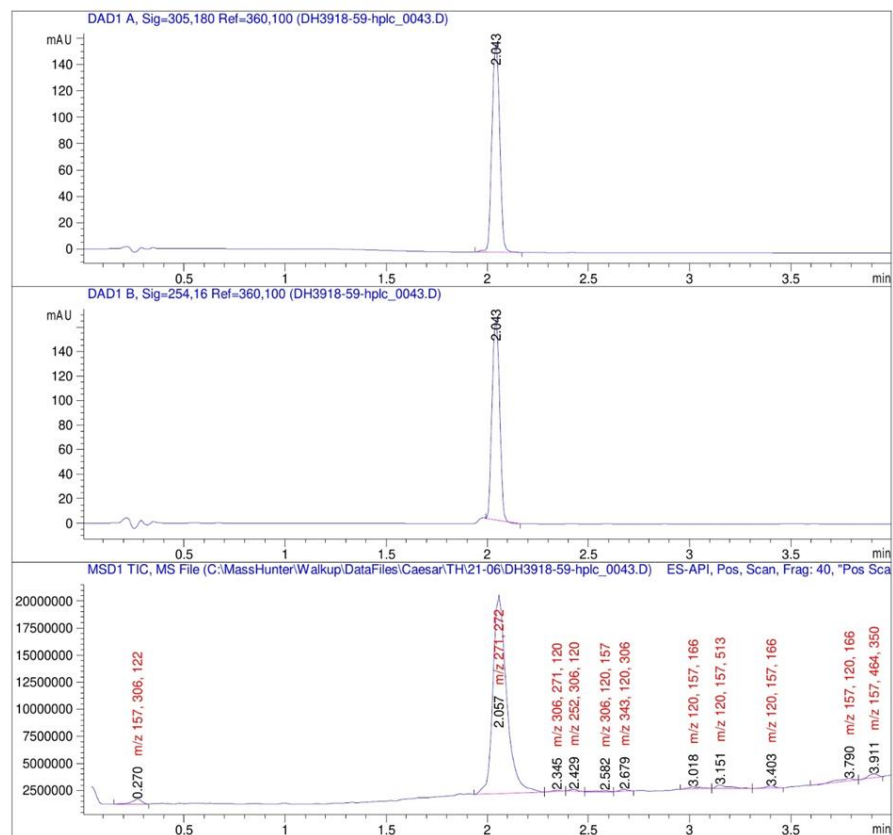


Compound (S51):

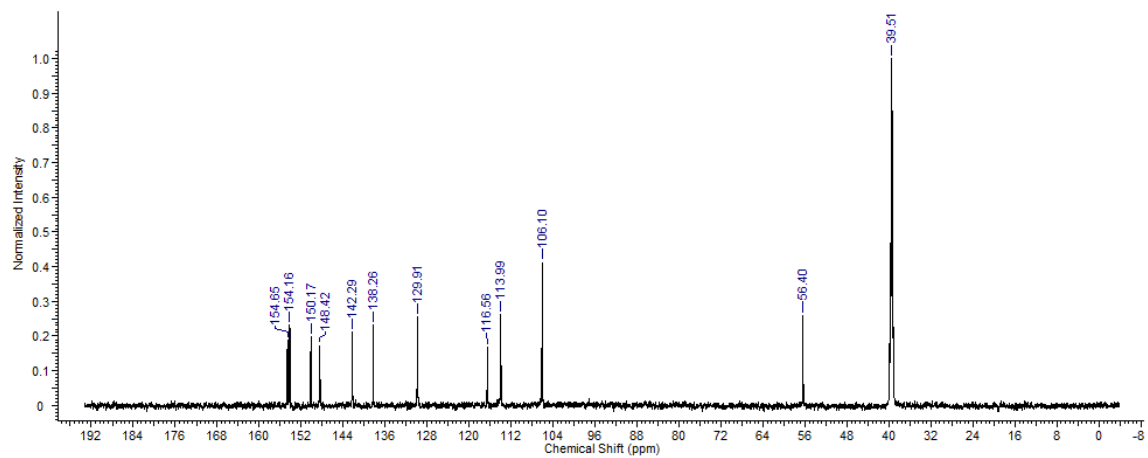
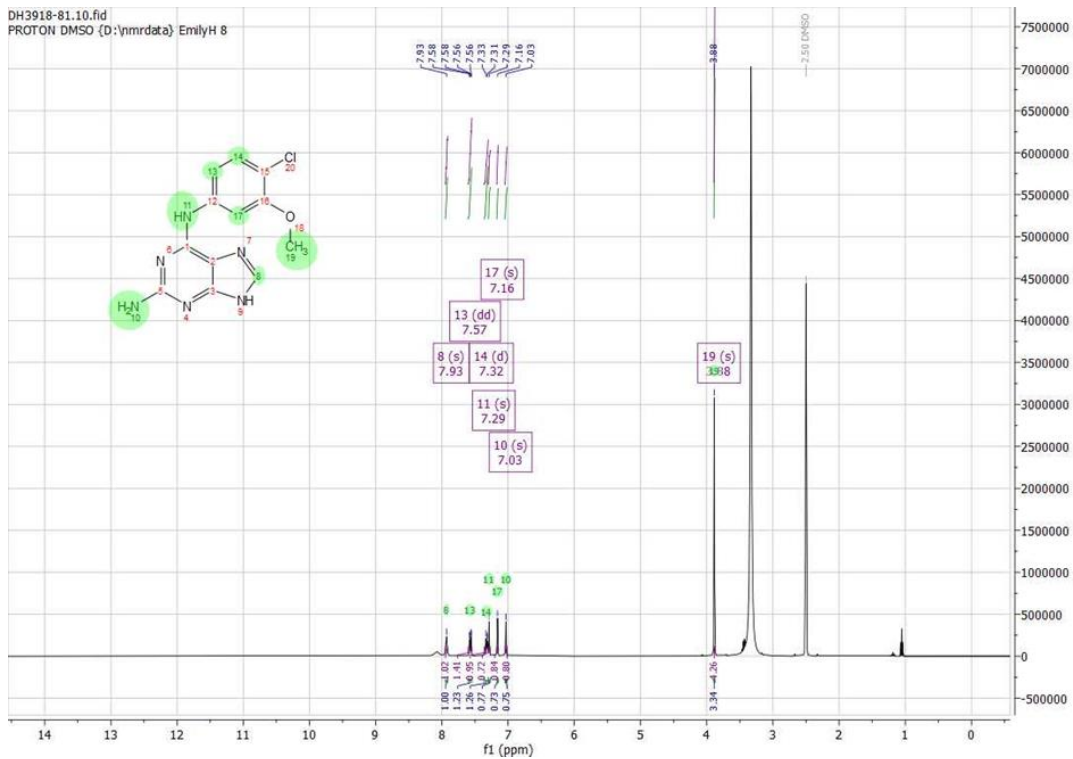


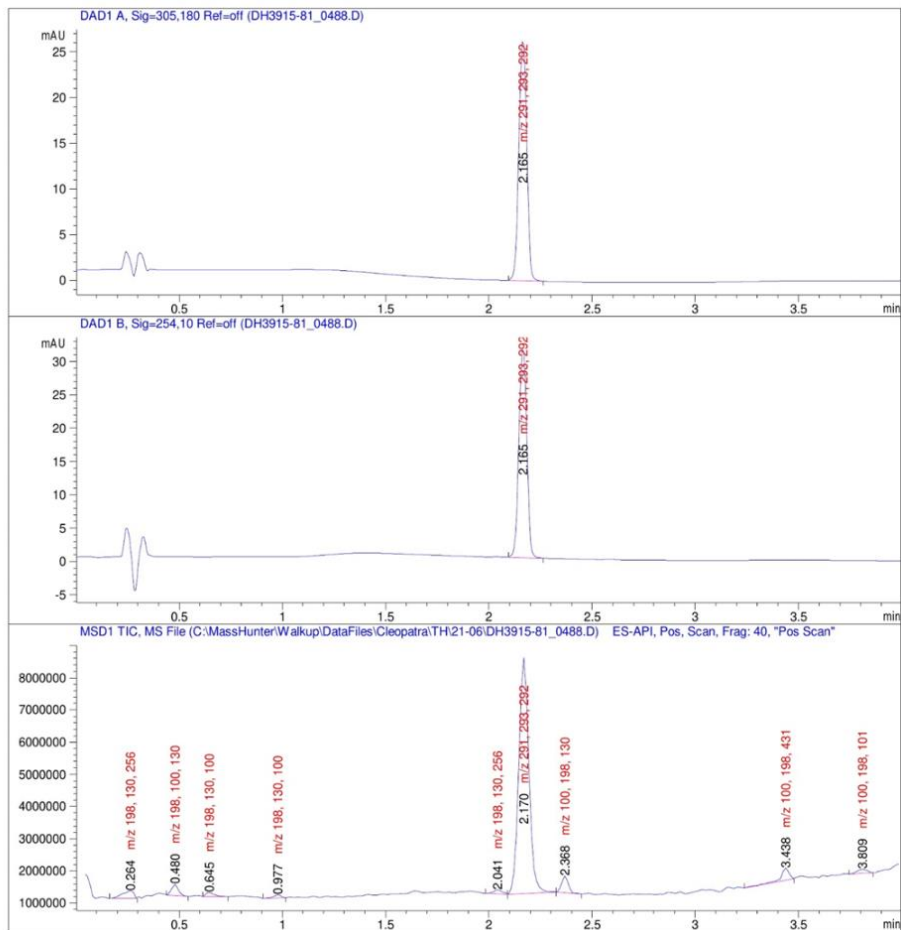
Method Info : X-bridge C18, 50x3.0 mm, 3.5u, 10-97% MeCN 3min,1mL/min, B: MeCN C: NH4HCO3

Sample Info : Walkup method: 'X1097-3'
Target:

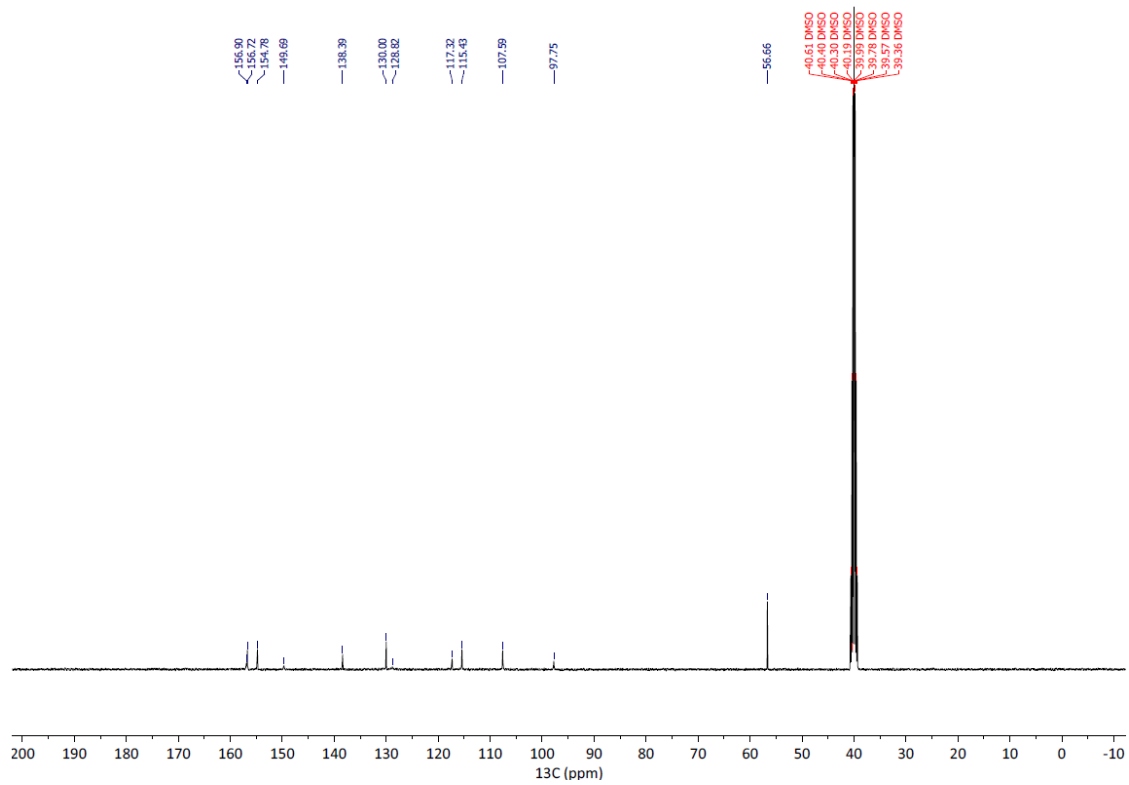
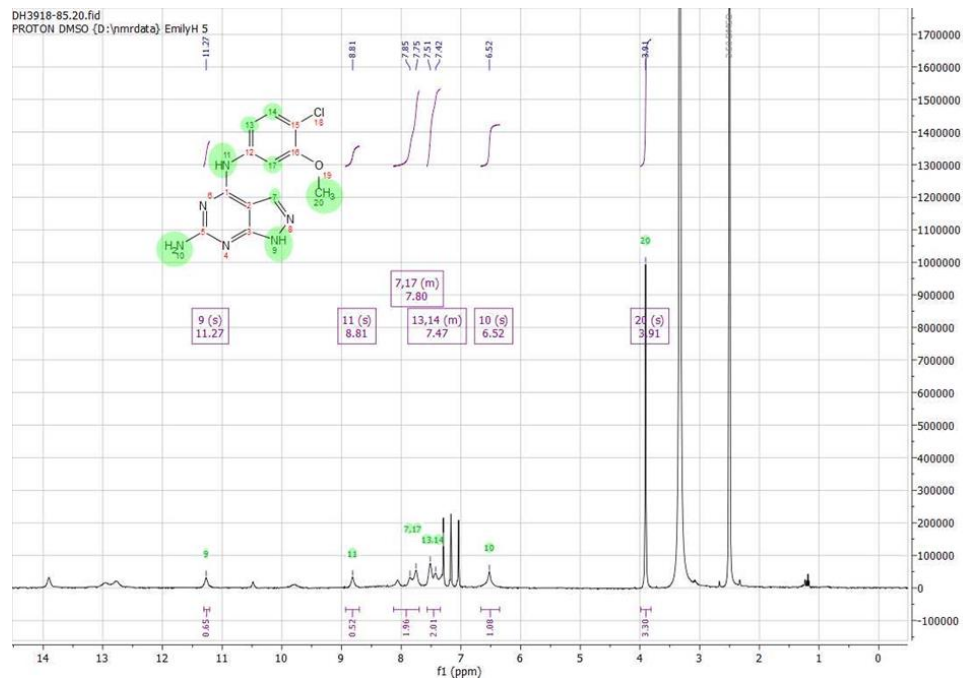


Compound (S52):



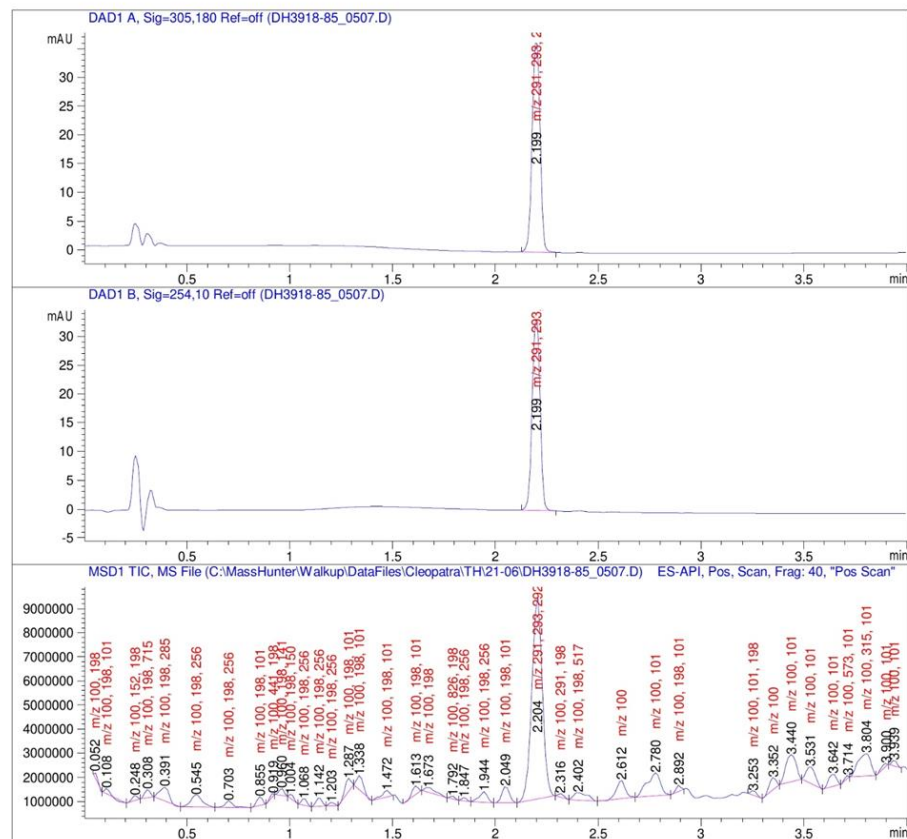


Compound (S53):

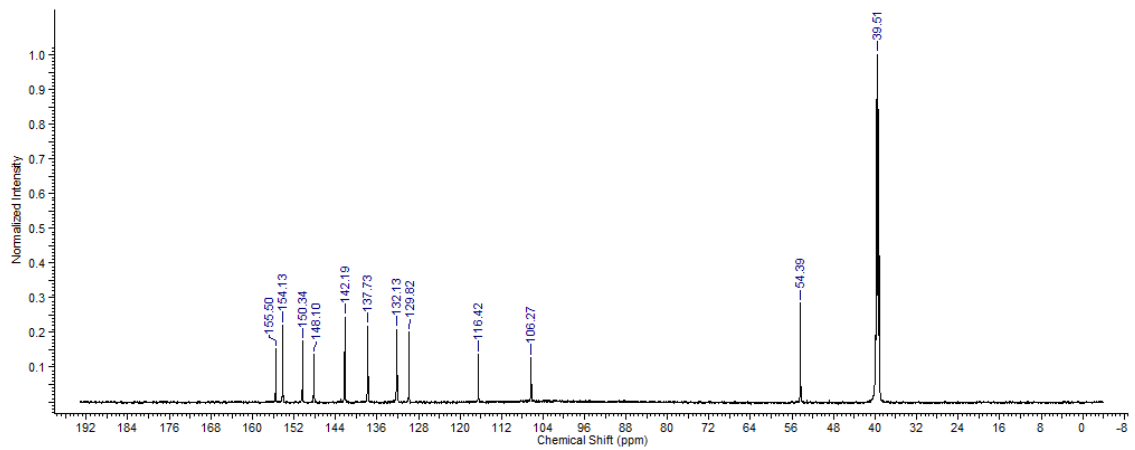
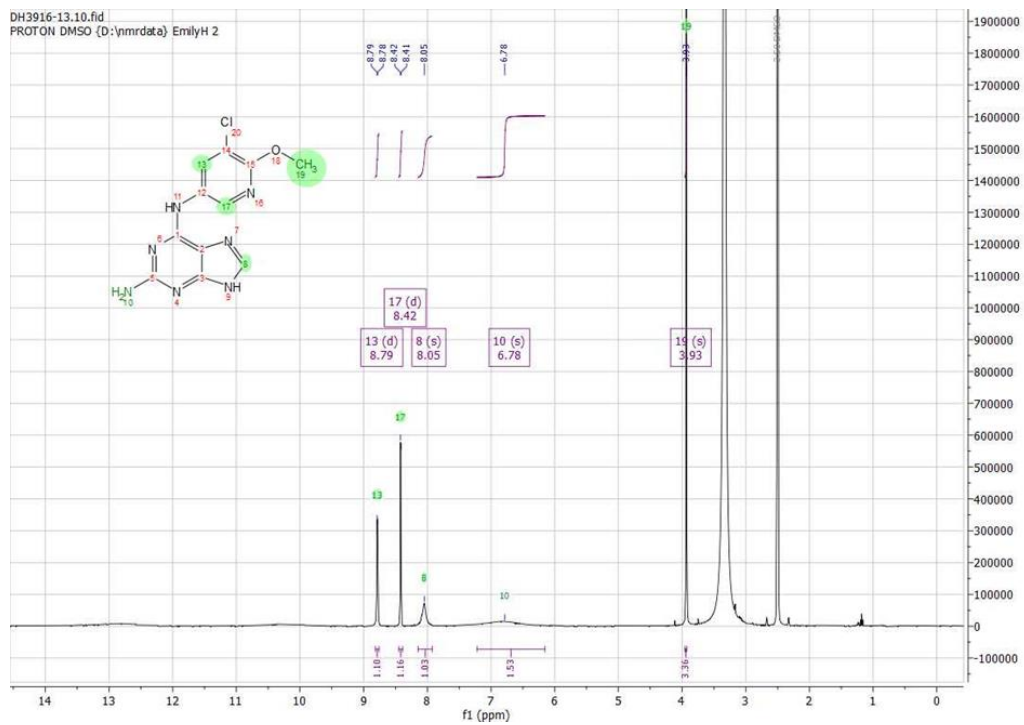


Method Info : X-bridge C18, 50x3.0 mm, 3.5u, 10-97% MeCN 3min,1mL/min, B: MeCN C: NH4HCO3

Sample Info : Walkup method: 'X1097-3'
Target:

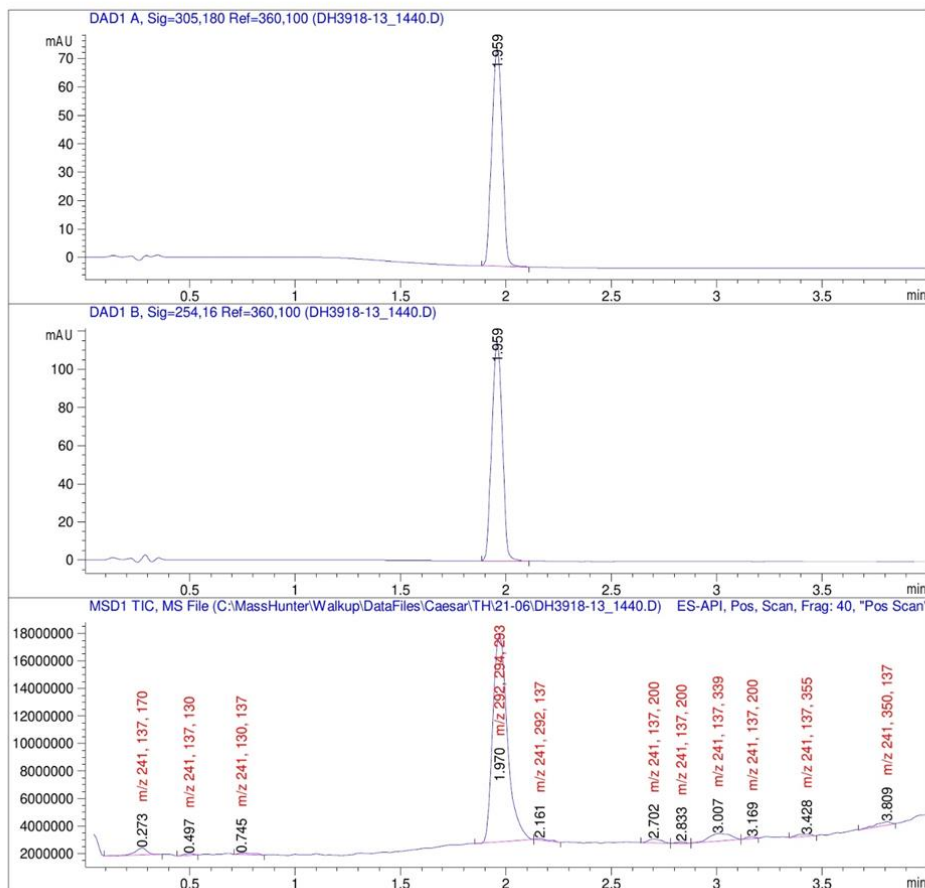


Compound (S54):

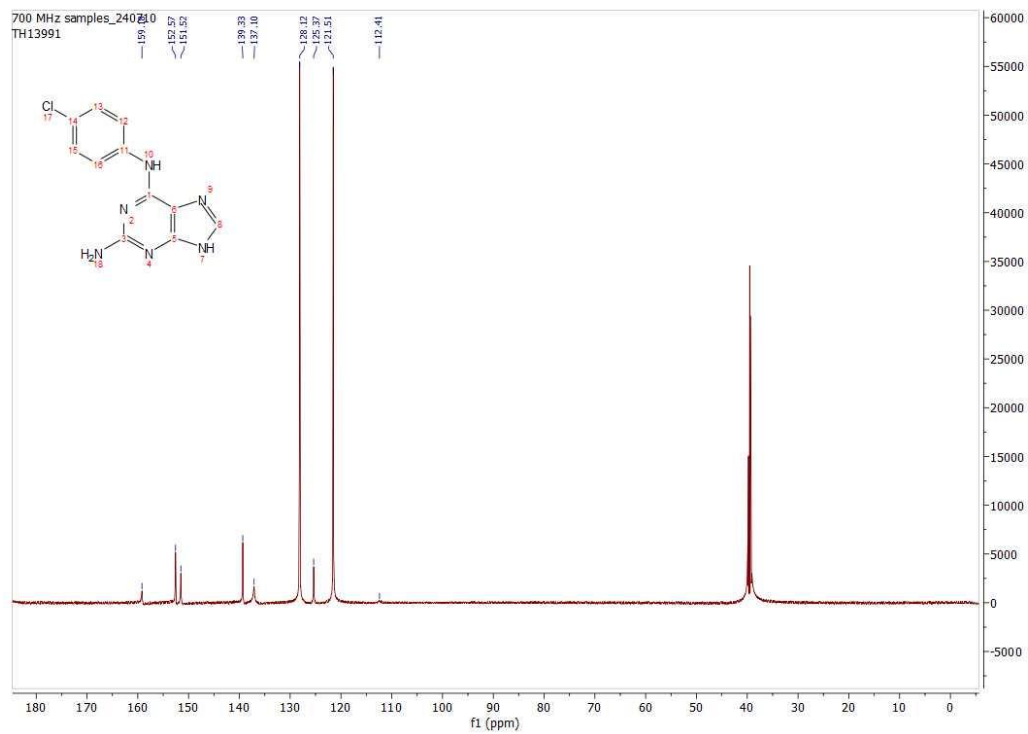
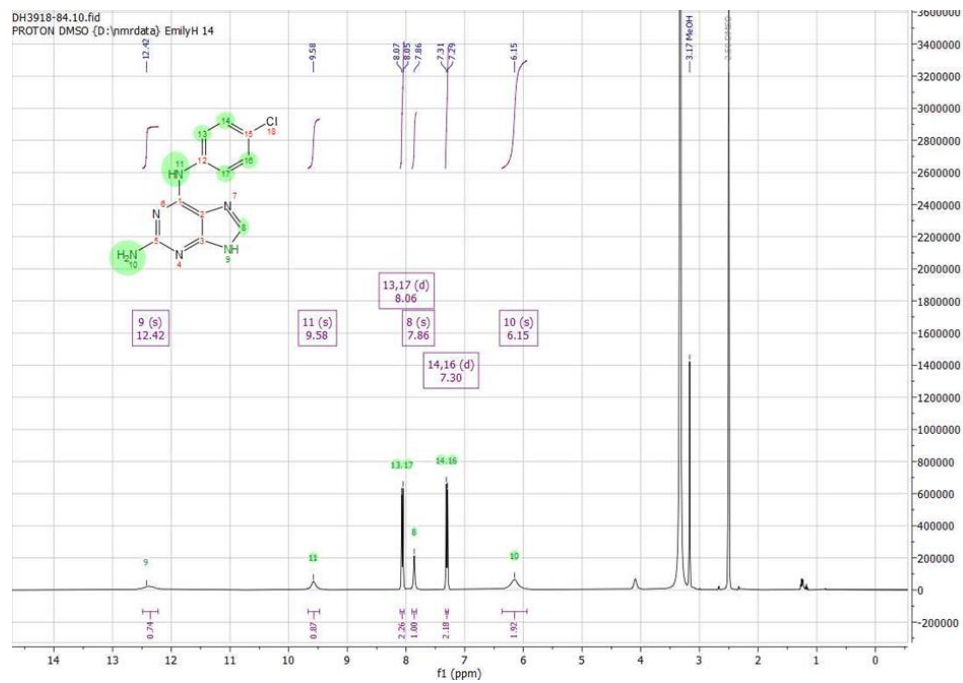


Method Info : X-bridge C18, 50x3.0 mm, 3.5u, 10-97% MeCN 3min,1ml/min, B: MeCN C: NH4HC03

Sample Info : Walkup method: 'X1097-3'
Target:



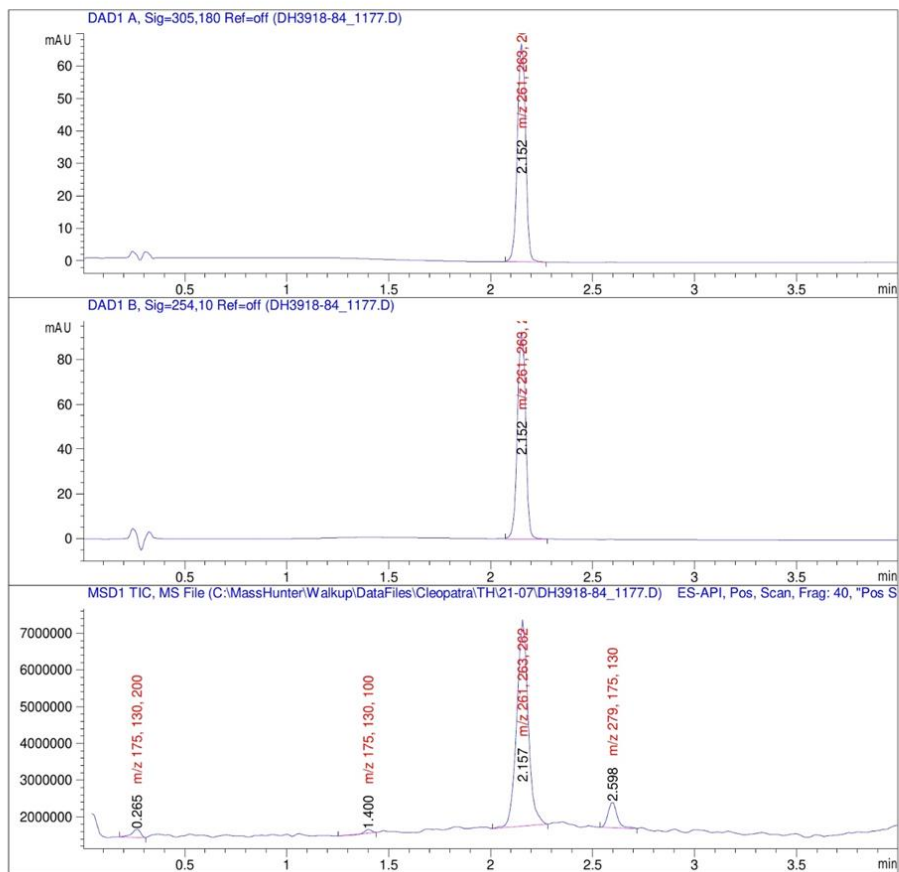
Compound (S55):



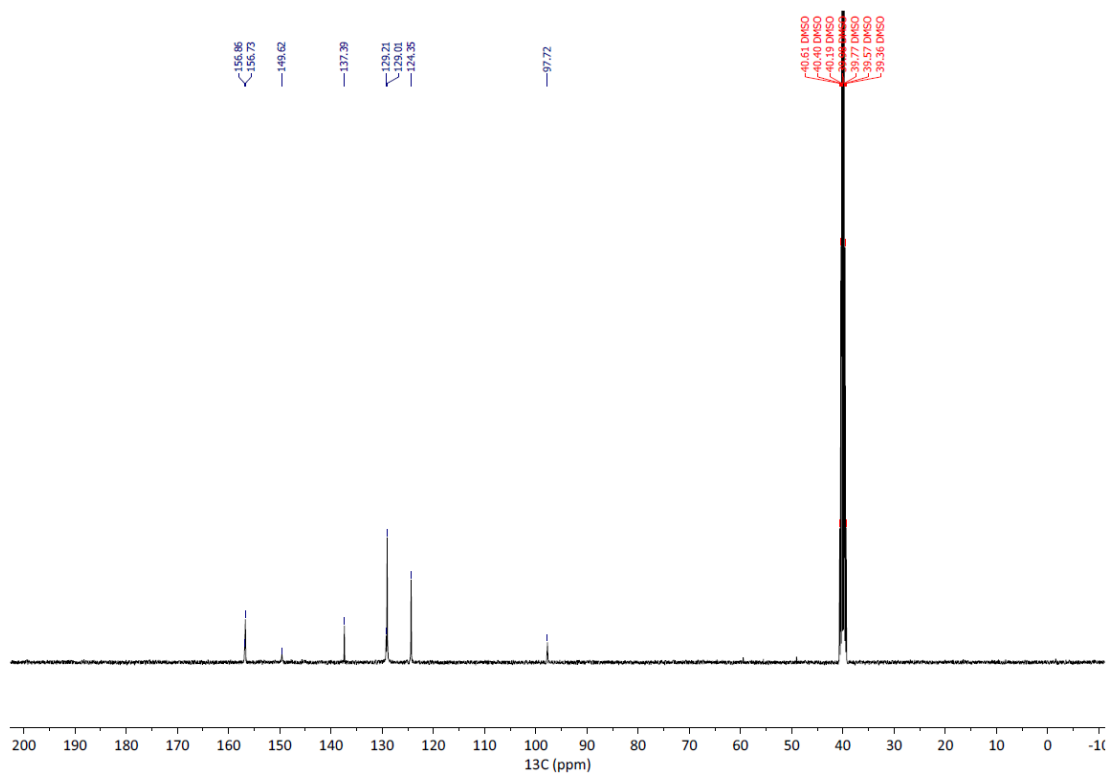
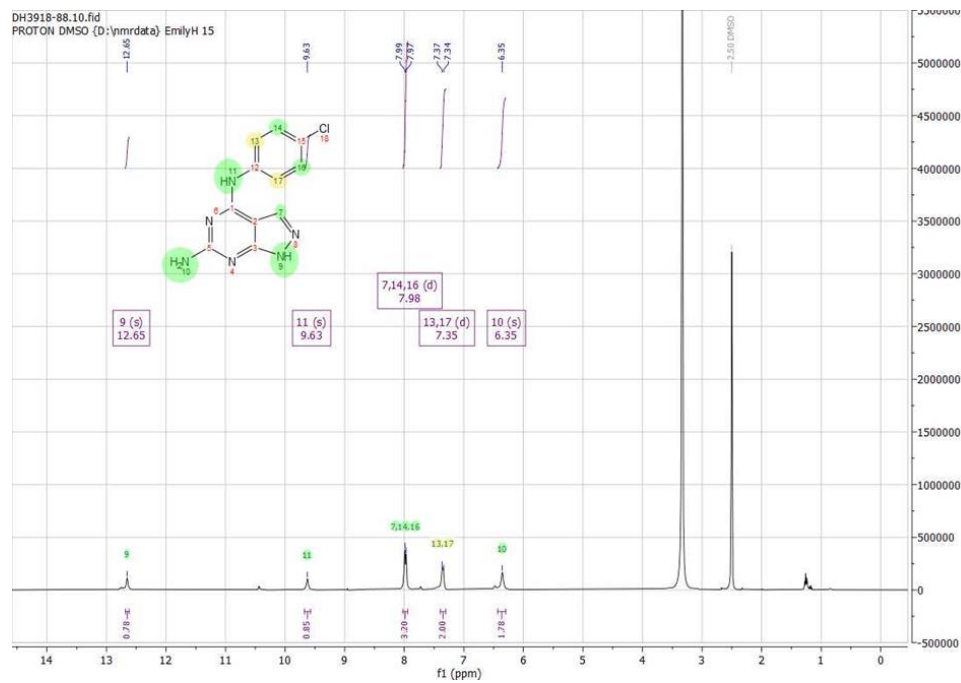
Method Info : X-bridge C18, 50x3.0 mm, 3.5u, 10-97% MeCN 3min,1ml/min, B: MeCN C: NH4HCO3

Sample Info : Walkup method: 'X1097-3'

Target:

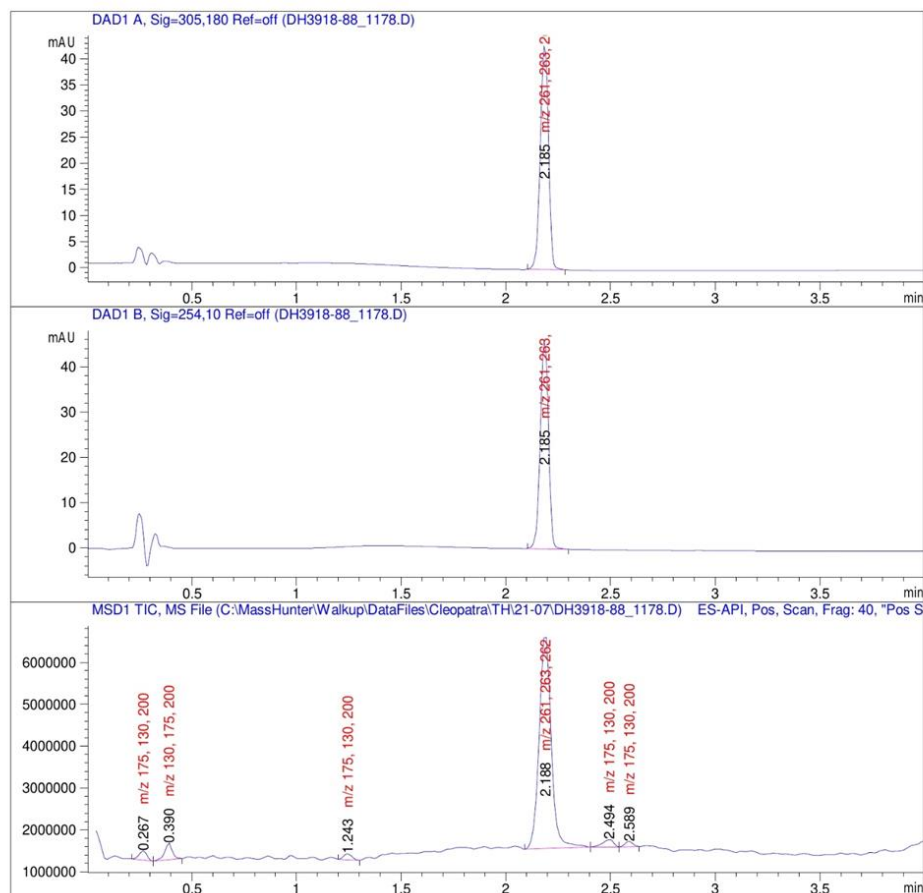


Compound (S56):



Method Info : X-bridge C18, 50x3.0 mm, 3.5u, 10-97% MeCN 3min,1ml/min, B: MeCN C: NH4HC03

Sample Info : Walkup method: 'X1097-3'
Target:



Supplementary References:

- [1] T. Visnes, A. Cázares-Körner, W. Hao, O. Wallner, G. Masuyer, O. Loseva, O. Mortusewicz, E. Wiita, A. Sarno, A. Manoilov, J. Astorga-Wells, A.-S. Jemth, L. Pan, K. Sanjiv, S. Karsten, C. Gokturk, M. Grube, E. J. Homan, B. M. F. Hanna, C. B. J. Paulin, T. Pham, A. Rasti, U. W. Berglund, C. von Nicolai, C. Benitez-Buelga, T. Koolmeister, D. Ivanic, P. Iliev, M. Scobie, H. E. Krokan, P. Baranczewski, P. Artursson, M. Altun, A. J. Jensen, C. Kalderén, X. Ba, R. A. Zubarev, P. Stenmark, I. Boldogh, T. Helleday, *Science* **2018**, 362, 834–839.
- [2] M. Michel, C. Benítez-Buelga, P. A. Calvo, B. M. F. Hanna, O. Mortusewicz, G. Masuyer, J. Davies, O. Wallner, K. Sanjiv, J. J. Albers, S. Castañeda-Zegarra, A.-S. Jemth, T. Visnes, A. Sastre-Perona, A. N. Danda, E. J. Homan, K. Marimuthu, Z. Zhenjun, C. N. Chi, A. Sarno, E. Wiita, C. von Nicolai, A. J. Komor, V. Rajagopal, S. Müller, E. C. Hank, M. Varga, E. R. Scaletti, M. Pandey, S. Karsten, H. Haslene-Hox, S. Loevenich, P. Marttila, A. Rasti, K. Mamonov, F. Ortis, F. Schömborg, O. Loseva, J. Stewart, N. D’Arcy-Evans, T. Koolmeister, M. Henriksson, D. Michel, A. de Ory, L. Acero, O. Calvete, M. Scobie, C. Hertweck, I. Vilotijevic, C. Kalderén, A. Osorio, R. Perona, A. Stolz, P. Stenmark, U. W. Berglund, M. de Vega, T. Helleday, *Science* **2022**, 376, 1471–1476.
- [3] J. Carreras-Puigvert, M. Zitnik, A.-S. Jemth, M. Carter, J. E. Unterlass, B. Hallström, O. Loseva, Z. Karem, J. M. Calderón-Montaño, C. Lindskog, P.-H. Edqvist, D. J. Matuszewski, H. A. Blal, R. P.

- A. Berntsson, M. Häggblad, U. Martens, M. Studham, B. Lundgren, C. Wählby, E. L. L. Sonnhamer, E. Lundberg, P. Stenmark, B. Zupan, T. Helleday, *Nature Communications* **2017**, *8*, 1541.
- [4] B. L. Carroll, K. E. Zahn, J. P. Hanley, S. S. Wallace, J. A. Dragon, S. Doublie, *Nucleic Acids Research* **2021**, *49*, 13165–13178.
- [5] J. M. Parkhurst, G. Winter, D. G. Waterman, L. Fuentes-Montero, R. J. Gildea, G. N. Murshudov, G. Evans, *J Appl Cryst* **2016**, *49*, 1912–1921.
- [6] P. Evans, *Acta Crystallogr D Biol Crystallogr* **2006**, *62*, 72–82.
- [7] Collaborative Computational Project, Number 4, *Acta Crystallogr D Biol Crystallogr* **1994**, *50*, 760–763.
- [8] W. Kabsch, *Acta Crystallogr D Biol Crystallogr* **2010**, *66*, 125–132.
- [9] A. J. McCoy, R. W. Grosse-Kunstleve, P. D. Adams, M. D. Winn, L. C. Storoni, R. J. Read, *J Appl Cryst* **2007**, *40*, 658–674.
- [10] A. Vagin, A. Teplyakov, *Journal of Applied Crystallography* **1997**, *30*, 1022–1025.
- [11] P. Emsley, B. Lohkamp, W. G. Scott, K. Cowtan, *Acta Crystallogr D Biol Crystallogr* **2010**, *66*, 486–501.
- [12] G. N. Murshudov, P. Skubák, A. A. Lebedev, N. S. Pannu, R. A. Steiner, R. A. Nicholls, M. D. Winn, F. Long, A. A. Vagin, *Acta Cryst D* **2011**, *67*, 355–367.
- [13] A. Krämer, C. G. Kurz, B.-T. Berger, I. E. Celik, A. Tjaden, F. A. Greco, S. Knapp, T. Hanke, *Eur J Med Chem* **2020**, *208*, 112770.
- [14] O. Fedorov, F. H. Niesen, S. Knapp, *Methods Mol Biol* **2012**, *795*, 109–118.
- [15] M. Michel, T. Visnes, E. J. Homan, B. Seashore-Ludlow, M. Hedenström, E. Wiita, K. Vallin, C. B. J. Paulin, J. Zhang, O. Wallner, M. Scobie, A. Schmidt, A. Jenmalm-Jensen, U. Warpman Berglund, T. Helleday, *ACS Omega* **2019**, *4*, 11642–11656.
- [16] M. Michel, E. J. Homan, E. Wiita, K. Pedersen, I. Almlöf, A.-L. Gustavsson, T. Lundbäck, T. Helleday, U. Warpman Berglund, *Front. Chem.* **2020**, *8*, DOI 10.3389/fchem.2020.00443.
- [17] S. M. Zhang, M. Desroses, A. Hagenkort, N. C. K. Valerie, D. Rehling, M. Carter, O. Wallner, T. Koolmeister, A. Throup, A.-S. Jemth, I. Almlöf, O. Loseva, T. Lundbäck, H. Axelsson, S. Regmi, A. Sarno, A. Krämer, L. Pudelko, L. Bräutigam, A. Rasti, M. Göttmann, E. Wiita, J. Kutzner, T. Schaller, C. Calderén, A. Cázares-Körner, B. D. G. Page, R. Krimpenfort, S. Eshtad, M. Altun, S. G. Rudd, S. Knapp, M. Scobie, E. J. Homan, U. W. Berglund, P. Stenmark, T. Helleday, *Nat Chem Biol* **2020**, *16*, 1120–1128.
- [18] B. D. G. Page, N. C. K. Valerie, R. H. G. Wright, O. Wallner, R. Isaksson, M. Carter, S. G. Rudd, O. Loseva, A.-S. Jemth, I. Almlöf, J. Font-Mateu, S. Llona-Minguez, P. Baranczewski, F. Jeppsson, E. Homan, H. Almqvist, H. Axelsson, S. Regmi, A.-L. Gustavsson, T. Lundbäck, M. Scobie, K. Strömberg, P. Stenmark, M. Beato, T. Helleday, *Nature Communications* **2018**, *9*, 250.